Adaptability improvement and expanded application of unmanned aerial vehicles in the indoor construction environment

YI YU

PhD

The Hong Kong Polytechnic University

2025

The Hong Kong Polytechnic University

Department of Building and Real Estate

Adaptability improvement and expanded application of unmanned aerial vehicles in the indoor construction environment

YI YU

A thesis submitted in partial fulfilment of the requirements for the degree of Doctor of Philosophy

July 2024

CERTIFICATE OF ORIGINALITY

I hereby declare that this thesis is my own work and that, to the best of my knowledge and belief, it reproduces no material previously published or written, nor material that has been accepted for the award of any other degree or diploma, except where due acknowledgement has been made in the text.

Yi Yu

July 2024

Abstract

Currently, drones are widely used in construction industry. However, compared with the already mature application of drones in outdoor construction environments, the application potential of drones in indoor environments has not been fully developed. The reason is that drones still face many challenges in indoor construction environments. The core challenges include the following four points: (1) Indoor construction environments usually have small spaces, many obstacles and complex distribution, and are also accompanied by frequent flows of people and frequent changes in the environment, which requires drones have greater real-time obstacle avoidance capability. (2) Indoor airflow is complex and unstable, especially when the air conditioning or ventilation system is running, which will affect the flight stability of the drone. (3) Indoor tasks usually require precise flight, resulting in greater energy consumption and affecting the efficiency of UAVs. (4) There is a lack of GPS signals in the indoor environment, making it difficult for UAVs to rely on satellite navigation for positioning and path planning. These challenges directly affect the safety and efficiency of drone applications in indoor environments.

The purpose of this study is to improve the current application status of drones in indoor construction environments and explore the application potential of drones in indoor construction environments. Therefore, in response to the first and second core challenges, this research improves the real-time obstacle avoidance capability and flight stability of UAVs in indoor construction environments by improving the flight control algorithm of UAVs. In response to the third challenge, this research also aims

to achieve efficient route re-planning capabilities by developing and improving flight control algorithms. At the same time, in order to fit the connection between the algorithm and the targeted field, this study integrated the 3D Building Information Model (BIM) with flight simulation software and developed a flight simulation platform for indoor construction environments. The algorithm was simulated and analyzed through this platform, to verify the advancement and feasibility from the software level. In response to the fourth challenge, this research develops a construction waste recycling collaboration framework that combines UAVs with improved flight control algorithms with ground robots to solve the problem of lack of GPS signals through the related capabilities of ground robots and conduct field verification of the improved flight control algorithm.

The collaboration framework and flight control algorithm were rigorously verified through a series of laboratory simulations and field experiments. Research results show that the improved flight control algorithm enhances the UAV's obstacle avoidance capabilities, flight stability, and real-time path adjustment functions. The collaborative framework effectively improves the efficiency of construction waste management, thereby helping to achieve sustainable smart construction management practices and laying the foundation for subsequent related cluster research. Overall, this research work provides an innovative UAV flight control algorithm and UAV application, which solves the current problems encountered by UAV applications in indoor construction environments and improves its obstacle avoidance capabilities and flight stability, and reducing working energy consumption.

Publications

Publish results

Yu Y, Zhang G, He P, et al. Tracking Attitude With Sum-of-Squares Programming for A Fixed-Wing Air Vehicle[J]. IEEE Transactions on Circuits and Systems II: Express Briefs, 2022.5.3 Research schedule

Antwi-Afari M F, Li H, Anwer S, Li D, Yu Y, et al. Assessment of a passive exoskeleton system on spinal biomechanics and subjective responses during manual repetitive handling tasks among construction workers[J]. Safety science, 2021, 142: 105382

Han, S., Li, H., Li, M., Tian, H., Qin, L., Yu, Y., & Ma, J. (2022). Intelligent short-term forecasting for mud concentration in CSD dredging construction. Ocean Engineering, 266, Article 113151.

Under-reviewed papers

Yu Y, Lyu Y, Li H, Zhang G, Fang X, Cost-effective collaborative framework between UAV and robot for recycling construction waste, Journal of Building Engineering, Under review

Zhang G, Yu Y, Li H, Safety-Critical Contraction Tubes with Robust Barrier Functions, IEEE Transactions on Automation Science and Engineering, Under review

Yu Y, Zhang G, Li H, Fang X, Optimization of fully automatic UAV application in indoor construction environment, Developments in the Built Environment, Under review

Acknowledgements

First and foremost, I would like to express my sincere gratitude to my supervisor, Prof. Heng Li. As my Ph.D. advisor, Professor Li has provided me with invaluable inspiration and support in my academic pursuits, as well as meticulous care and assistance in my personal development. His knowledge, wisdom and dedication have been the driving force behind my learning and research efforts. His patient and detailed guidance along with his selfless dedication have greatly benefited me and laid a solid foundation for my Ph.D. research.

Second, I would like to thank my classmates and colleagues in the Smart Construction Lab. Throughout my Ph.D. research, their support and encouragement have been immensely important to me. Discussing problems and sharing research findings with all of them has enabled me to make continuous progress. I am especially grateful to those who helped and advised me during my experiments. Their friendship and cooperation have made the journey of scientific research less lonely.

I would also like to express my special gratitude to my collaborators, Zhang Guo and Dr. Lyu Yifan. Working with them not only improved my research skills, but also broadened my scientific horizons. The process of overcoming research challenges together is one of my most memorable experiences. Their professionalism and spirit of cooperation were crucial to our success.

I am deeply grateful to my wife, Zhao Kewei. Her understanding and support have been the unwavering backbone that has allowed me to fully dedicate myself to my research. Whether I faced difficulties or made progress, she was always there to give me endless love and encouragement. Without her dedication and companionship, I would not have been able to complete this dissertation.

Additionally, I want to thank my one-year-old son, Yu Chen'an. His arrival has brought boundless joy and motivation to our lives. Every time I see his innocent and charming smile, I feel immensely happy and fulfilled. He is the greatest source of motivation for my perseverance and determination.

Finally, I would like to thank my family. The nurturing and selfless dedication of my parents has given me the opportunity to pursue my dreams. Their support and love have been the source of my strength to overcome all challenges. My family has been the strong backbone of my life and career. Without their support, I could not have reached this point.

Once again, I would like to thank everyone who has helped and supported me during my Ph.D. research. Your care and encouragement have allowed me to move forward and complete this dissertation. Thank you all!

Chapter table of content

List of Figures

List of Tables

List of Abbreviations

AEC: Architecture, Engineering, and Construction

AI: Artificial Intelligence

BIM: Building Information Modeling

CDW: Construction and Demolition Waste

CNN: Convolutional Neural Network

DOF: Degrees of Freedom

GPS: Global Positioning System

IMU: Inertial Measurement Unit

IoT: Internet of Things

LiDAR: Light Detection and Ranging

MPC: Model Predictive Control

PID: Proportional-Integral-Derivative

PRM: Probabilistic Roadmap Method

RCBF: Robust Control Barrier Function

RCCM: Robust Control Contraction Metric

RF: Radio Frequency

RL: Reinforcement Learning

RPN: Region Proposal Network

SLAM: Simultaneous Localization and Mapping

SOS: Sum of Squares

UAV: Unmanned Aerial Vehicle

UE4: Unreal Engine 4

UWB: Ultra-Wideband

VSLAM: Vision-based Simultaneous Localization and Mapping

YOLO: You Only Look Once

List of Symbols

α: Angle

β: Sideslip Angle

ϕ: Roll Angle

θ: Pitch Angle

ψ: Yaw Angle

p: Roll Rate

q: Pitch Rate

r: Yaw Rate

m: Mass

g: Gravitational Acceleration

S: Wing Surface Area

b: Wingspan

c̄: Mean Aerodynamic Chord

VT: Airspeed

ρ: Air Density

CL: Lift Coefficient

CM: Pitch Moment Coefficient

CN: Yaw Moment Coefficient

σα1, σα2: Left and Right Aileron Deflection Angles

σe1, σe2: Left and Right Elevator Deflection Angles

σr: Rudder Deflection Angle

Ω: Angular Velocity

I: Inertia Matrix

M: Moment

G: Control Contraction Metric

δx: Differential State Vector

δu: Differential Control Vector

γ: Minimizing Geodesic

t: Time

x: State Vector

u: Control Vector

w: Disturbance Vector

K: Intrinsic Parameter Matrix

Chapter 1. Introduction

1.1 Unmanned Aerial Vehicles in the construction industry

Construction is a sector that has traditionally made a significant contribution to economic development [1]. However, despite this, the industry has been slow to adopt new technologies [2]. The recent integration of unmanned aerial vehicles (UAVs), or drones, into the construction process marks a critical shift towards embracing technological advancements [3]. These tools have a number of technical advantages, but they also face a number of unique challenges that may hinder their full implementation. The technical advantages of drones in construction are manifold. Firstly, drones provide an unparalleled aerial perspective, allowing for precise and comprehensive site surveys [4]. This feature allows the creation of accurate three-dimensional models and terrain maps while reducing the need for labour and time [5]. Secondly, drones facilitate real-time monitoring and inspection of construction sites, which is crucial for project managers to track progress and identify issues without the need for frequent physical presence [6]. Thirdly, drone technology significantly improves the safety of the construction environment. The deployment of drones to perform high-risk tasks, such as inspecting high-rise buildings or large machinery, greatly reduces the need for human workers to physically enter hazardous areas [7]. This minimizes the risk of accidents and ensures compliance with health and safety regulations, thereby reducing the construction company's liability [8].

Despite the aforementioned advantages, it is important to note that drone technology is not without limitations in the field of construction. One of the most significant technical challenges in the field of construction is the limited applicability of drones in specialized environments and the inherent limitations of the drone itself [9]. These factors restrict the dependability and efficiency of work of drones in intricate environments, such as those found in the construction industry [10]. As a consequence, the dependability and efficiency of work have become the significant obstacle to the promotion and development of drones in the construction environment. This introduces an additional layer of complexity and cost. These factors may reduce the efficiency and accuracy of drone data collection, and even cause safety accidents at the construction site, thus posing various challenges to project management [11]. It may even result in the overall production effect being inferior to traditional construction methods [12].

While drones have significant technological advantages that can revolutionize traditional construction practices by improving construction management efficiency, relative personnel safety, and data accuracy, these advantages are hampered by their environmental limitations and their own hardware limitations offset by associated challenges [13]. It is therefore imperative that these technical shortcomings be addressed if the construction industry is to fully utilise drone technology and ensure its sustainable integration into future construction practices.

In the future, the continued growth of the construction industry is expected to generate huge socioeconomic value, but will also place pressure on the human resources of the construction industry [14]. In short, problems such as heavy workload, manpower shortage and aging population in the traditional construction industry have a negative impact on the develop of the global construction industry [15]. It is therefore of great importance to provide the construction industry with powerful helpers in order to improve safety management and efficiency management. This is why research on smart construction is currently being vigorously promoted [16]. Among these helpers, the hardware device of the drone has technical advantages and potential that other devices do not have [17].

To better understand the application of UAV technology in the construction industry, it is essential to analyze its technical background and the challenges it faces. The integration of UAV technology in construction management requires seamless interfacing with existing management software systems, while also overcoming specific challenges in construction environments, such as complex spatial layouts and variable weather conditions. Furthermore, it is necessary to explore improvements in navigation and obstacle avoidance technologies for UAVs on construction sites to enhance operational efficiency and safety.

1.2 Research scope

This section has the objective of defining the scope of the study in a more precise manner, focusing it on drones in indoor built environments. First, the rationale for selecting the indoor construction environment as the subject of this study is presented, the intricacies of the indoor construction environment are elucidated, and the research topic is narrowed to the utilization and enhancement of drones in indoor settings

1.2.1 From outdoor construction environment to indoor

construction environment

The utilization of Unmanned Aerial Vehicles (UAVs) in outdoor construction has undergone a notable evolution, with functions such as terrain mapping, progress monitoring, and safety inspections becoming increasingly prevalent [18]. However, the application of UAVs in indoor construction environments presents a greater challenge than in outdoor environments.

Firstly, the spatial constraints of indoor construction environments necessitate a higher degree of maneuverability from UAVs. The necessity for precision control in flying in a narrow space is paramount to avoid collisions with walls, ceilings, beams, or equipment under construction. Furthermore, indoor environments frequently lack GPS signals, necessitating the use of more sophisticated navigation technologies such as vision or laser navigation systems (VSLAM). These systems enable drones to locate and navigate by analyzing images captured by a camera or laser scans. Secondly, lighting conditions in indoor construction environments are often variable and unpredictable, thereby challenging the UAV's vision system. In order to ensure the accuracy of visual measurements and data collection in low light or reflective conditions, it is necessary for UAVs to be equipped with high-performance cameras and other sensors. Furthermore, poor air flow in indoor construction sites may affect the stability and flight efficiency of UAVs. For example, airflow from air conditioning systems, vents, or other mechanical equipment operations may cause the drone to oscillate or deflect during flight. Additionally, radio frequency interference in indoor environments is a significant issue that cannot be overlooked. In indoor construction sites, various electronic devices and machinery may generate interference signals, which may affect the communication system of the UAV, resulting in unstable data transmission or delayed control commands. Finally, the dynamic changes in the indoor construction environment also place higher demands on the UAV's real-time response capability. Factors such as temporary structural changes and frequent personnel movements at the construction site require the UAS to be able to update its flight path and operation plan in real time [19].

In summary, the application of UAVs in indoor construction environments is more complex than in outdoor environments, requiring the resolution of a series of technical issues such as spatial constraints, navigation technology, lighting conditions, air mobility and radio frequency interference. Despite the challenges, the potential for UAVs in indoor construction monitoring and management remains huge as technology continues to evolve [12].

1.2.2 The importance of improvement in UAV in the indoor construction environment

Enhancing Unmanned Aerial Vehicles (UAVs) for indoor construction environments is crucial due to the unique challenges and significant benefits they provide. UAVs can navigate dangerous or inaccessible areas, reducing the risk of injuries by minimizing the need for workers to perform high-risk inspections or operations in confined spaces [13]. By conducting rapid and frequent inspections, UAVs save time and labor costs. Equipped with advanced sensors, UAVs can ensure higher accuracy in data collection such as measurements and 3D mapping, crucial for maintaining construction quality and adherence to plans. Improving UAV technology for indoor use is essential for advancing safety, efficiency, and data quality in construction, addressing these challenges will unlock their full potential in transforming indoor construction operations [15]. Serving as the important step of UAV in construction environment, the development and improvement of UAV applications in indoor environments is the subject of this study.

1.3 Research problem statement

Given the global significance of the construction industry in economic development, the sector's slow adoption of advanced technologies notably impedes its operational efficiency and safety standards [20]. The integration of Unmanned Aerial Vehicles (UAVs), or drones, into indoor construction processes represents a progressive shift; however, their full potential is far from being realized due to several pronounced issues:

Adaptability Challenges: UAVs are currently challenged by the demanding environments of construction sites that require high maneuverability and stability [21]. The existing UAV technologies, although advanced, often fall short in meeting these specific operational demands, thus limiting their effective deployment in varied construction activities [22]. Technological Limitations: The technological infrastructure supporting UAVs in construction is yet to fully cater to the sector's unique needs. This includes capabilities for precise data collection, real-time monitoring under diverse environmental conditions, and robust safety protocols that are critical in densely populated or structurally complex construction sites [8]. Safety and Regulatory Concerns: The integration of UAVs introduces significant safety risks and regulatory challenges. These include potential accidents and the need for stringent compliance with evolving safety regulations, which can impose additional burdens on construction firms [14]. Inefficient Collaboration: There is an absence of an effective framework for integrating UAVs with other robotic systems such as ground robots, especially in tasks like recycling construction waste. Such collaborative frameworks are essential for enhancing operational efficiency and promoting sustainable construction practices [15]. Moreover, current UAV applications do not account for individual differences among construction sites and projects, which can vary widely in terms of environmental and operational conditions.

The core problem is that while UAVs have the potential to revolutionize construction practices by enhancing efficiency, safety, and data accuracy, their implementation is hindered by these technological, operational, and regulatory challenges. This dissertation aims to solve safety issues such as obstacle avoidance of drones in complex indoor environments by developing advanced drone flight control algorithms and collaboration frameworks suitable for indoor construction environments, and ensure their effective and safe integration into indoor construction management processes [22].

1.4 Research aim and objectives

The overall objectives of this dissertation are multiple:

1) To critically assess the current state and limitations of UAV technology in the construction management arena and provide an empirical basis for its potential optimization.

2) To develop a state-of-the-art flight control algorithms tailored to the specific needs of the construction environment, thereby improving the performance and reliability of UAVs.

3) To optimize the application of UAVs in indoor construction scenarios through the integration of Building Information Modeling (BIM) 3D models and advanced autonomous navigation techniques, paving the way for increased operational efficiency and precision in construction processes.

4) To develop a cost-effective collaborative framework to integrate drones with improved flight control algorithms with ground-based robots, especially in the context of construction waste recycling.

This study aims to enhance the adaptability and application potential of drones in indoor construction environments by improving flight control algorithms and developing a collaborative framework, addressing key issues such as obstacle avoidance, flight stability, path planning, and construction waste recycling in complex settings, thereby advancing the safety, efficiency, and sustainability of smart construction management.

1.5 Research significance

The thesis's significance on the adaptability and expanded application of unmanned aerial vehicles (UAVs) in the construction environment is multifaceted and substantial. At its core, this research addresses critical gaps in current indoor construction management practices by integrating advanced UAV technology, thereby catalyzing a transformative shift in how indoor construction projects are managed and executed.

Firstly, the thesis makes a pivotal contribution by developing sophisticated UAV flight control algorithms that enhance maneuverability and stability in the challenging conditions of indoor construction sites. They are critical to ensure the obstacle avoidance capabilities of UAVs operating in dangerous and dynamically changing indoor environments and to modify flight paths with precision and efficiency in real time. The research improves the precision and reliability of UAVs, thereby facilitating their deployment in indoor critical tasks such as site surveying, progress monitoring, and safety inspections, which traditionally involve high risks and significant human resources.

Secondly, the thesis extends the functionality of UAVs in indoor construction environments through the integration of 3D Building Information Modeling (BIM) and autonomous navigation systems. This advancement is critical to optimizing the project planning and execution phases of drone work, enabling more precise and automated control of complex tasks without compromising construction safety and construction quality.

In addition, the cost-effective collaboration framework proposed in this thesis combines UAVs with improved flight control algorithms and ground robots to work together, representing an innovative method for recycling construction waste. This is particularly important in the context of sustainable building practices, where reducing waste and improving resource efficiency are pressing concerns. And the previously proposed algorithm was also verified from the level of field experiments. The framework addresses both environmental sustainability and the practical solutions needed to reduce construction project costs and improve operational efficiency. And provide reliable data support for all previous theoretical results.

In essence, this dissertation not only pushes the boundaries of existing UAV technology but also sets a robust foundation for future research and implementation in the field of construction technology. By addressing the technological challenges, the research significantly enhances the potential of UAVs to improve construction management practices, aligning with broader goals of efficiency, safety, and sustainability in the industry.

1.6 Research instruments

The following research instruments are applied in this study to answer the following research questions.

1) Literature review. A review of pertinent literature was conducted, primarily comprising peer-reviewed journal articles and conference papers, with the objective of gaining insight into the existing knowledge base pertaining to drone flight control and previous construction drone technology. Based on the findings of the literature review, potential research gaps in the field of feasible UAV technology and flight control algorithms were identified.

2) Laboratory experiments. This study conducted a series of laboratory simulation experiments and calculations to evaluate the accuracy of the proposed flight control algorithm and to improve its performance. In addition, the feasibility of the constructed hardware framework was assessed.

3) Field experiments. The feasibility of the proposed hardware framework in actual construction sites was verified through field experiments, and the applicability of this method in construction site management was demonstrated.

1.7 Overview of the thesis

The remainder of this thesis is divided into three parts and comprises eight chapters. The remainder of the first part is a literature review of construction management automation, which outlines the relevant technologies that support this research. These include computer vision techniques, unmanned aerial vehicle (UAV) path planning algorithms, and flight control algorithms, etc. Part II describes the construction of new UAV flight control algorithms. Chapter 3 outlines the design of this study, while Chapter 4 presents a study on the improvement of a fixed-wing UAV flight control algorithm. Chapter 5 describes a multi-rotor UAV flight control algorithm based on the fixed-wing UAV flight control algorithm in Chapter 4, and Chapter 6 describes the development of a simulation software that can be used to evaluate the proposed flight control algorithm. Finally, the Chapter 7 of third part describes the application of the developed UAV collaboration framework in construction site management and describes the experimental setup and results. The discussion of this study and possible future research directions are given in Chapter 8.

Chapter 2. Literature Review

In order to review the literature that laid the foundation for this study, this chapter is organized as follows. Section 2.1 outlines the UAV in construction industry and explains the main trends of the application research, and studied related literature on drone-robot collaboration. Section 2.2 specifically reviews the research on UAV flight control algorithm. Section 2.3 studies on related technologies of drones in construction waste recycling. Finally, research gaps are revealed in section 2.4.

2.1 Overview of UAV in construction industry

2.1.1 Related applications of drones in construction

The past five years have seen a remarkable integration of Unmanned Aerial Vehicle (UAV) technology into the construction industry, revolutionizing traditional practices through enhanced data collection, monitoring, and management processes. This literature review aims to encapsulate the significant strides made in this domain, highlighting the advancements, challenges, and future potential of UAV applications in construction. A significant leap has been the development of UAVs equipped with advanced sensors and imaging technologies. In the application of drone technology, multi-rotor drones have become essential tools in construction management due to their flexibility and ease of operation. According to a study [23], multirotor drones show significant advantages in construction monitoring, progress tracking, and safety inspections. The study indicates that by providing real-time data and comprehensive site views, drones can optimize construction management processes, reduce reliance on manpower, and enhance site safety. This finding provides empirical support for the application of drone technology in the construction industry and highlights potential directions for further technological development. For instance, the work by Setyawan (2022) illustrates the use of LiDAR-equipped drones for creating high-resolution 3D site models, enabling precise volume measurements and structural inspections [24]. Similarly, advancements in photogrammetry, as discussed by Agueera-Vega (2018, have allowed for detailed topographic mapping, which is invaluable in site planning and design [25]. UAVs have been increasingly adopted for real-time site monitoring, offering a bird's-eye view that facilitates project management. A study by Jacob-Loyola et al. (2021) showcases the implementation of UAVs for tracking construction progress, identifying discrepancies between planned and actual construction works [26]. Furthermore, the integration of UAV data into Building Information Modeling (BIM), as explored by Sulaiman et al (2022), has provided project stakeholders with an interactive platform to visualize progress and make informed decisions [27]. Worker safety has been a critical area of application for UAVs. The research by Kas, K. A., (2020) highlights how UAVs can perform hazardous site inspections, reducing the need for human exposure to potential risks [28]. UAVs have also been used to monitor compliance with safety regulations, as shown in the study by Alizadehsalehi, S., (2020), which describes a UAV-based system for detecting safety equipment usage on-site [2]. Despite these advancements, several challenges impede the widespread adoption of UAVs in the construction industry. Privacy and legal concerns, limited flight endurance, and vulnerability to environmental factors are issues discussed by York (2020) [29]. The need for skilled operators and the integration of UAV operations with existing workflows, as noted by Onososen et al. (2023), also present significant hurdles [30].

Looking forward, the potential of UAVs in construction is vast. Autonomous UAVs, machine learning for data analysis, and improved collaboration between UAVs and ground robots are areas ripe for research and development. The work by Liang (2023) predicts that advancements in artificial intelligence will enable UAVs to make real-time decisions, further enhancing their application in construction [31].

In conclusion, the literature indicates that UAVs have become indispensable tools in the construction industry, improving efficiency, safety, and decision-making processes. Although challenges remain, ongoing research and technological developments are likely to overcome these barriers, paving the way for more innovative and integrated UAV applications in the future.

2.1.2 BIM and UAV technology

Building Information Modeling (BIM) serves as a comprehensive digital database designed to gather, manage, analyze, and process information related to construction activities throughout the project lifecycle [32]. Unlike traditional construction management systems, BIM excels in creating multi-dimensional and data-rich models, making it an advanced technology for enhancing construction quality, cost-effectiveness, efficiency, and sustainability [33]. Specifically, BIM is a versatile management tool applicable at various stages of new or existing infrastructure projects. It can be utilized for numerous purposes, including site selection, energy analysis, scheduling, cost estimation, visualization, equipment management, and design revision. Moreover, the increasing emphasis on safety within the architecture, engineering, and construction (AEC) industry has led many researchers to employ BIM for safety inspections [34].

Innovative technologies integrated with BIM are often proposed to enhance its capabilities and monitor construction progress. Drones, or unmanned aerial vehicles

(UAVs), represent one such technology used for construction safety monitoring within the AEC industry [35]. Initially developed for military use [36], drones have recently gained popularity in fields like construction due to advancements in technology. UAVs equipped with real-time monitoring capabilities can capture images or videos of construction sites as they evolve [37, 38]. As a result, UAVs are extensively used for site surveys, visual inspections, monitoring construction progress, and detecting security risks in various infrastructure projects [37-39]. Compared to other monitoring technologies, UAVs offer benefits such as portability, flight stability, ease of use, real-time responsiveness, low cost, and high resolution [39].

Currently, researchers are exploring two primary methods to integrate BIM and UAVs based on the UAVs' functionalities [38]. In the first method, UAVs capture geometric information of construction sites, which is then used to generate BIM models [40]. In the second method, BIM models are created before deploying UAVs.

2.1.3 Combining Drones and BIM applications

Asnafi (2016) [41] and Alizadehsalehi et al. (2017, 2020) [2, 42] pioneered the use of UAVs to monitor potential hazard locations identified using BIM. They developed a framework encompassing a 4D BIM-based model, safety regulations, UAV-based safety inspections, dynamic data, and project safety analysis. This safety framework is divided into preconstruction and construction stages. During the preconstruction stage, 4D BIM is used to simulate site hazards, and safety regulations from OSHA are integrated into the model. This allows for the identification and prevention of potential hazards. At the construction stage, UAVs can monitor and enforce safety regulations. Safety managers can compare UAV-captured images with the preconstruction 4D model to confirm that potential hazards are controlled and prevention methods are effective.

Furthermore, BIM can be instrumental in designing UAV flight paths for safety inspections. For instance, Freimuth and König (2015) [43] suggested a system to survey construction sites using semiautonomous UAVs, generating 3D building and site models from aerial images. In this system, UAVs capture images to create dense point cloud data for the 3D model. The UAV waypoints are determined by survey tasks, objectives, and building element types derived from BIM. UAVs then capture necessary images based on these waypoints. Although not explicitly stated by the authors, this system could be adapted for regular safety inspections. The safety issues of UAVs on construction sites are critical, and Freimuth and König [43] leveraged BIM to calculate the safety distance between UAVs and all operational objects automatically.

BIM aids UAVs by designing safety waypoints, and facilitating semiautonomous and fully autonomous UAV safety inspections.

2.1.4 The application of drones and robots in construction management

The application of drones in the construction domain is not only conducive to improving the quality of construction projects, accelerating construction progress, and reducing labor costs, but also conforms to the development of digitalization, industrialization, and intelligence in the construction industry. Chen et al. [44] developed an application that combines building information modeling (BIM) and drones for the safety management of construction sites. Although the application is still in the early stages of adoption, it shows the potential to significantly improve safety performance of buildings. Kaamin et al. [45] developed a way to improve the schedule management of construction sites using drone technology. These authors used drones to replace the conventional method of shooting on construction sites. They found that the entire view of the construction site can produce better images, videos, and 3D models, and can also simplify the work of site engineers' jobs, so this research has proven that using drones, better images, and videos can provide a better overview of construction sites and monitor any defects in high-altitude building structures.

Additionally, the progress of the construction sites can effectively be tracked by using drones. Asadi et al. [46] presented a cooperative UAV-UGV system for autonomous data collection in construction. It also shows another direction of the current UAV construction site application, which is related to using construction robots on the ground. Regarding construction waste recycling, several robot-related application studies have been conducted. Ku et al. [47] proposed a robot for sorting construction and demolition waste, which is used to finely sort a large number of objects before mixing and crushing. It was found that the use of robots has improved the resource utilization level of construction and demolition waste. However, it aimed at the problem of low efficiency of industrial sorting robots using traditional vision algorithms to identify and locate targets in complex environments. The system proposed by Zhang et al. [48] introduces a deep learning technology to detect and locate solid waste based on existing algorithms, and to also build an industrial robot sorting system platform. Gao et al. [49] presented a new method for capturing and reconstructing indoor scenes using mini-UAVs and ground robots, which considers the completeness of capture and the accuracy of reconstruction.

2.1.5 Specific challenges of UAV in Construction Workspace

Unmanned Aerial Vehicles (UAVs) have become a focal point of research in autonomous systems, particularly in the context of path planning and navigation in changing environments. While significant progress has been made in various domains, construction workspaces present unique challenges that extend beyond the capabilities of current UAV technologies. This review highlights these specific challenges and discusses how novel methods can advance data engineering and science in construction and building environments.

I. Unique Challenges of UAV in Construction Workspace

Construction sites present unique challenges due to their highly dynamic and unpredictable nature, which complicates UAV path planning and autonomous operation. The presence of dynamic obstacles, such as moving equipment, cranes, vehicles, and workers, requires UAVs to continuously adapt their flight paths [50]. Traditional path planning systems, reliant on static or semi-static maps, are inadequate in these scenarios. UAVs must be equipped with real-time obstacle detection and avoidance systems that can process and respond to the rapid movement of objects and people [51]. This involves employing advanced sensor technologies such as LiDAR, cameras, and radar for real-time obstacle detection [52], coupled with adaptive path planning algorithms that dynamically adjust flight paths based on real-time data, potentially using predictive models to anticipate obstacle movements [53].

Furthermore, the unstructured and cluttered environment of construction sites, filled with materials, debris, and incomplete structures, poses significant navigational challenges. Traditional algorithms effective in structured environments struggle here. Therefore, UAVs need sophisticated perception systems to interpret complex environments and robust navigation algorithms that can process and integrate data from various sensors to understand and navigate the site effectively [54]. The rapid temporal changes in construction site layouts, with new structures constantly emerging and old ones being modified or removed, necessitate UAVs to perform real-time map updates and path recalculations [55]. They must integrate new sensor data continuously to maintain accurate maps and develop algorithms for quick path recalculations in response to environmental changes.

Ensuring the safety and compliance of UAV operations is critical in construction sites. UAVs must not only avoid obstacles but also predict and respond to human movements, adhering to strict safety protocols to prevent accidents [56]. This requires human detection and behavior prediction systems, potentially using machine learning models trained on construction site data to recognize common behaviors and patterns [57]. Additionally, UAVs must comply with site-specific safety protocols and regulatory standards, maintaining safe distances from workers and equipment and avoiding restricted areas [58].

II. Advancing new methods to the data engineering and science of UAV in construction and building environments

To address these challenges, Innovative methods are required that integrate advanced principles of data engineering and science. Key areas of research include real-time sensor fusion, which involves combining data from multiple sensors, such as LiDAR, cameras, and GPS, to create a comprehensive and real-time map of the environment [51]. This approach enhances the situational awareness and responsiveness of UAVs. Additionally, machine learning for dynamic path planning employs algorithms to anticipate environmental changes and optimize path planning in real-time [53]. Reinforcement learning, for example, can enable UAVs to learn from their experiences and refine their navigation strategies [54]. Another crucial area is the development of adaptive and predictive algorithms that can adjust to both immediate and long-term changes in environments such as construction sites [59]. These algorithms must be capable of rapidly recalculating paths and forecasting future changes to maintain efficient navigation [60]. Human-UAV interaction is also a significant focus, aiming to improve the interaction between UAVs and human workers through advanced perception and prediction models. This involves understanding human behavior and movements to ensure safe and effective coexistence on the site [57]. Finally, the exploration of collaborative multi-UAV systems is essential, as it involves using multiple UAVs working together to cover larger areas, share data, and enhance overall efficiency [61]. Developing coordination algorithms that allow UAVs to communicate and adjust their paths in real-time is a key component of this research [62].

2.1.6 Summary

The integration of unmanned aerial vehicles (UAVs) into the construction industry has significantly changed traditional practices by improving data collection, monitoring, and management processes. This chapter reviews the significant advances in UAV applications, highlighting their contributions to creating high-resolution 3D site models, real-time site monitoring, and improving worker safety through advanced sensor technologies and machine learning algorithms. It also discusses the synergistic use of UAVs with Building Information Modeling (BIM) for better project visualization and decision making. Despite the obvious benefits, challenges remain, such as obstacle avoidance problem, limited endurance, and the need for skilled operators. This part highlights the potential for future research in autonomous UAVs, real-time sensor fusion, and collaborative multi-UAV systems to further improve the efficiency, safety, and sustainability of construction sites, and ultimately advance data engineering and science in the built environment.

2.2 Researches on UAV flight control algorithm

2.2.1 Overview of UAV flight control algorithm

Recent years have seen a surge in the development of adaptive control algorithms capable of handling the nonlinear dynamics of UAVs and the uncertainties in their operating environments. For instance, the work by Kazim et al. (2021) introduced a robust adaptive flight control algorithm that improves UAV stability in turbulent atmospheric conditions [63]. Similarly, Wu, J and Wang, H (2022) developed a machine learning-based control algorithm that allows UAVs to learn from their environment and adjust their flight parameters in real-time [64].

The push for autonomous UAVs has led to the integration of advanced sensory and processing capabilities. Research by Lin et al. (2023) demonstrated an algorithm that uses visual-inertial odometry to navigate in GPS-denied environments with a high degree of accuracy [65]. Furthermore, the deep reinforcement learning approach by Bouhamed (2020) for UAV navigation in urban environments shows promise in enabling UAVs to make intelligent pathfinding decisions autonomously [66].

Ensuring safe operation, collision avoidance algorithms have been a critical area of focus. A notable study by Du, Y (2019) proposed a real-time collision avoidance algorithm that dynamically adjusts the flight path of UAVs in response to moving and static obstacles [67]. This work is instrumental in paving the way for UAV integration into crowded airspace and complex urban settings.

Energy efficiency in UAV flight control is essential for extending mission durations and operational efficiency. The research by Gudmundsson. (2019) on bio-inspired energy-efficient flight control algorithms draws from the flight patterns of birds, resulting in significant energy savings for UAVs during long flights [68].

Although substantial progress has been made, challenges persist in the field of UAV flight control algorithms. The limitations in computational resources on UAVs, as noted by Ebeid, E (2018), restrict the complexity of algorithms that can be implemented onboard [69]. Additionally, the regulatory landscape and safety concerns necessitate the development of highly reliable and fail-safe flight control systems.

The future of UAV flight control algorithms lies in the advancement of artificial intelligence and edge computing, which can enable real-time processing and decision-making. The integration of these technologies, as projected by Santos and Rezwan (2020), will likely lead to more robust, intelligent, and adaptive control systems for UAVs [70].

The research conducted in the field of UAV flight control algorithms over the last five years has made significant strides in improving UAV performance and autonomy. As computational technologies advance and regulatory frameworks evolve, it is expected that UAVs will become increasingly capable and reliable, with flight control algorithms playing a central role in their evolution.

2.2.2 Overview of Fixed-Wing UAV Flight Control Systems

Fixed-wing UAVs are preferred for missions requiring long endurance and high-speed travel due to their aerodynamic efficiency. Unlike rotary-wing UAVs, they require continuous forward motion to generate lift. This intrinsic characteristic influences the design of their flight control algorithms, which must continuously balance stability and maneuverability [71]. Flight control systems in fixed-wing UAVs typically involve the regulation of the pitch, roll, and yaw axes to maintain flight stability and navigate through waypoints [72].

Early flight control algorithms were heavily reliant on classical control theory, primarily utilizing PID (Proportional, Integral, Derivative) controllers due to their simplicity and effectiveness in many linear control systems [73]. However, the dynamic environments and the non-linear nature of UAV flight dynamics prompted the development of more sophisticated algorithms. In the last two decades, there has been a shift towards using advanced control strategies like Linear Quadratic Regulators (LQR), Model Predictive Control (MPC), and adaptive control systems.

LQR provides a method to determine the optimal gain settings to minimize a quadratic cost function, making it highly effective for systems where the model dynamics are well understood [74].

MPC has emerged as a powerful control strategy in scenarios requiring the handling of multiple constraints and prediction of future states. This is particularly useful in UAVs where future state prediction can significantly enhance the robustness of the control system against disturbances like wind gusts [75]. Adaptive control algorithms are designed to adjust their control parameters in real-time, compensating for model uncertainties and external disturbances. This feature is crucial in UAV applications due to the variability in payload, weather conditions, and system dynamics over time.

Otherwire, Deep learning has also found applications in UAV flight control, particularly in tasks requiring image recognition and environment sensing for autonomous navigation. Convolutional Neural Networks (CNNs) and Reinforcement Learning (RL) are being increasingly used to enable UAVs to learn from their environment and improve their flight behavior autonomously (Mnih et al., 2015) [76].

Despite these advancements, several challenges remain. The computational demand of advanced algorithms like MPC and the training requirements for ML-based systems pose limitations on their deployment in smaller UAVs with limited on-board processing capabilities. Furthermore, ensuring the safety and reliability of AI-driven UAVs in all operational scenarios is still a subject of ongoing research.

Future research is likely to focus on the development of more energy-efficient AI algorithms that can operate on low-power computing platforms suitable for UAVs.

Additionally, the integration of AI with traditional control methods in a hybrid approach could potentially offer a balance between adaptability and reliability.

In conclusion, the research on flight control algorithms for fixed-wing UAVs has made substantial strides in moving from basic PID controllers to more sophisticated, adaptive, and AI-enhanced systems. As these technologies continue to evolve, they hold the promise of making UAVs more autonomous, efficient, and capable of handling complex tasks in dynamic environments. Nevertheless, balancing computational demands with operational efficiency and safety remains a critical challenge for researchers and engineers in the field.

2.2.3 Control Barrier Functions

Control Lyapunov Functions with Control Barrier Functions.The topic of control barrier functions (CBFs), constructing invariant sets satisfying safety feasibility provides a suitable tool to maintain the safety of control systems. Furthermore, the quadratic-program-based-based approaches, called CLF-CBF-OP, were utilized to unify stability and safety via the control Lyapunov functions and control barrier functions [77]. Several applications of CLF-CBF-OP can be seen in the historical view [78]. The further literature [79]-[81] studied different problems through such quadratic optimization schemes. Control barrier functions with the input-to-state property were presented to address the safety-critical control for nonlinear dynamical systems under input disturbances [79]. An adaptive estimation law was introduced in

CBFs to guarantee safety for nonlinear systems subject to time-varying and state-dependent uncertainties [80]. The adaptiveCLFs and adaptive CBFs were unified in one adaptively stabilizable and adaptively safe framework [81].

Model Predictive Control with Control Barrier Functions: The well-known MPC is available for the tracking problems of a large class of nonlinear systems and has attracted lots of concentrations in the fields of CBFs. The main operation of MPC with CBFs usually converts barrier constraints into the cost function instead of the safety-critical control [82]. The discrete-time CBFs were presented to ensure system safety, where MPC was utilized for optimal performance [83]. In [84], a multi-layered locomotion framework was proposed for the safe motion of legged robots by unifying CBFs with MPC. However, the safety verification of CBFs heavily relies on a precise model, leading the conservative safety behavior. In the presence of uncertainties, the systems may take unsafe action, which is unacceptable with the principle of safety first.

Confracfion analysis: Contraction analysis is a universal tool for studying the stability of nonlinear systems, specialized in analyzing the convergence between any feasible solutions [85]. A constructive control technique using the contraction analysis can be found in [86], which develops an optimization-based control framework by solving the off-line control contraction metric (CCM). Then, the control can be constructed from a real-time calculation of geodesics. Recently, a few of the literature have taken advantage of CCM to solve problems in motion plans, accomplishing several tubes. Certified trajectory tracking methods [87]-[89]. Such tube-certified methods are inspired by model predictive control tubes [90], but utilize fewer computational resources than model predictive control. In addition, those tubes are extremely useful to assist collision-free path planning while there exist uncertainties in control systems.

2.2.4 UAV flight planning

The flight planning of UAVs in a construction environment is a typical motion task, generally speaking, investigating how to make UAVs move to a goal placement by applying comfortable force over avoiding some unsafe factors like obstacles, collision, and unsteady flight. The current research can be attributed to the control area, given a feasible trajectory that connects the final goal and initial goal in the building environment. Besides, the resulting trajectory must be dynamically feasible for the positions and orientations of UAVs. Before discussing flight planning, we must clarify some concepts to distinguish general terms among path, trajectory, and motion planning. In addition, there is a strong request to introduce the configuration space of UAVs, which is a space consisting of all possible points of UAVs [91]. The normal definition can be applied to most robot systems: one UAV has six degrees of freedom, also called the dimension of the UAV's configuration space Q = IR'. Then, explain the path planning problem and claim it is to find a path satisfying (a) : [0 1] - Q, while many effective algorithms have sufficiently studied it during the last decades.

The most classical method. The variational method intuitively explains how to get the shortest path in a local area if the optimizing cost function that has a finite-dimensional vector can be solved through nonlinear continuous optimization techniques. In order to shorting and smooth the path UAY used, a variational method was applied to the artificial potential field by considering to reconstructed optimization problem that combines additional force, solving the dead point problem [92] approach solved path planning problem was proposed for large degree serial manipulators by variational principle, represented moving total joint in configuration s.pace by constrained minimization of a functional [93]. However, it is easier to find the global optimal solution if the initial guesses are appropriate. Several papers concentrate on the graph search method, where the configuration space was discredited and viewed as a graph whose vertices and edges can represent most information in such configuration space. Based on the graph search framework, Liu and Li [94] used a tangent intersection and target guidance strategy to generate autonomous path planning that enables UAVs to avoid obstacles and reach the target; Li and Chen et al. [95] proposed improved rapidly-exploring random tree to address the path planning problem of narrow passages; Economouand Kladis et al., [96] presented to use 4-zone strategy using Dijkstras Algorithm to solve UAV path planning process with on-board UAV energy constraints; Yan and Fei et al., [97] introduced random sampling in 3D space UAV worked into probabilistic roadmap method for guaranteeing safety requirements of planned path. Bai. Xiong et al., [98] improved the A* algorithm. They combined it with the dynamic window approach f, which constructs a globally optimal path by adapting the evaluation function for the UAV's safety threshold obstacles — and environment information. Although the graph-based method can address the local convergence problem of path planning, the optimization space can still be limited to a finite set of paths.

Another extremely important research is about the planning for trajectory, especially in some scenarios the traditional path planning is unavailable in a dynamic environment [99]. Trajectory planning is similar to finding a trajectory rather than a path in the configuration, which can be defined by a time-parametrized function*(t) : [0 T] - Q prescribing the dynamic process of the vehicle's configuration. It has been shown that the relationship between path form and trajectory form can be mutually converted once a path planning algorithm can handle differential constrain. This operation copes with path planning in a configuration with an added time dimension. However, directly utilizing numerical methods to solve trajectory planning is a more popular choice because some tractable path planning algorithms sometimes cause more complexities for nontrivial trajectory planning.

In trajectory optimization, the usual recognition to clarify solving trajectory optimization problems is to distinguish it by direct and indirect methods. That is, for a cost function of that problem, the process takes firstly discretization or firstly optimization, where the previous one requires the discrete state point should collocate to the approximate trajectory that satisfies some constraints, and the latest one requires a better initialization for constructing the necessary and sufficient conditions of optimization problem [100]. Benefiting from the advantage of being easier to pose and solve, the direct method has been extensively investigated in recent decades. An algorithm of trajectory generation based on the direct method was applied to a UAV to provide the maximum sensor coverage time [101]. In order to achieve the flighting of a solar-powered UAV during longer periods, a method was provided to produce an appropriate trajectory for that UAV under a wind field, which applied a direct method to solve the optimal energy path [102]. An interpolating global radial basis function combined with the direct method was provided to solve a nonlinear programming problem that discretized from a continuous-time optimal control problem [103]. However, the cost of obtaining a convenience calculation must be more accurate to solve the optimization problem. The indirect method was an advisable choice to get the trajectory to improve the accuracy. An algorithm based on Pontryagin-s minimum principle was presented to find a trajectory that gave a quadrotor UAV a maximum payload to solve the problem of transporting a cable-suspended load [104]. An indirect projected gradient method was applied to solve optimal control problems for addressing the problem of energy-optimal trajectories of planner quadrotors, where an accurate electrical model of the brushless DC motors and the rest-to-remanoeuvresers were considered [105]. Although the above papers have contributed to the trajectory planning for UAVs in various tasks, it is still challenging to form an effective trajectory planner if UAVs face the indoor flighting environment. In such cases, rotorcraft UAVs that are more flexible than fixed UAVs are more likely to be adopted and pose higher requirements for indoor trajectory planning.

2.2.5 Summary

This part provides a comprehensive overview of recent advancements in UAV flight control algorithms, emphasizing their importance in managing the nonlinear dynamics and uncertainties inherent in UAV operations. It highlights various adaptive control strategies, including robust adaptive algorithms, machine learning-based controls, and deep reinforcement learning, which enhance UAV stability, autonomy, and energy efficiency in diverse environments. The chapter also explores the specific control systems for fixed-wing UAVs, discussing the evolution from basic PID controllers to sophisticated Model Predictive Control (MPC) and adaptive control systems. Furthermore, it introduces control barrier functions (CBFs) and their integration with Model Predictive Control for ensuring safety and stability in UAV operations. Finally, the chapter delves into flight planning and trajectory optimization, underscoring the significance of advanced algorithms in navigating complex and dynamic construction environments. Despite the progress, challenges such as computational limitations and ensuring safety and reliability remain, pointing to future research directions in energy-efficient AI algorithms and hybrid control approaches.

2.3 Research on related technologies of drones in construction waste recycling

2.3.1 UAV localization and detection scanning

Localization is crucial for UAVs as precise position data is necessary for stable hovering and trajectory following. The objective of localization is to estimate the 6-DOF (Degrees of Freedom) vehicle state, encompassing three positional DOFs (x, y, z) and three orientation DOFs (yaw, pitch, roll) [106]. Localization can be integrated with mapping, forming a SLAM problem where both the vehicle state and the environmental map are estimated [107].

Typically, localization for outdoor UAV applications is resolved using the Global Navigation Satellite System (GNSS), which provides position data without cumulative drifts. However, in GNSS-denied environments like indoor facilities, alternative sensory systems are required for localization and mapping [108]. Indoor localization techniques are essential when global signals such as GPS are unreliable [109, 110]. According to Ibrahim and Moselhi (2016) [111], indoor localization methods fall into three main categories:

Wave characteristics and propagation: Various waves and receivers, including radio frequency (RF), ultra-wideband (UWB), and wireless local area network (WLAN), are employed for indoor localization [109, 112, 113]. While ultrasound waves offer an accuracy of 9 cm, they need direct and interference-free access to objects. Techniques like UWB and RFID report accuracies of 5-9 m, which may not suffice for high-precision applications. Such systems are generally used for sensing and roughly locating materials in warehouses and other indoor environments.

Image-based/vision-based localization: This method employs computer vision to identify object locations within the global coordinate system. Image-based localization is divided into global feature detection (e.g., edge and corner detection) and local feature detection (e.g., fiducial tag and marker detection). The effectiveness of this approach can be hampered by dynamically changing environments and marker deterioration over the project lifecycle. Nevertheless, simultaneous localization and mapping (SLAM) remains reliable for indoor localization and mapping [114].

Inertial navigation systems: This approach involves using onboard accelerometers, inertia measurement units (IMUs), and other motion sensors for indoor localization, given an initial location. Inertial navigation and IMU-based localization may drift from actual measurements if motion components are not updated appropriately as movement progresses. Ibrahim and Moselhi [111] proposed an IMU-based localization technique combined with a Kalman filter, which proved more accurate than wave-based methods. However, relying solely on IMUs for UAV navigation can be hazardous, leading to potential loss of control and collisions. SLAM [114] can also be used with IMUs or other motion sensors to facilitate localization, making the processing less computationally demanding and closer to real-time.

2.3.2 Real-time target detection

Ren et al. [113] introduced a Region Proposal Network (RPN) that shares full-image convolutional features with the detection network, enabling nearly cost-free region proposals. An RPN is a fully convolutional network that predicts object bounds and scores simultaneously at each position. It is trained end-to-end to generate high-quality region proposals used by Fast R-CNN (Region proposals-Convolutional Neural Networks) for detection. The deepening of the detection task with the RPN network marked the success of Faster R-CNN. The sliding window method for generating anchor boxes, used in later works like YOLO v2, was also inspired by this approach [116]. Ren et al. [115] established the two-stage method structure "RPN+RCNN," influencing subsequent research. Although Faster RCNN offers higher accuracy and speed and is close to real-time performance, it still exhibits computational redundancy during detection.

Lin et al. [117] proposed Feature Pyramid Networks (FPN) based on Faster RCNN. Before FPN, detection heads were typically located at the network's deepest layer. While deep features are rich in semantic information, which aids object classification, they lack spatial information, affecting positioning accuracy. FPN addresses this by introducing a top-down architecture with horizontal connections, ensuring high-level semantic information at all levels. This innovation significantly improved detection network accuracy.

One-stage detection algorithms, unlike the two-stage approach, do not require a region proposal stage. They directly generate object category probabilities and position coordinates, resulting in faster detection speeds.

YOLO v1 [118] was the first deep learning detection algorithm designed for speed. It divides images into multiple grids, predicting bounding boxes and corresponding probabilities for each grid cell. If a target's center falls within a grid cell, that cell predicts the target's location and category. YOLO v1 achieves real-time performance with the VOC-07 dataset at 155 fps and an mAP of 52.7%, with improved versions performing even better (VOC-07 mAP=63.4%, 45 fps; VOC-12 mAP=57.9%). Despite its speed, YOLO v1's accuracy is lower than two-stage algorithms.

YOLO v2 [119] improved accuracy, speed, and classification capabilities over YOLO v1. It used DarkNet19 for feature extraction, faster than VGG-16 used in YOLO v1. Combining target classification and detection techniques expanded YOLO v2's detection types. On the VOC 2007 dataset, YOLO v2 achieved 67 FPS with an mAP of 76.8 (40 FPS, mAP=78.6). However, YOLO v2's single detection branch and lack of multi-scale context capture affected performance, particularly for small targets.

YOLO v3 [120] further enhanced the architecture by replacing the feature extraction network with DarkNet53, switching Softmax to Logistic for classification, and using three branches for detecting different-sized objects. On the VOC dataset, YOLO v3 reached 20FPS on Titan X, with an mAP@0.5 of 57.9% on the COCO test dataset. Although YOLO v3's accuracy rivals Faster RCNN and outperforms SSD, its speed is at least twice that of SSD, RetinaNet, and Faster RCNN, with the simplified YOLOv3 tiny being even faster.

2.3.3 Improved treatment of construction waste

The recycling of construction waste is an integral part of the overall waste management strategy, and waste management is costly for construction companies as it requires personnel, equipment, and efficient methods of operation [121]. Currently, the successful and mainly used method of assessment in the construction industry relies on human intervention, which requires waste sorting, and constant inspection of the contents of construction site waste bins [122]. This method is costly for both construction companies and their clients, who end up bearing these unnecessary costs [123]. The literature shows that waste management in the construction industry has attracted the attention of many researchers. Bao et al. [124] reported on the barriers and facilitators of implementing on-site construction waste recycling in Hong Kong. Unlike the current traditional recycling method in which construction waste is transported to off-site facilities for processing, construction managers and related researchers are actively exploring the possibility of on-site recycling where treating construction waste directly at the source. Several improvements were proposed including the development of customized on-site recycling equipment. Ali et al. [125] mentioned that construction waste is inevitably generated under any circumstances, and their disposal is always a threat to managers. Additionally, their study developed a conceptual framework for an effective construction waste management system (EMS) by applying artificial intelligence (AI). Davis et al. [119] designed and described a deep convolutional neural network (CNN) for on-site construction waste classification using techniques that automatically identify different materials. Their study argued that the use of automatic classification of construction waste on construction sites would improve productivity, reduce the cost of construction projects, and promote the reuse of construction waste to provide environmental benefits.

2.4 Summary and research gaps

This chapter provides a comprehensive overview of the integration of unmanned aerial vehicles (UAVs) and related technologies in the construction industry, emphasizing advances, applications, and challenges. It highlights the significant contributions of UAVs in data collection, real-time monitoring, and improving worker safety through advanced sensors and machine learning algorithms. The synergistic use of UAVs with Building Information Modeling (BIM) is discussed, highlighting improvements in project visualization and decision-making. The chapter also covers the evolution of UAV flight control algorithms, from basic PID controllers to sophisticated adaptive and AI-enhanced systems, as well as the integration of control barrier functions and model predictive control for safety and stability. It also addresses the complexities of UAV localization and target detection, particularly in GNSS-denied environments, and explores various methods, including image-based and inertial navigation systems. Finally, the chapter reviews the challenges and advances in construction waste management, highlighting the role of UAVs and AI in improving efficiency and sustainability. To better understand the application of UAV technology in the construction industry, it is essential to analyze its technical background and the challenges it faces. The integration of UAV technology in construction management requires seamless interfacing with existing management software systems, while also overcoming specific challenges in construction environments, such as complex spatial layouts and variable weather conditions.

Furthermore, it is necessary to explore improvements in navigation and obstacle avoidance technologies for UAVs on construction sites to enhance operational efficiency and safety.

According to above analysis, the research gaps are identified as below.

1) There exists a lack of enhanced flight obstacle avoidance and autonomous navigation capabilities of drones, especially for complex indoor construction environments.

2) There lacks a flight simulation platforms to validate algorithms in the construction environment.

3) There is a lack of a fully automated on-site recycling collaborative system that can more effectively handle various types of construction waste.

4) There lacks field experimental data on drones in indoor construction environments.

Chapter 3. Research design

3.1 Introduction

The objective of this thesis is to improve the UAV flight control algorithm to enhance its adaptability(Obstacle avoidance, re-planning, etc.) to complex indoor construction environments, and to develop a collaborative framework for construction waste recycling that can efficiently and automatically inspect construction sites, detect and automatically pick up construction waste. This will improve the efficiency and recycling rate of construction waste and verify the results of the improved flight control algorithm through field experiments. To address these issues, this study employs a quantitative analysis approach so that the authors can measure and statistically evaluate the effectiveness of the flight control algorithms and the effectiveness of the collaborative framework efforts.

In order to achieve the established research goals, this study focuses on the design, development, and verification of UAV flight control algorithms and collaboration frameworks. This chapter is divided into two parts: 1) Research framework 2) Research methodology.

3.2 Research framework

This research is mainly divided into two parts, the first part is the flight control system, and the second part is the collaborative framework system.

The main purpose of the flight control system is to complete the mobile task of the drone in the indoor construction environment, including the full coverage path planning of the drone and the real-time positioning system of the drone. Therefore, starting from a fixed-wing UAV with the same flight control system but a simpler architecture, we first tried to optimize the flight control algorithm of this type of UAV, and obtained corresponding results. A safety-critical motion planning system for a planar quadcopter UAV system was subsequently optimized. Finally, the algorithm results were verified through the development of flight simulation software. The verification results show that the new flight control algorithm can enable the UAV to have an obstacle avoidance path with smaller disturbance error than before when facing various complex movable obstacles, and can make real-time supplementary modifications to the path.

The collaborative framework system is an important part of realizing drone applications. This study first collects image data of target construction waste, processes it, and then identifies different types of construction waste through a computer vision system. At the same time, in order to enable ground robots to successfully determine detailed positions, this study uses UAVs equipped with new flight control algorithms as detection support, using a wider aerial view as the first step in target detection and target positioning. Finally, based on the above research, this thesis proposes an innovative picking scheme that can successfully pick up construction waste of different types and shapes. In order to verify the practical feasibility of the robot-drone collaboration framework developed in this study, this study conducted a series of experiments, including laboratory experiments and organized field experiments. The field experiment also further verified the feasibility of the developed UAV flight control algorithm.

3.3 Research method

3.3.1 Data Collection Methods

This study involves a variety of data sources, including literature data, laboratory experimental data, and field experimental data. In order to verify the feasibility of the collaborative system, laboratory experiments and field experiments are usually organized, and test data are collected by cameras. Details of the literature and experimental data are given below:

In this study, the literature review is conducted by retrieving relevant background knowledge for specific keywords, including fixed-wing UAV flight control algorithms, planar multi-rotor UAV flight control algorithms, pre-existing applications of architectural robots and UAVs, path planning, synchronized localization, and computer vision. Most of the data is obtained from academic journals and books. The experiments were the atmosphere simulation experiment and the field test as described above.

3.3.2 Data Analysis Methods

Data processing and data analysis were performed throughout the experiment. We checked the validity of the data before the analysis, and deleted the data that could affect the experimental results before each experiment. Data analysis in this study included not only the evaluation of experimental results, but also the comparative evaluation of experimental results under different conditions.

3.4 Chapter summary

This chapter has briefly described the general research framework of this study, as well as the data collection and analysis methods used to empirically test the framework. In order to have a more comprehensive understanding of existing related technologies, this study conducted a multifaceted literature review. At the same time, this study employs a variety of experimental methods to validate the feasibility of the flight control algorithm and the collaboration framework.

Chapter 4. Improvement of Attitude Control System for Fix-Wing Aircraft

This chapter introduces a controller using sum of squares programming for attitude control of fixed-wing aircraft. According to the previous article, the flight control system of fixed-wing UAVs is relatively simple compared to the flight control algorithm of multi-rotor UAVs, so this is the first step to improve the flight control algorithm. First, the vehicle state space form of the controller is designed to achieve the desired attitude tracking performance by solving the contraction control metric associated with the linearized region near the equilibrium point. Finally, the effectiveness of the control algorithm was verified through comparative simulation experiments.

4.1 Introduction

The design of the attitude controller of the aircraft system is a classic problem as old as the aircraft itself [126]. Many aircraft of current interest are fixed-wing in the military field [127]. Traditional PID control which has a mature method for adjusting proportional, integral, and differential parameters widely used in aircraft attitude control . Modern control theory includes dynamic inverse control [128, 129], sliding mode control [130–132], fuzzy control [133], back stepping [134–136], model predictive control [137, 138], linear quadratic optimal Control [139, 140], have also been introduced into attitude control and achieved good results. Whether classical control theory or the modern control theory mentioned above, it's not to stabilize attitude systems over their maximal basin of attraction by a generally applicable method. Briefly, the motivation of this chapter is to extend a general control method to fixed-wing attitude control for more precise tracking.

One recent approach called contraction control metric in [141] is used to design a controller based on optimization-based methods. It generates controllers that solve by sum-of-squares theory and has benefits of tractability beyond verifying a basin of attraction, that is, just by setting two suitable parameters and proving the existence of a square sum polynomial, an outstanding performance controller can be provided, it will be revealed in Section 4.3.

This chapter focuses on the converge problem that the given reference attitude can be tracked at any initial conditions by using straight-line geodesic optimal principles. In particular, it is easy to obtain a simplified constant-coefficient inequality constraint by linearization, which has an advantage for avoiding the complicated geodesic calculation problems caused by multivariable and multidimensional systems.

Based on the aforementioned discussion, precise attitude control for fixed-wing air vehicles using contraction control metric is practically necessary, but yet challenging so far when real-time geodesic calculation for complex attitude systems. Contributions of this chapter are the following: 1) In the framework of contraction theory, avoiding complex computation of geodesics due to the metric used for a linearized fixed-wing attitude model. 2) An outstanding control effect that unifying attitude trajectory to the equilibrium point was achieved by using the square sum programming technology.

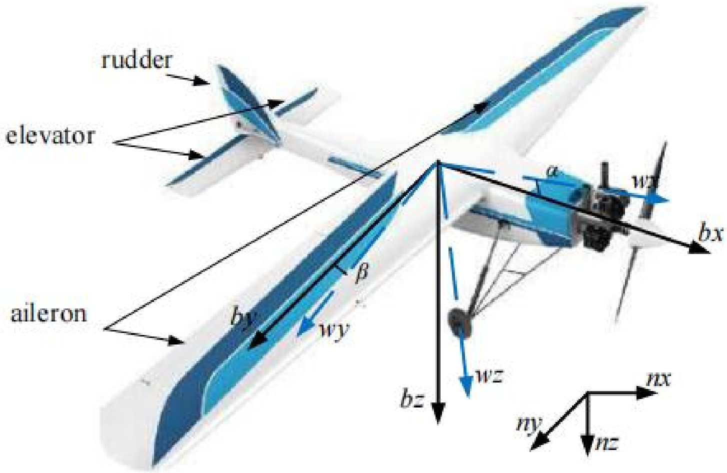

Fig. 4.1. The vehicle's configurations and coordinates.

4.2 Attitude system of the fixed-wings air vehicle

The vehicle attitude motion has three degrees of freedom about its centroid, which includes pitch, roll and yaw motion. The vehicle's configuration shown in Fig.4.1 permits the pitch torque and the roll torque to be produced by ailerons and elevators, the yaw torque to be produced by the rudder. The navigation frame, the body-fixed frame and the wind frame are shown in Fig.4.1 by the letters n, b, and w, respectively. The equations concern the angle of attack α and the side slip angle β are as follows:

$$\dot{\alpha} = q + \frac{\kappa V_T S C_{Z\alpha}}{2m}, \quad \dot{\beta} =- r + \frac{\kappa V_T S C_{Yl}}{2m}\beta,$$

where m is the quality of the vehicle, the remaining parameters are described below. Considering the roll, pitch, and yaw attitude angles of the vehicle relative to the inertial coordinate system are represented by Euler angles ϕ, θ and ψ respectively. The angular velocity of the vehicle relative to the body coordinate system is represented by p q and r respectively. The relationship between these variables is as follows:

$$[p \quad q \quad r]^T = \mathbf{C}_n^b[\dot{\varphi} \quad \dot{\theta} \quad \dot{\psi}]^T,$$

where C_n^{b} is the rotation matrix from the inertial coordinate system to the body coordinate system, expressed as follows:

$$\mathbf{C}_n^b = \begin{bmatrix} 1 & 0 & -\sin\theta \\ 0 & \cos\varphi & \sin\varphi\cos\theta \\ 0 & -\sin\varphi & \cos\varphi\cos\theta \end{bmatrix}.$$

According to Newtonian mechanics, the dynamic equation of the vehicle's attitude system can be deduced as:

$$\dot{\Omega} = \left(\mathbf{I}^b\right)^{-1}\left(\mathbf{M}^b - \Omega \times \left(\mathbf{I}^b \cdot \Omega^b\right)\right), \tag{1}$$

where $\mathbf{I^b}$ is the inertia matrix of the vehicle

$$\mathbf{M}^b = \begin{bmatrix} \bar{q}SbC_L \\ \bar{q}SbC_M \\ \bar{q}SbC_N \end{bmatrix}, \mathbf{I}^b = \begin{bmatrix} I_{xx} & 0 & I_{xz} \\ 0 & I_{yy} & 0 \\ I_{zx} & 0 & I_{zz} \end{bmatrix},$$

where $q^{-} = \rho VT2/2$ is dynamic pressure, VT is airspeed, ρ is air density, S is wings surface, b is wingspan, c^{-} is mean aerodynamic chord, vehicle roll $CL = CLa1\sigma\alpha1$ $+CLa2\sigma\alpha2 + CLe1\sigma e1 + CLe2\sigma e2 + CL\beta\beta + CLp\tilde{}p\tilde{} + CLr\tilde{}r\tilde{}$, pitch $CM = CM\,l\sigma\alpha1 +$ $CMe1\sigma e1 + CMe2\sigma e2 + CM\alpha1\sigma\alpha1 + CM\alpha2\sigma\alpha2 + CMq\tilde{}q\tilde{} + CM\alpha\ \alpha$, and yaw $CN =$ $CN\sigma r\ \sigma r + CNr\tilde{} + CN\beta\beta$, where the coefficient similar to the structure of $C(\cdot)(\cdot)$ are shown in Tab I. $\sigma\alpha1$ and $\sigma\alpha2$ are the left and right aileron's deflection, respectively.

$\sigma e1$ and $\sigma e2$ are the left and right elevator's deflection, respectively. σr is the rudder's deflection.

The dimensionless angular rates is defined as $p\tilde{} = bp/2VT$, $q\tilde{} = c\bar{}q/2VT$ and $r\tilde{} = br/2VT$. Let $x = [p, q, r]T$ and $u = [\sigma\alpha 1, \sigma\alpha 2, \sigma e1, \sigma e2, \sigma r]^T$. The state space model of (1) can be derived as:

$$\dot{x} =- f(x, - t) + B(x, - t)u. \tag{2}$$

Note that equation (2) is the nominal model of the vehicle's attitude system, that is, the vehicle model without model uncertainty.

$$f(x,t) = \begin{bmatrix} \frac{I_{zz}Sb^2C_{L\bar{p}}}{2D_1V_T}p - \frac{N_1}{D_1}qp + \frac{-N_1p + N_2r}{D_1}q + \frac{(I_{zz}C_{L\bar{r}} - IxzC_{N\bar{r}})sb^2\tilde{q}}{2D_1V_T}r + \frac{N_2q}{D_1}r \\ \frac{(I_{xx} - Izz)r - 2I_{zx}p}{I_{\mathrm{y}}}p + \frac{S\tilde{c}^2C_{M\bar{q}}\tilde{q}}{2V_{\mathrm{y}}I_{\mathrm{y}}\mathrm{y}}q + \frac{-(I_{xx} - Izz)p - 2Ixzr}{I_{\mathrm{yy}}}r \\ -\frac{I_{xz}Sb^2C_{L\bar{p}}\tilde{q}}{2D_1V_T}p - \frac{N_3}{D_1}qp + \frac{N_3p + N_1r}{D_1}q + \frac{\left(I_{xx}C_{N\bar{r}} - lx\xi C_{L\bar{p}}\right)sb^2\tilde{q}}{2D_1V_T}r + \frac{N_1q}{D_1}r \end{bmatrix}$$

$$\mathrm{A} = \begin{bmatrix} \frac{I_{zz}Sb^2C_{L\tilde{p}}}{2D_1V_T} & 0 & \frac{(I_{z\bar{z}}C_{L\tilde{r}} - IxzC_{N\tilde{r}})sb^2\tilde{q}}{2D_1V_T} \\ 0 & \frac{S\bar{c}^2C_{M\tilde{q}}\tilde{q}}{2V_TI_y\mathrm{y}} & 0 \\ -\frac{I_{x\bar{z}}Sb^2C_{L\tilde{p}}\tilde{q}}{2D_1V_T} & 0 & \frac{(I_{x\bar{x}}C_{N\tilde{r}} - Ix\bar{z}C_{L\tilde{r}})sb^2\tilde{q}}{2D_1V_T} \end{bmatrix}$$

$$B(x,t) = \begin{bmatrix} \frac{I_{zz}SbC_{La1}}{D_1} & \frac{I_{zz}SbC_{La2}}{D_1} & \frac{I_{zz}SbC_{Le1}}{D_1} & \frac{I_{zz}SbC_{Le2}}{D_1} & \frac{-I_{zz}SbC_{N\delta r}}{D_1} \\ \frac{SC_{Ma1}}{D_1} & \frac{SC_{Ma2}}{D_1} & \frac{SC_{Me1}}{D_1} & \frac{SC_{Me2}}{I_{yy}} & 0 \\ \frac{-I_{xz}SbC_{La1}}{D_1} & \frac{-I_{xz}SbC_{La2}}{D_1} & \frac{-I_{xz}SbC_{Le1}}{D_1} & \frac{-I_{xz}SbC_{Le2}}{D_1} & \frac{-I_{Xx}SbC_{N\delta r}}{D_1} \end{bmatrix}$$

where $N_1 = I_{xz}\left(I_{xx} - I_{yy} + I_{zz}\right), N \quad V_2 = I_{\mathrm{yy}}I_{zz} - I_{xz}^2 - I_{zz}^2, N_3 = I_{xz}^2 - I_{xx}I_{yy} + I_{xx}^2, D_1 = I_{xx}I_{zz} - I_{xz}^2$

4.3 Controller design

Given a smooth nonlinear dynamic system (2) and a smooth manifold M with each $x \in M$. Let $\Gamma(a, b)$ be a set of piecewise-smooth paths between two points a and b in M, for each curve $c \in \Gamma(a, b)$ satisfying $c(0) = a$ and $c(1) = b$, the time-derivatives of each path are defined as

$$\dot{C}(s) = f(c(s,t),t) + B(c(s,t),s)u(s,t),$$

where a feedback law $v(s,t) = k(c(s,t),t) \in \mathcal{U} \subseteq \mathcal{M}$, an infinitesimal displacement is defined in the tangent bundle of M with $\delta x = \frac{\partial c}{\partial s} \in \mathcal{T}_x\mathcal{M}$ and $\delta u = \frac{\partial k}{\partial c}\frac{\partial c}{\partial s} \in T_u\mathcal{U} \subseteq T_x\mathcal{M}$ at a fixed time [142], the tangent vectors $c_s = \frac{\partial c}{\partial s}$ obey

$$\dot{c}_s = \frac{\partial f(c,t)}{\partial c} c_s + \sum_{j=1}^{m} \frac{\partial b_j}{\partial c} u_j + B(c,t)v_s,$$

where b_j denotes the j^{th} column of B(x, t) and u_j denotes the j^{th} element of u. Consider all the point x of all c in $\mathcal{M}$, each δx also obeys

$$\delta_{\dot{x}(t)} = \frac{\partial f(x,t)}{\partial x}\delta_{x(t)} + \sum_{j=1}^{m} \frac{\partial b_j}{\partial x} u_j + B(x,t)\delta_u. \tag{3}$$

Definition 1: A symmetric and uniformly positive definite matrix $G(x, t)$[1] is called a contraction matrix and a constant β is called a contraction rate if there exist the inequality

$$\frac{d}{dt}\langle \delta_x, \delta_x \rangle_G \leq -\beta \langle \delta_x, \delta_x \rangle_G.$$

Lemma 1 [141]: For a control system of the form (2), if $\delta x \neq 0$ satisfies $\delta_x^T G B = 0$, then

$$
\begin{aligned}
\frac{d}{dt}\langle\delta_x,\delta_x\rangle_G \quad &= \delta_x^T(\frac{\partial G}{\partial x}\cdot(f(x,t)+B(x,t)u) \\
&+ \frac{\partial(f(x,t)+B(x,t)u)}{\partial x}^T G \\
&+ G\frac{\partial(f(x,t)+B(x,t)u)}{\partial x})\delta_x <-\beta\langle\delta_x,\delta_x\rangle_G.
\end{aligned}
$$

and for each $j=1,2,\dots,m,\left(\frac{\partial b_j}{\partial x}\right)^T G+G\frac{\partial b_j}{\partial x}+\frac{\partial G}{\partial x}\cdot b_j=0$, then the system (2) can be stabilized on the given trajectory with rate β, such a metric is referred to as a *control contraction metric* (CCM).

Definition 2 [143]: Polynomials $p(x_1,x_2,\dots,x_n)\triangleq p(x)$ are called sum of square polynomials , if there exists polynomials *h1 (x), h2 (x),..., hm (x)* satisfied

$$p(x)=\sum_{i=1}^{m}h_i^2\,(x).$$

It is easy to see that $p(x)\geq 0,\forall x\in\mathbb{R}^n$, which corresponds to global no-negative sufficient conditions for the sum-of-square (SOS) polynomials.

The detailed steps in the controller design of the fixed-wing UAV are as follows:

1. Linearize the attitude system at the equilibrium point, it yields

$$\dot{x}=Ax+Bu, \tag{4}$$

where $A=\frac{\partial}{\partial x}(f+Bu)\Big|_{x=0,u=0}, B=\frac{\partial}{\partial u}Bu\Big|_{x=0,u=0}$. Taking the incremental form for the linear system (4-4), it is easy to get

$$\delta_{\dot{x}}=A\delta_x+B\delta_u, \tag{5}$$

note that the linear time-varying system represent the differential dynamics at the equilibrium point.

2. Design a contraction feedback law that can stabilize the linear attitude system (4) by solving the CCM via sum-of-square polynomials theory, that is

$$-A^T G - GA - \dot{G} - \beta G + 2\kappa GBB^T G \in \Omega_{SOS}, \tag{6}$$

where $\alpha_1 I < G < \alpha_2 I, \alpha_1 \in \mathbb{R}^+, \alpha_2 \in \mathbb{R}^+, \kappa \in \mathbb{R}^+, \beta \in \mathbb{R}^+$, Ω_{SOS} denotes a SOS constraint with respect to the abstract variable in the argument.

The above conditions come from the closed-loop system formed by the designed contraction controller $\delta_u = -\kappa B^T G \delta_x$. Taking δ_u into (5), it yields

$$\delta_{\dot{x}} = A\delta_x - B\kappa B^T G \delta_x, \tag{7}$$

so the rate of change of $\langle \delta_x, \delta_x \rangle_G = \delta_x^T G \delta_x$ over t can be written as

$$\begin{aligned} \frac{d}{dt}\langle \delta_x, \delta_x \rangle_G = &\ \delta_{\dot{x}}^T G \delta_x + \delta_x^T G \delta_{\dot{x}} + \delta_x^T \dot{G} \delta_x \\ = &\ \delta_x^T (A^T - GB\kappa B^T) G \delta_x \\ &+ \delta_x^T G (A - B\kappa B^T G) \delta_x \\ &+ \delta_x^T \left(\frac{\partial G}{\partial x} \cdot (Ax + Bu) + \frac{\partial G}{\partial t} \right) \delta_x \\ = &\ \delta_x^T \left(A^T G + GA - 2\kappa GBB^T G + \dot{G} \right) \delta_x, \end{aligned}$$

where $\dot{G} = \frac{\partial G}{\partial x} \cdot (Ax + Bu) + \frac{\partial G}{\partial t}$. For each $j = 1, 2, \ldots, m$, we known that $\frac{\partial b_j}{\partial x} = 0$, hence a constant G which satisfied $\frac{\partial G}{\partial x} = 0$ would make

$$\left(\frac{\partial b_j}{\partial x} \right)^T G + G \frac{\partial b_j}{\partial x} + \frac{\partial G}{\partial x} \cdot b_j = 0.$$

By Lemma 1, we can find that any trajectory, which starts near the equilibrium point trajectory, converges to this trajectory via solving ΩSOS.

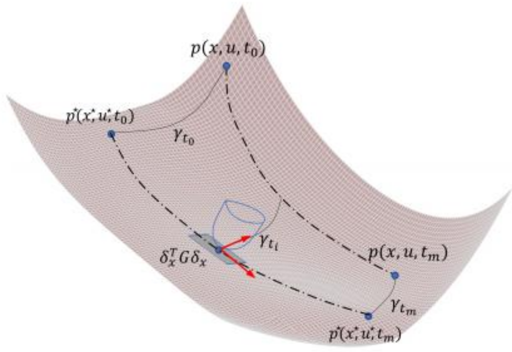

Fig. 4.2. Graphical interpretation of the solution.

3. Calculate the control signal along geodesic which connects the actual trajectory x and the given trajectory $x^{\star}$:

$$u(t) = u^{\star} + \kappa B^T G(x - x^{\star}).$$

The minimizing geodesic $\gamma(s)$ is related with the manifold M in which the dynamic (4). For each parameterized differentiable curve $c(s)$: $[0,\ 1] \rightarrow \mathcal{M}$, the minimizing geodesic is defined as

$$\gamma(s) = \operatorname*{argmin}_{c} \int_0^1 \left[\frac{\partial c(s)}{\partial s}^T G(c) \frac{\partial c(s)}{\partial s} \right] ds,$$

then to calculate γ through the variation of (8) when G is a constant metric, it can be obtained

$$-\frac{\partial}{\partial s}\frac{\partial c_s^T G c_s}{\partial c_s} + \frac{\partial c_s^T G c_s}{\partial c} = 0.$$

For the geodesic, it can be known that $\frac{\partial c_s^T G c_s}{\partial c} = 0$ and $c(\mathrm{s})$ is linear equation related s, let the parameterized form of this curve is $c(s) = \mathfrak{a}s + \mathfrak{b}$, according to the start point $s = 0 \Rightarrow c(0) = x^{\star}$ and the end point $s = 1 \Rightarrow c(1) = x$ it can be solved that

$$c(s) = xs + (1-s)x^{\star}, \tag{8}$$

which equivalents to the geodesic $\gamma(s) = xs + (1-s)x^{\star}$. As shown in Fig. 4.2, given a manifold $\mathcal{M}$, the tracking purpose is to unify a given trajectory (crossing point $p^{\star}$) with the actual trajectory (crossing point p) at t_i in which i denotes the continuous time point. The actual controller $u = k(x) + u^{\star}$ is the integral of the shortest geodesic γ at t_i , such that

$$\begin{aligned} \mathrm{u} &= u^{\star} + k(x, x^{\star}) = u^{\star} + \int_0^1 \delta_u \, ds \\ &= u^{\star} + \int_0^1 \kappa B^T G \delta_x ds \\ &= u^{\star} + \kappa B^T G(x - x^{\star}). \end{aligned}$$

(9)

Remark 1: To construct the actual control signal a, one of the critical tasks is geodesic calculations, an algorithm to calculate minimizing geodesics at each time step can be found in [144], the complicated calculations are avoided in this thesis since the linearization of the fixed-wing UAV model.

The fundamental process of the solution algorithm consists of alternating between the dynamics and metric derived from problem (6). The SOS programming is used for searching for the contraction metric online, which is flexible for inequality constraints. The full pseudo code is summarized below in Algorithm 1.

```
Algorithm 1: Simulation-solve controller
Data: Current period t, initial vehicles roll p, pitch q, and yaw r,
      given system trajectory x* , u* , matrix A and B ,
      parameters β , κ
Result: The feed back controller u(t)
  r - t;
  converged - false;
  ε - 0.01;
  while   r < T do
          G - Solve (6);
          u - Solve (8);
          x - Update p, q, r using (4);
          if Δ < ε then
             |     converged - True;
       end
          r - r + 1;
end
```

TABLE I PARAMETERS IN (2) [145] [146]

Term	Value	Umit	Term	Value	Unit
I_{xx}	2.56	$\mathrm{kg}\cdot\mathrm{m}^2$	$C_{L\beta}$	−0.087	/
I_{yy}	10.9	$\mathrm{kg}\cdot\mathrm{m}^2$	m	28	kg
I_{zz}	11.3	$\mathrm{kg}\cdot\mathrm{m}^2$	b	3.1	m
I_{xz}	0.5	$\mathrm{kg}\cdot\mathrm{m}^2$	$\bar{c}$	0.58	m
I_{zx}	0.5	$\mathrm{kg}\cdot\mathrm{m}^2$	$C_{N\beta}$	0.087	/
$C_{N\delta}$	0.053	/	ρ	1.29	$\mathrm{kg}\cdot\mathrm{m}^2$
S	1.8	m^2	V_T	15	m/s
$C_{M\alpha}$	−0.09	/	C_{LF}	0.036	/
$C_{L\bar{p}}$	−0.19	/	$C_{N\bar{p}}$	0.21	/
C_{Yl}	−0.38	/	$C_{L\alpha 1}$	−0.03	/
$C_{M\bar{q}}$	−9.83	/	$C_{L\alpha 2}$	−0.03	/
$C_{Z\alpha}$	−3.25	/	C_{Le1}	−0.05	/
C_{Me1}	0.272	/	C_{Le2}	−0.05	/
C_{Me2}	0.272	/	$C_{M\alpha 2}$	0.038	/
$C_{M\alpha 1}$	0.272	/			

4.4 Numerical simulation

The parameters of fixed-wing aircraft are shown in Tab. I. The initial state was set to $[p(0), q(0), r(0)]^T = [0.5, 1, 1.5]^T$. The desired tracking state was set to $p^* = 0$, $q^* = 0$, $r^* = 0$. The standard solution calculated by Matlab is $u^* = 0$.

Set $\beta = 10$ and the maximum order of the decision variable of SOS programming to 2. The amount of decision variables solved was 510. In order to illustrate the advantages of the proposed control method, comparing with the controller designed by the dynamic inverse control $u = B^{-1}((\dot{x} - \dot{x}_s) - a(x - x_s) - b\int(x - x_s)dt - f)$, where $a = 5$, $b = 5$ [144] and with the PID controller which has parameters $K_p = 15$, $K_i = 10$. In this simulation, a parameter error $0.1Ax$ is added to the model (2) to test robustness, noted that SC denotes the control method based on SOS polynomial and contraction theory, DI denotes the dynamic inverse control method, PID denotes the PID control.

As shown in Fig.4.3 to Fig.4.5, the close loop response of the yaw, pitch and roll angles has different for applying the above control methods. From figures its clear that system is achieving the reference input in very short time by PID, SC also finished the track tasks, followed by DI. It is worth noting that the DI controller has small error fluctuations, which may be caused by parameter errors. However, SC and PID of error fluctuations are not obvious, which shows that the SC method can handle small parameter errors to achieve robust tracking. Fig.4.6 indicates that the input signal is reliable, thus further illustrating the feasibility of the SC method.

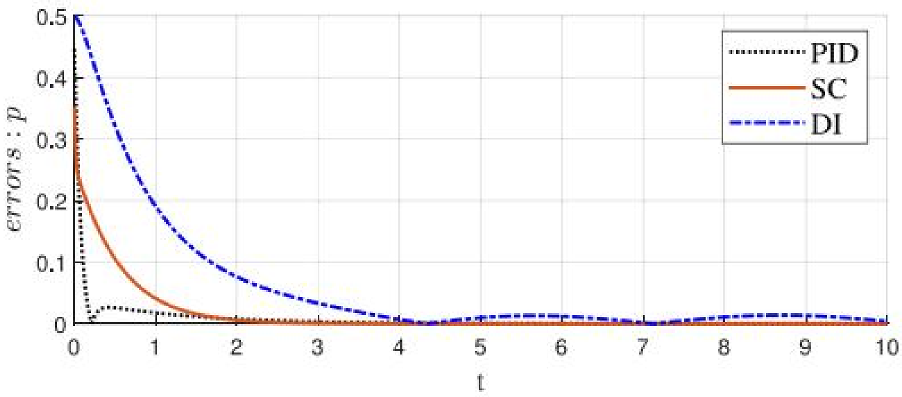

Fig. 4.3. The tracking and errors of p.

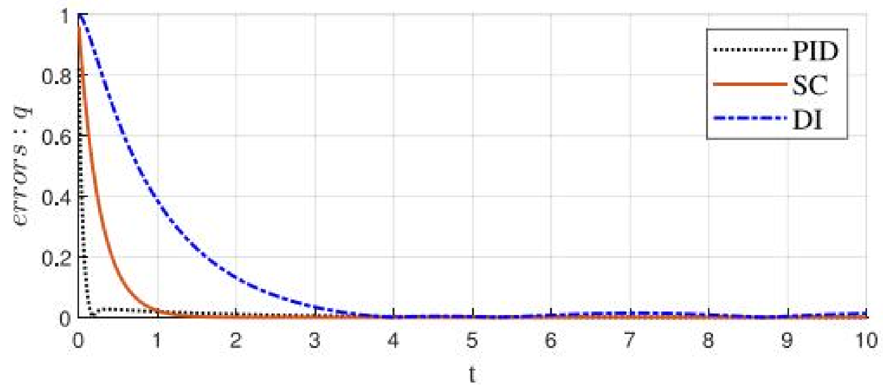

Fig. 4.4. The tracking and errors of q.

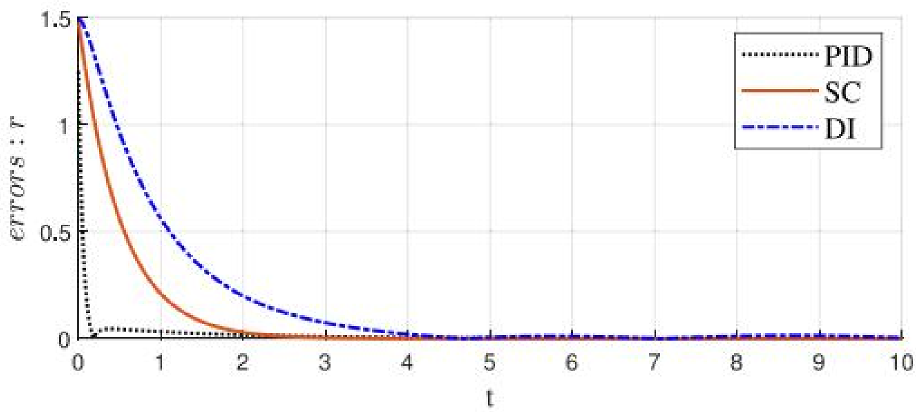

Fig. 4.5. The tracking and errors of r.

The Input with SC

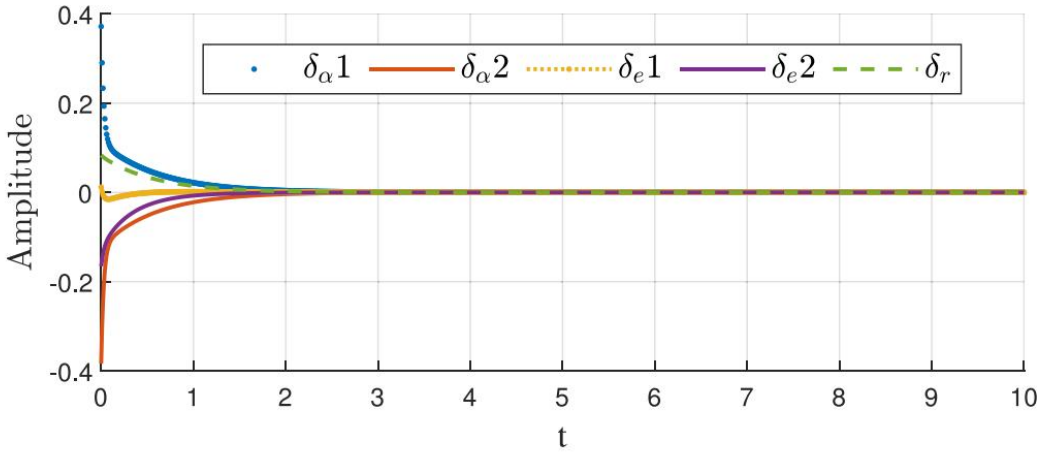

Fig. 4.6. The input uses SC method and DI method.

TABLE II Performance Comparison

Term	PID	SC	DI
Average Errors p_t>2	0.00125	0.00091	0.00916
Average Errors q_t>1	0.00174	0.00095	0.0085
Average Errors r_t>2	0.00206	0.00093	0.0071
Fast Coverage p	0.2s	2s	4s
Fast Coverage q	0.2s	1s	3.5s
Fast Coverage r	0.22s	2s	4s

Tab.II shows comparison result of fastest convergence time and average error after attitude stabilization. The average error of SC is the best in attitude tracking. PID has a faster convergence time $0.2s$ compared with SC $1s$, but the average error does not exceed 0.001 level. The DI controller has no advantage in convergence time and average tracking error.

Based on the comparison of the previous, in the case of a small model error, the SC control has a certain robustness and can obtain a small tracking error, which shows that the method in this chapter can achieve accurate attitude tracking of fixed-wing air vehicles. The tracking error can also be explained as the distance $[x - x^{\star}]^T G[x - x^{\star}]$

of the trajectory in Fig. 4.2, where $\delta x = x - x^{\star}$ since the case of constant metric produced straight line (8). When t > 3, γ of system (4) will appear very short on the manifold due to the fundamental properties of contraction theory.

4.5 Chapter summary

This chapter focuses on enhancing the attitude control system for fixed-wing UAVs by introducing a controller based on sum of squares (SOS) programming. Given the relatively simpler architecture of fixed-wing UAVs compared to multi-rotor UAVs, this chapter serves as the initial step in improving flight control algorithms. The local stability control of attitude system of fixed-wing air vehicles is often described by linear dynamics. In this chapter, the design of attitude controller for a fixed-wing air vehicle is presented by contraction metric and SOS programming. The linearization condition relaxes the calculation of CCM, that is, the geodesic of the nonlinear system is regarded as a straight line here, so a brief algorithm flow is presented, which is similar to the solving process of linear matrix inequality under the framework of contraction theory.

The newly designed controller utilizes a contraction control metric, which simplifies the computational process and ensures precise tracking of the desired attitude by solving a linearized region near the equilibrium point. Through comparative simulation experiments, the effectiveness of this control algorithm is validated, demonstrating superior performance in terms of robustness and tracking accuracy compared to traditional PID and dynamic inversion control methods.

The insights and methodologies developed in this chapter lay the groundwork for addressing more complex control challenges in UAV systems. Specifically, the successful application of SOS programming to enhance the stability and maneuverability of fixed-wing UAVs provides a robust foundation for the subsequent chapter, which will extend these concepts to multi-rotor UAVs. This progression from simpler to more complex systems ensures a comprehensive approach to optimizing UAV flight control in diverse and challenging environments, ultimately aiming to improve their operational efficiency and safety in indoor construction settings.

Chapter 5. Safety-Critical Contraction Tubes with Robust Barrier Functions For Unmanned aerial vehicles

After completing the fixed-wing flight control algorithm optimization in the previous chapter, this chapter addresses the safety-critical control issues of UAV systems subject to external interference. The proposed scheme can efficiently track any feasible nominal trajectory, creating safe and predictable tubes with fixed dimensions through robust control of contraction metrics. For added safety assurance within the tube, powerful barrier functions are utilized to avoid safety-critical restrictions. Additionally, this research proposes a robust barrier function with a relative degree of 1 or 2 to solve the robust security problem by ensuring that the defined security set is forward invariant. The method is validated using planar quadrotor and aircraft pitch dynamics, achieving the purpose of optimizing the flight control algorithm of multi-rotor UAVs.

5.1 Introduction

5.1.1 Motivation

The safety-critical motion planning of robotic systems is a challenging problem, particularly with uncertain interferences. Some investigations formulate this problem using a combination of control Lyapunov functions (CLFs) and control barrier functions. However, in nonlinear systems, it is difficult to determine such CLFs because nonlinear properties do not guarantee the existence of feasibility conditions. Advanced model predictive control (MPC) for nonlinear systems can solve these issues but requires large amounts of computing resources. High real-time requirements limit the applications of MPC in complex problems. This chapter addresses the above challenges for control-affine nonlinear systems using a hybrid of contraction analysis and barrier constraints, yielding dynamic robustness and reducing the conservativeness of safe sets. This result develops an efficient safety-critical control framework, unifying the provided robust control contraction metric and robust control barrier functions. Unlike the high expense of nonlinear MPC, this method handles uncertainties in safe sets effectively. We explain this by utilizing the contraction-based robust control invariant tube and unsafe regions (see Fig. 5.1 and Fig. 5.2), and demonstrate that the results can lead a planar quadrotor to safely complete motion tasks as well as simple aircraft dynamics.

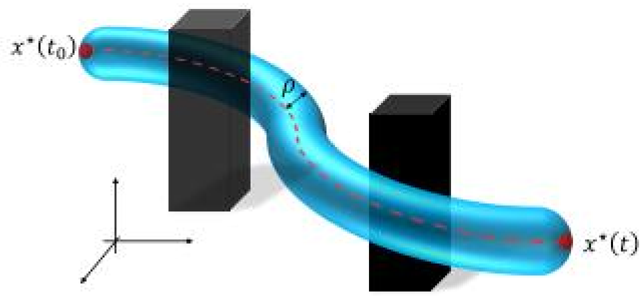

Fig. 5.1. The explanation of tube has been supposed systems is 3-degree state, where the read dotted line denotes a normal or given trajectory $x^{å}$, and the virtual tube denoted by the blue region around that has a ρ-norm ball.

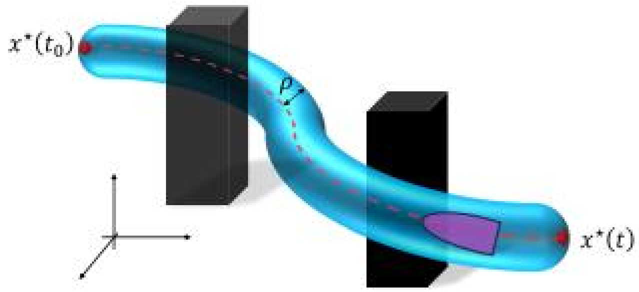

Fig. 5.2. The explanation of tube with a barrier has a barrier region compared to the tube in Fig. 5.1, where the purple region denotes unsafe set $h(x) < 0$ that has an intersection set with the virtual tube.

5.1.2 Contribution

To address the safety-critical control problem of a large class of control-affine nonlinear systems with uncertain disturbances, this chapter presents a safe controller based on contraction analysis and barrier constraints. By utilizing universal input-to-state L^{∞} gain theorem, the proposed stronger condition of robust contraction control metric produces predictable tubes that guarantee the robustness of a planned trajectory. In the control architecture, worst-case disturbances are considered in constructing metrics and robust control barrier functions, allowing for the safety certification of invariant sets inside such tubes despite existing uncertain disturbances. The quadratic program of provided robust control barrier functions can merge with the robust control contraction metric, which is more general than current safety-critical control using CLFs with control barrier functions, and is less expensive than MPC with control barrier functions. We verify the properties of our safety-critical tube using a planar quadrotor. The method is generally validated and also applicable in scenarios with multiple obstacles. Specifically, emergency situations involving obstacles that the path planner does not previously consider can be safely avoided.

Notations: Let $\mathbb{R}^n, \mathbb{R}^{n\times m}$ denote the n-dimensional real vector space, and the set of real n by m matrices, respectively. Let $\mathcal{M}$ denote a smooth manifold equipped with a Riemannian metric $M(x,t)$ that defines an inner product $\langle\cdot,\cdot\rangle$ on the tangent space $T_x\mathcal{M}$ at every point x. Let $\langle P\rangle$ denote the shorthand notation of $P+P$. Let $\|\cdot\|$ denotes the 2-norm of a vector or a matrix. The space of vector signals is denoted $\mathcal{L}^\infty$, where signals $\|x\|_{\mathcal{L}^\infty} := \sup_{t\geq 0}\|x(t)\|$ for each $x\in\mathcal{L}^\infty$. A continuous function $\gamma:[0,a)\to[0,\infty)$ is a class $\mathcal{K}$ function if it is strictly increasing and $\gamma(0)=0$. A continuous function $\beta:[0,a)\times[0,\infty]\to[0,\infty]$ is a class $\mathcal{KL}$ function if for each fixed s , the map $\beta(r,s)$ belongs to $\mathcal{K}$ with respect to r and for each fixed $r=0$. A continuous function $\alpha:(-b,c)\to(-\infty,\infty)$ is said to belong to extended class $\mathcal{K}$ for some $b>0, c>0$ if it is strictly increasing and $\alpha(0)=0$.

5.2 Problem description and preliminaries

5.2.1 Trajectory tracking and tube

Given a nonlinear control system, describe it as

$$\dot{x} = f(x,t) + B(x,t)u + D(x,t)w, \tag{1}$$

where the system state vector is $x(t)\in \mathbb{R}^{n}$, the system input is $u(t)\in \mathbb{R}^{m}$, function $f(x,t)\in \mathbb{R}^{n}, B(x,t)\in \mathbb{R}^{n\times m}$ and $D(x,t)\in \mathbb{R}^{n\times m}$ is known, and disturbances $w(t)\in \mathbb{R}^{m}$ is unknown. Consider the desired state x^{*}, desired input u^{*} and desired disturbance w^{*}, it satisfies

$$\dot{x}^{*}=f\left(x^{*},t\right)+B\left(x^{*},t\right)u^{*}+D\left(x^{*},t\right)w^{*} \tag{2}$$

where the desired disturbance is considered to be zero $\left(w^{*}=0\right)$ in the assumption of one ideal situation.

Reference [147] studied universal input-output stability by differential L^{2} gain and universal L^{∞} gain theorems respectively. In contrast, the definition applied universal input-to-state L^{∞} gain bounds give a more comprehensive analysis in robust control contraction metric, producing three methods to solve the involved metric (see formula (31) to (34)), and naturally creating a tube assisting nonlinear control systems to avoid unsafe factors.

Definition 1 A control system (1) achieves a universal input-tostate L^{∞}-gain bound of σ, if there is a KL function β and a feedback controller $u=k\left(x(t),x^{*}(t)\right)+u^{*}$ for any trajectory x^{*},u^{*},w^{*} satisfying nominal system (2), any initial condition $x(0)$, and disturbance w such that $w-w^{*}\in \mathrm{L}^{\infty}$,

$$\begin{aligned} x(t)-x^{*}(t)^{2} \leq \beta\left(\| x(t_{0})-x^{*}(t_{0}) \|^{2}, t-t_{0}\right) \\ +\sigma w(t)-w^{*}(t)_{\mathrm{L}^{\infty}}^{2} \end{aligned}$$

Another difference with the general L^{∞} gain is that the universal form of that presents a wide stable region instead of the equilibrium point, ensuring a convergence ball around x^{*}, while disturbances can also be viewed as input in most cases.

The following is about the virtual tube. A ρ -norm ball is consist of the system state, desired state and a positive scalar ρ , the Euclidean distance between $x(t)$ and $x^{\text{å}}(t)$ for all $t > 0$ has

$$\Omega\left(\rho, x^{*}(t)\right) := \left\{x(t) - x^{*}(t) \le \rho\right\}, \tag{3}$$

Definition 2 (Robust control invariant tube) If there exists a tracking controller $k\left(x, x^{\text{å}}\right)$ for each $x(t_0) \in \Omega\left(\tilde{n}, x^{\text{å}}(t_0)\right)$, then for all allowable realizations of the disturbance $w, x(t) \in \Omega\left(\tilde{n}, x^{\text{å}}(t)\right)$, we call $U_{t\ge 0}\Omega\left(\tilde{n}, x^{\text{å}}(t)\right)$ a robust control invariant tube centered on the trajectory $x^{\text{å}}(t)$.

The description of this virtual tube is also used in [148], and here, it can be simply illustrated in Fig. 5.1, where the black cubes represent some outside unsafe factors such as obstacles in a 3-D UAV's flying path. A similar property among them is helpfully improving control performance, in which system dynamics have modeling errors or external disturbances. Similarly, we give the definition of the tube for solving the invariant region problem around a given trajectory. Before discussing that, the following remarks about contraction theory are introduced because it describes the convergence of systems and tubes by the universal input-to-state L^{∞} gain and the energy degradation.

5.2.2 Remarks on Contraction

For a nonlinear dynamic systems

$$\dot{x} = f(x, t), \tag{4}$$

contraction analysis, presented in [85], provides a comprehensive understanding of the property of systems, mainly applying the differential (a.k.a. linearized, variational, prolonged) dynamics along particular solutions:

$$\dot{\delta}_x = \frac{\partial f(x,t)}{\partial x}\delta_x \tag{5}$$

An alteration form of (5), with the differential geometric tools, is also

$$\dot{c}_s(s,t) = \frac{\partial f\left(c(s,t),t\right)}{\partial c(s,t)} c_s(s,t) \tag{6}$$

Both of above illustrations show the dynamic property between trajectories at a fixed time t instead of one trajectory along times. The reason for getting two different forms is that a valid calculation formula obtaining the differential value δ_x needs to be approximate by the following

Definition 3 (Riemanian Energy). On a manifold $\mathcal{M}$, a Riemannian metric $M(x,t)$ always can define an inner $\langle\cdot,\cdot\rangle$ on the tangent space $T_x\mathcal{M}$, it is

$$E(c,t) = \int_0^1 c_s\, M(c,t) c_s ds$$

where $c(s,t):[0,1]\to\mathcal{M}$, at a fixed time t, is a regular parameterized differentiable curve.

Now, suppose on some time interval $t\in[t_i, t_i+\epsilon)$ and for each $s\in[0,1]$, we fix the control and disturbance inputs to their values at $t=t_i$, and the state $c(t,s)$ evolves according to (2). Here the time interval $[t_i, t_i+\epsilon)$ can be arbitrarily short so as to guarantee existence of solutions. As a result of this, adopt the equivalent notation $\delta_x = c_s$, and more references doing this can see in [147].

5.2.3 System Safety

In the context of safety, we consider a set $\mathcal{C}$ defined as the 0 superlevel set of a continuously differentiable function $h:\mathbb{R}^n \to \mathbb{R}$, yielding:

$$\mathcal{C} = \left\{ x \in \mathbb{R}^n \mid h(x) \geq 0 \right\} \tag{7}$$

$$\partial\mathcal{C} = \left\{ x \in \mathbb{R}^n \mid h(x) = 0 \right\} \tag{8}$$

$$\mathrm{int}\mathcal{C} = \left\{ x \in \mathbb{R}^n \mid h(x) > 0 \right\} \tag{9}$$

refer $\mathcal{C}$ as the safe set. According to the safe set, the barrier function examines the safe property of nonlinear systems by set invariance principle [149], and has been widely studied in the robot field. It is

Definition 4 (Barrier Function (BF)). Let $\mathcal{C} \subset \mathbb{R}^n$ be the 0 superlevel set of a continuously differentiable function $h:\mathbb{R}^n \to \mathbb{R}$. Function h is called BF for system (4) if there exists an open set D with $\mathcal{C} \subset \mathcal{D} \subseteq \mathbb{R}^n$ an extended class $\mathcal{K}_\infty$ function α such that

$$\dot{h}(x) \geq -\alpha\left(h(x)\right)$$

for all $x \in \mathcal{D}$.

The central conclusion is that system (4) is safe with respect to set $\mathcal{C}$ if the $\mathcal{C}$ is an invariant set. In this chapter, we consider a case where some unsafe factors are in the virtual tube, which comes from the instant situation that needs safety-critical control. For instance, an obstacle stands in the given way while a trajectory planner did not deal with it, and the simple illustration is shown in Fig. 5.2.

Now, designing the safety-critical tubes is the main purpose of this chapter. We aim to find a feedback control $k\left(x, x^{*}\right)$, for control systems (1), making the control system successfully run in the virtual tube with unsafe constraints. Specifically, we desire the tube containing a finite capacity can avoid some obstacles, meanwhile, this tube allows systems to pass through the tube when there are dangerous regions.

5.3 Robust control contraction metric

In [147], a nonlinear version of $\mathcal{H}^{\infty}$ control was proposed for nonlinear systems, primarily using the robust control contraction metric (RCCM). Then, in [91], the specific scenario in tube design was expanded to a modified RCCM, achieving more effective performance in tube width. In this chapter, what is different from them is that the RCCM was expanded to a comprehensive evaluation by the new definition, so there is a strong condition for RCCM, by which leading three equivalent descriptions of the universal input-to-state $\mathcal{L}^{\infty}$ gain. The following subsections provide more details and can check it.

Now, giving the basis for how to get RCCM, which is about a uniformly lower-bounded Riemannian metric M that is supposed to be found by

$$\delta_x Mb_i = 0 \Rightarrow \frac{d}{dt}\langle \delta_x, \delta_x \rangle_M \leq -2\lambda\delta\langle {}_x, \delta_x \rangle_M + \mu^2 \langle \delta_w, \delta_w \rangle \qquad (10)$$

for all $x \in \mathcal{M}$, $t \in \mathbb{R}^{+}$, and $\delta_x, \delta_w \in T_x M$, then the system is universal input-to-state stable. Such a metric is referred to as a robust control contraction metric. The explanation of RCCM is that if the span of actuated directions b_i is keeping a bound distance with a gain μ^2 on the every tangent vector δ_x orthogonal, then every solution of the system has universal input-to-state L^{∞} gain.

This section is divided into several parts as a response to the problem description of Subsection II-A and II-B, and all are based on the basis formula (10) (seeing details in Subsection III-A). The controller design, the duality form of RCCM and how to calculating the approximate metric will be given. Besides, a specific case of RCCM with an affect of w, and some connections with virtual tube will be presented in the last two subsections.

5.3.1 Strong condition for RCCM

Let us verify (10) for the system (1), so the first consideration is the differential forms connecting each particular solution such as

$$\dot{\delta}_x = A\delta_x + B\delta_u + D\delta_w, \tag{11}$$

which helps system to become contraction by constructed Riemannian metric $M\left(x,t\right)$ if the RCCM condition was verified to be ture, where

$$A\left(x,u,w,t\right) = \frac{\partial f}{\partial x} + \sum_{i=1}^{m}\frac{\partial b_i}{\partial x}u_i + \sum_{i=1}^{m}\frac{\partial d_i}{\partial x}w_i$$

The second, considering the following dynamic behaviour of the squared differential length

$$\frac{d}{dt}\delta_x^{\mathrm{T}} M\delta_x = \delta_x^{\mathrm{T}}\left(\dot{M} + \langle MA\rangle\right)\delta_x + 2\delta_x^{\mathrm{T}} MB\delta_u + 2\delta_x^{\mathrm{T}} MD\delta_w. \tag{12}$$

where the candidate RCCM $M\left(x,t\right)$ is arbitrary and waiting to be verified, and it's derivative holds $M = \frac{\partial M}{\partial t} + \frac{\partial M}{\partial x}\cdot\left(f + Bu + Dw\right)$. Finally, the RCCM condition (10) become that for every $\delta_x = 0$ and every x, u, w, t,

$$\begin{aligned} &\delta_x^{\mathrm{T}} MB = 0 \Rightarrow \\ &\delta_x^{\mathrm{T}}\left(\dot{M} + \langle MA \rangle\right)\delta_x + 2\delta_x^{\mathrm{T}} MD\delta_w \le -2\lambda\delta_x^{\mathrm{T}} M\delta_x + \mu^2\delta_w^{\mathrm{T}}\delta_w . \end{aligned} \tag{13}$$

Since w is independent on x, let's specify the change of δ_w a prolonged straight line. The representation of geometry of δ_w now can be written as $\delta_w = w - w^{å}$ because of the straight line form $w(t) = (1-s)w + w^{å}$ in any two connected trajectories.

Theorem 1 Given a control system of the form (1), suppose there exists a bounded metric $M(x,t)$, a constant $\lambda > 0$ and $\mu > 0$. such that the following two conditions hold:

C1: if $\delta_x = 0$ satisfies $\delta_x MB = 0$. , then

$$\delta_x \left(\frac{\partial M}{\partial t} + \frac{\partial M}{\partial x} \cdot f + \left\langle M \frac{\partial f}{\partial x} \right\rangle + \frac{MDD^T M}{\mu^2} \right) \delta_x \le -2\lambda \delta_x M \delta_x$$

C2: for each $i = 1, 2, \ldots, m$

$$\begin{aligned} &\frac{\partial M}{\partial x} \cdot b_i + \left\langle \frac{\partial b_i}{\partial x} M \right\rangle = 0 \\ &\frac{\partial M}{\partial x} \cdot d_i + \left\langle \frac{\partial d_i}{\partial x} M \right\rangle = 0 \end{aligned} \tag{14}$$

Then the system (1) achieves universal input-to-state L^{∞}. gain.

Proof: Using substitutions of δ_x, δ_w in inequality (13) and integrating along $s \in [01]$, one can get

$$\frac{d}{dt}\int_0^1 c_s^{\mathrm{T}} M c_s ds \le -2\lambda \int_0^1 c_s^{\mathrm{T}} M c_s ds + \mu^2 \left\| w(t) - w^*(t) \right\|^2 .$$

The inequality about Riemanian energy can be obtained as

$$\frac{d}{dt}E\left(c,t\right)\leq -2\lambda E\left(c,t\right)+\mu^{2}\left\|w\left(t\right)-w^{å}\left(t\right)\right\|^{2}. \qquad (15)$$

For sufficiently small $\grave{o}$, for any $t\in\left[t_i,t_i+\grave{o}\right]$, try to solve above inequality, it yields

$$\begin{aligned}E\left(c,t\right) &\leq E\left(c,t_i\right)e^{-2\lambda\left(t-t_i\right)}\\ &+\int_{t_i}^{t}e^{-2\lambda\left(t-\tau\right)}\mu^{2}\left\|w\left(\tau\right)-w^{å}\left(\tau\right)\right\|^{2}d\tau\end{aligned}$$

Since t_i was arbitrary, for all $t\geq 0$ there is

$$\begin{aligned}E\left(c,t\right)\leq\ & E\left(c,0\right)e^{-2\lambda t}\\ &+\int_{0}^{t}e^{-2\lambda\left(t-\tau\right)}\mu^{2}\left\|w\left(\tau\right)-w^{å}\left(\tau\right)\right\|^{2}d\tau\\ &\leq E\left(c,0\right)e^{-2\lambda t}+\frac{\mu^{2}}{2\lambda}\sup\left\|w\left(t\right)-w^{å}\left(t\right)\right\|^{2},\end{aligned}$$

Suppose M has bound satisfying $\underline{\alpha}I<M<\overline{\alpha}I$, there is

$$\begin{aligned}\underline{\alpha}\left\|x\left(t\right)-x^{*}\left(t\right)\right\|^{2} &=\underline{\alpha}\int_{0}^{1}c_s^{\mathrm{T}}c_s ds\leq\int_{0}^{1}c_s^{\mathrm{T}}Mc_s ds=E\left(c,t\right)\\ &\leq\overline{\alpha}\int_{0}^{1}c_s^{\mathrm{T}}c_s ds=\overline{\alpha}\left\|x\left(t\right)-x^{*}\left(t\right)\right\|^{2},\end{aligned}$$

then $\underline{\alpha}x\left(t\right)-x^{å}\left(t\right)^{2}\leq E\left(c,t\right)$ and $E\left(c,0\right)\leq\overline{\alpha}\left\|x\left(0\right)-x^{å}\left(0\right)\right\|^{2}$. Hence, the system (1) is universal input-to-state stable such that

$$\begin{aligned}\left\|x\left(t\right)-x^{*}\left(t\right)\right\|^{2} &\leq\frac{\overline{\alpha}e^{-2\lambda t}}{\underline{\alpha}}\left\|x\left(0\right)-x^{*}\left(0\right)\right\|^{2}\\ &+\frac{\mu^{2}}{2\lambda\underline{\alpha}}\left\|w\left(t\right)-w^{*}\left(t\right)\right\|_{\mathrm{L}^{\infty}\infty}^{2},\end{aligned} \qquad (16)$$

one can observe that $\frac{\mu^{2}}{2\lambda\underline{\alpha}}=\sigma$ is the universal input-to-state L^{∞}-gain bound. When $\delta_x=0$ satisfies $\delta_x MB=0$, making

$$\begin{aligned}H\left(x,u,w,\delta_x,\delta_w,t\right) &=\delta_x^{\mathrm{T}}\left(\dot{M}+\left\langle MA\right\rangle\right)\delta_x+2\delta_x^{\mathrm{T}}MD\delta_w\\ &+\lambda\delta_x^{\mathrm{T}}M\delta_x-\mu^{2}\delta_w^{\mathrm{T}}\delta_w\leq 0,\end{aligned} \qquad (17)$$

then consider the worst-case δ_w in $H\left(x,u,w,\delta_x,\delta_w,t\right)$ so that we have $\frac{H}{\partial\delta_w}=0$. It yields

$$\delta_w = \frac{\delta_x MD}{\mu^2}. \qquad (18)$$

Take (18) into RCCM condition (13), there is

$$\delta_x^{\mathrm{T}} \left(\dot{M} + \langle MA \rangle + \frac{MDD^{\mathrm{T}}M}{\mu^2} + 2\lambda \delta_x^{\mathrm{T}} M \delta_x \right) \delta_x \leq 0. \quad (19)$$

We can note that $\dot{M} = \frac{\partial M}{\partial t} + \frac{\partial M}{\partial x} \cdot (f + Bu + Dw)$, and $A(x,u,w,t) = \frac{\partial f}{\partial x} + \sum_{i=1}^{m} \frac{\partial b_i}{\partial x} u_i + \sum_{i=1}^{m} \frac{\partial d_i}{\partial x} w_i$. For eliminating the affects regarding u and w, using the equality condition $C2$ to enforce M into it. Suppose $C2$ is true, then the term in parenthesis of (20) will be

$$\frac{\partial M}{\partial t} + \frac{\partial M}{\partial x} \cdot f + \left\langle M \frac{\partial f}{\partial x} \right\rangle + \frac{MDD^T M}{\mu^2}. \qquad (20)$$

Now, the strong condition for RCCM is the negative definite (20) such that $C1$, with an equality constrain on $M(x,t)$ such that $C2$.

One should notice that worst-case δ_w is also dependent on $w^{å}$, while we concentrate on a normal disturbance $w^{å} = 0$ in this chapter, which means w has an influence on each solution of system (1) with a normal disturbance $w^{å}$.

5.3.2 Construction of control law

To construct the control signal, the differential value δ_x should be solved first. There is an online scheme that minimizes Riemannian energy such that

$$\mathrm{c}(s) = \underset{c(s)\in\Gamma(x,x^{å})}{\operatorname{argmin}} \int_0^1 c_s M(c,t) c_s ds, \quad (21)$$

where $\mathrm{c}(s)$ represents a geodesic at a fixed time t, the reason calling it a realtime and online optimization control comes from to the requirement to find a geodesic $c(s)$ in family of curves connecting point connected x and $x^{å}$ in real time.

In this section, two types of control laws can achieve feedback control through RCCM. Both of them depend on $c(s)$ if the chosen target trajectory $x^*(t), u^*(t), w^*(t)$ have been given and the differential value $c_s = \delta_x$ that enables such control laws to be feasibly calculated. The subsequent analysis is about to construct a differential control δ_u that produce the input-to-state L^∞ gain along any particular solution for the control system (1).

Proposition 1 If Condition C1 holds then there exists a scalar multiplier $\rho(x,t)$ for which

$$\frac{\partial M}{\partial t} + \frac{\partial M}{\partial x} \cdot f + \left\langle M \frac{\partial f}{\partial x} \right\rangle + \frac{MDD^T M}{\mu^2} - \rho MB \;\; BM + 2\lambda M \leq 0 \qquad (22)$$

Proof: Reference in the explanation from Finsler's theorem. A scalar multiplier ρ satisfying $H - \rho GG \;\; < 0$ in which H is a given square matrix and G is a matrix, then for all $\delta_x = 0$ that satisfies $\delta_x \; G = 0$, there is $\delta_x \; H \delta_x < 0$. One can discover that Condition C1 is established if to use the strict inequality (22) in each point $x(t)$. Hence, this proposition holds the negative property for a scalar multiplier ρ.

Supposing there is a feedback gain $K(x,t)$ in system (11), by which we denote a differential controller $\delta_u = K(x,t)\delta_x$, and for which the closed-loop differential dynamics become

$$\dot{\delta}_x = \big(A(x,u,w,t) + B(x,t)K(x,t)\big)\delta_x + D(x,t)\delta_w,$$

then the derivative of the differential squared-length will be

$$\frac{d}{dt}\delta_x^{\mathrm{T}} M \delta_x = \delta_x^{\mathrm{T}}\left(\dot{M} + \langle MA \rangle\right)\delta_x + 2\delta_x^{\mathrm{T}} MBK\delta_x + 2\delta_x^{\mathrm{T}} MD\delta_w \quad (23)$$

Now, the existence of the differential gain $K(x,t)$ can be guaranteed if there are pre-known metric M and multiplier ρ according to Proposition 1. So the differential feedback law can be constructed by

$$\delta_u = -\frac{1}{2}\rho(x,t)B(x,t)\ \ M(x,t)\delta_x \qquad (24)$$

where $-\frac{1}{2}\rho(x,t)B(x,t)\ \ M(x,t) = K(x,t)$. Next, the inequality respect with the bound for the derivative of the differential squaredlength is

$$\frac{d}{dt}\delta_x^{\mathrm{T}} M \delta_x \leq -2\lambda \delta_x^{\mathrm{T}} M \delta_x + \mu^2 \delta_w^{\mathrm{T}} \delta_w,$$

which ensure system (1) to be universal input-to-state stable.

Once the geodesic $\mathrm{c}(s)$ is successfully identified by (21), along which the differential feedback law (24) is always existing by constructing the differential gain $K\left(\mathrm{c}(s,t),t\right) = -\frac{1}{2}\rho\left(\mathrm{c}(s,t),t\right)B(\mathrm{c}(s,t),t)\ \ M\left(\mathrm{c}(s,t),t\right)$. To integrate the differential feedback law along $\mathrm{c}(s)$, the control law with a integration form is the following

$$u(t) = u^{\text{å}}(t) + \int_0^1 K\left(\mathrm{c}(s),t\right)\mathrm{c}_s(s)\,ds \qquad (25)$$

Notice that one equivalent to (25) is $u = u^{\text{å}} + \int_0^1 \delta_u ds$, where $u^{\text{å}}$ can be viewed as an open control and denoting the initial point, when $s = 0$, in controller part of the solution for the target trajectory, while the integrate part denotes the feedback gain along $\mathrm{c}(s)$, so in each produced trajectory x the corresponding control signal, when $s = 1$, is the combination of the open control and the integral feedback gain.

Proposition 2 If Theorem 1 holds then there exists a control set $\mathrm{U}_{\text{stable}}$ such that

$$U_{\text{stable}} := \Big\{ u \in ò^{m} : 2c_s(s) \ \ M\left(c(s)\right)\Big|_{s=1} \left(f(x) + B(x)u \right)$$
$$-2c_s(s)^{\mathrm{T}} M\left(c(s)\right)\Big|_{s=0} \left(f(x^*) + B(x^*)u^* \right) \qquad (26)$$
$$+\frac{1}{\mu^2} \left\| c_s(s)^{\mathrm{T}} M\left(c(s)\right)\Big|_{s=1} D(x) \right\|^2 + 2\lambda E(c,t) \le 0 \Big\}$$

achieving universal input-to-state L^{∞} gain.

Proof: Consider the time derivative of Riemanian energy between trajectories x and $x^{å}$, it is

$$\frac{d}{dt} E\left(c(s,t)\right) = \int_0^1 \frac{d}{dt} c_s(s,t) \ \ M\left(c(s,t),t\right) c_s(s,t)\, ds \qquad (27)$$

Referencing to [148] and [150], the first variation of energy with respect to time is

$$\frac{1}{2} \dot{E}\left(c(s,t)\right) = c_s(s), \dot{c}(s)\Big|_{s=0}^{s=1} - \int_0^1 \left\langle \frac{\partial}{\partial s} c_s, \dot{c} \right\rangle ds. \qquad (28)$$

In the situation of minimizing geodesic $c(s) = c(s)$, there is $\frac{\partial}{\partial s} c_s = 0$. Hence, by ignoring the term $\int_0^1 \left\langle \frac{\partial}{\partial s} c_s, \dot{c} \right\rangle ds$, the formula (28) can be rewritten as

$$\begin{aligned}
\frac{1}{2} \dot{E}\left(c(s,t)\right) &= \frac{\partial E}{\partial t} + \left\langle c_s(s), \dot{c}(s) \right\rangle\Big|_{s=0}^{s=1} \\
&= \frac{\partial E}{\partial t} + 2\gamma_s(s)^{\mathrm{T}} M\left(\gamma(s)\right)\Big|_{s=1} \dot{x} \qquad (29) \\
&\quad -2\gamma_s(s)^{\mathrm{T}} M\left(\gamma(s)\right)\Big|_{s=0} \dot{x}^*
\end{aligned}$$

where $\dot{x} = f(x) + B(x)u + D(x)w$ and $\dot{x}^* = f(x) + B(x^*)u + D(x^*)w$. According to the inequality (17) in Theorem 1 , we know the following inequality chain

$$\begin{aligned}
2c_s(s)^{\mathrm{T}} M\left(c(s)\right)\Big|_{s=1} & \left(f(x) + B(x)u + D(x)w \right) \\
& -2c_s(s)^{\mathrm{T}} M\left(c(s)\right)\Big|_{s=0} \left(f(x^*) + B(x^*)u^* + D(x)w^* \right) \\
& \le -2\lambda E\left(c(s,t)\right) + \mu^2 \left\| w(t) - w^*(t) \right\|^2.
\end{aligned}$$

where $w - w^{å} = \delta_w$ is the linear consideration of $w(s)$ in every trajectory. According to the worst-case δ_w in (18), we can obtain

$w = w^{å} + \frac{c_s(s)\ M\left(c(s)\right)\big|_{s=1} D(x)}{\mu^2}$. Now, for each state pari $\left(x(t), x^{å}(t)\right)$ the set of control inputs $u = u^{å} + k$ can be constructed by satisfying

$$
\begin{aligned}
&2c_s(s)^{\mathrm{T}} M\left(c(s)\right)\big|_{s=1}\left(f(x)+B(x)u\right) \\
&-2c_s(s)^{\mathrm{T}} M\left(c(s)\right)\big|_{s=0}\left(f\left(x^{å}\right)+B\left(x^{*}\right)u^{*}\right) \qquad (30) \\
&+\frac{1}{\mu^2}\left\|c_s(s)^{\mathrm{T}} M\left(c(s)\right)\big|_{s=1} D(x)\right\|^2 + 2\lambda E\left(c(s,t)\right) \le 0.
\end{aligned}
$$

So let's use $\mathrm{U}_{\text{stable}}$ showed in (26) to denote the control sets with the universal input-to-state L^{∞} gain.

In summary, the integration-form and energy-minimum-form controller were presented behind the provided RCCM condition, both of which depend on the online solution of the geodesic c(s), while the basis principle to the universal input-to-state L^{∞} gain are to search a metric M.

5.3.3 Dual robust control contraction metric

Because of the difficulties to solve the quadratic $MDD^T M$ of Theorem 1 introduced in Subsection III-A, and the dependency relationships between u and M introduced in Subsection III-B, the transform of RCCM is applied by the following: to definite dual robust control contraction metric a change of variables $W(x,t) = M(x,t)^{-1}$ and making $\eta = M(x,t)\delta_x$, now condition $C1$ is presented as if $\delta_x = 0$ satisfies $\eta\ B = 0$, then

$$\eta\ \left(-\frac{\partial W}{\partial t} - \frac{\partial W}{\partial x}\cdot f + \left\langle\frac{\partial f}{\partial x}W\right\rangle + \frac{DD^T}{\mu^2} + 2\lambda W\right)\eta \le 0. \quad (31)$$

Specifically, the basis for null space of B can be constructed by a matrix $B_{\perp}$ such that $B \; B_{\perp} = 0$. In this case, the inequality (31) is equivalent to

$$B_{\perp}\left(-\frac{\partial W}{\partial t}-\frac{\partial W}{\partial x}\cdot f+\left\langle\frac{\partial f}{\partial x}W\right\rangle+\frac{DD^{T}}{\mu^{2}}+2\lambda W\right)B_{\perp}\leq 0. \quad (32)$$

According to **Proposition 1**, Finslers theorem can replace above two inequalities by

$$-\frac{\partial W}{\partial t}-\frac{\partial W}{\partial x}\cdot f+\left\langle\frac{\partial f}{\partial x}W\right\rangle+\frac{DD^{T}}{\mu^{2}}-\rho BB \;\; +2\lambda W\leq 0. \quad (33)$$

This condition guarantee a differential feedback gain $K = \;\; -\frac{1}{2}\rho B \;\; W^{-1}$ is always existing.

We can also use the form $Y=\frac{1}{2}\rho B$ in which $Y:(x,t)\in \mathbb{R}^{m\times n}$ to definition a more explicit search for W :

$$-\frac{\partial W}{\partial t}-\frac{\partial W}{\partial x}\cdot f+\left\langle\frac{\partial f}{\partial x}W\right\rangle+\frac{DD^{T}}{\mu^{2}}+\left\langle BY\right\rangle+2\lambda W\leq 0. \quad (34)$$

So a differential feedback gain can be written $K=-YW^{-1}$ if satisfying condition (34).

Following the transforms for Condition $C2$, the equivalent constraints on W is written as $C2$: for each $i=1,2,\ldots,m$,

$$\begin{aligned}&\frac{\partial W}{\partial x}\cdot b_{i}-\left\langle\frac{\partial b_{i}}{\partial x}W\right\rangle=0\\&\frac{\partial W}{\partial x}\cdot d_{i}-\left\langle\frac{\partial d_{i}}{\partial x}W\right\rangle=0\end{aligned} \quad (35)$$

In contrast, this chapter trying to construct RCCM for reducing the impact by disturbance, which can be achieved through provided control law (25) and solving the stable set (26). It should be notice that all searched RCCM can be used in calculating geodesic (21), so **Proposition 2** with a quadratic index $\min u\ \ u$ is valid, while the differential feedback gain K is useful if the condition (33) or (34) get a verification.

5.3.4 Offline search of RCCM for gain minimization

In this subsection, the cost function μ^2 definite the gain minimization problem by the offline search of RCCM. Moreover, considered a compact set $x \in \Lambda$ to limit the searching in the infinite range. As discussed in [151], the elements of W can be parameterized as some finite-dimensional polynomial, solved by sum-of-squares programming. The optimization problem $0\mathrm{PT}_{RCCM_i}, i = 1,2,3$ involved in this chapter are follows:

$$
\begin{aligned}
&0\mathrm{PT}_{RCCM_1} : \min_{\lambda, W} \mu^2, \\
&\ \text{s.t} \quad \text{condition(32),condition(35)}, \underline{\alpha}^{-1} I \geq W \geq \overline{\alpha}^{-1} I. \\
&0\mathrm{PT}_{RCCM_2} : \min_{\lambda, W, \rho} \mu^2, \\
&\ \text{s.t} \quad \text{condition(33),condition(35)}, \underline{\alpha}^{-1} I \geq W \geq \overline{\alpha}^{-1} I. \\
&0\mathrm{PT}_{RCCM_3} : \min_{\lambda, W, Y} \mu^2, \\
&\ \text{s.t} \quad \text{condition(34),condition(35)}, \underline{\alpha}^{-1} I \geq W \geq \overline{\alpha}^{-1} I.
\end{aligned}
$$

where condition (32), (33) and (34) are strictly limited to sumof-squares constraints. The above three problems are equivalent, which can be verified in Subsection III-C. In terms of numerous computation, several computational tools such as [152], YALMIP [153] and Mosek [154] have provided some successful applications in search of control contraction metric [155].

5.3.5 Extension

This extension is about a modified RCCM reserving the influence of disturbance w whose boundary is pre-known. Because disturbance is easily to deal with when modeling the optimization problem about RCCM, we can eliminate $\frac{\partial M}{\partial x}\cdot d_i+\left\langle \frac{\partial d_i}{\partial x} M\right\rangle=0$ by the following

Corollary 1 Given a control system of the form (1), suppose there exists a bounded metric $M(x,t)$, a constant $\lambda>0$ and $\mu>0$ such that the following two conditions hold:

C3: if $\delta_x=0$ satisfies $\delta_x MB=0$, then

$$\delta_x^{\mathrm{T}}\left(\frac{\partial M}{\partial t}+\frac{\partial M}{\partial x}\cdot \mathrm{f}+\left\langle M\mathrm{A}\right\rangle+\frac{MDD^{\mathrm{T}}M}{\mu^2}\right)\delta_x \le -2\lambda\delta_x^{\mathrm{T}}M\delta_x .$$

where $\mathrm{f}=f+Dw$ and $\mathrm{A}=\frac{\partial f}{\partial x}+\frac{\partial D}{\partial x}w$.

C4: for each $i=1,2,\dots,m$,

$$\frac{\partial M}{\partial x}\cdot b_i+\left\langle \frac{\partial b_i}{\partial x} M\right\rangle=0. \quad (36)$$

Then the system (1) achieves universal input-to-state L^{∞} gain.

Now, the modified dual RCCM can do a similar change introduced in Subsection III-C, in which the corresponding optimization problem is able to produce a solution of modified dual RCCM. Following the condition (32) to (34), the modified dual form can be written as

$$B_{\perp}\left(-\frac{\partial W}{\partial t}-\frac{\partial W}{\partial x}\cdot \mathrm{f}+\left\langle \mathrm{A}\ W\right\rangle+\frac{DD^{T}}{\mu^2}+2\lambda W\right)B_{\perp}\le 0. \quad (37)$$

To use Finslers theorem, the second modified dual RCCM is

$$-\frac{\partial W}{\partial t}-\frac{\partial W}{\partial x}\cdot \mathrm{f}+\langle \mathrm{A}\ W\rangle+\frac{DD^T}{\mu^2}-\rho BB\ \ +2\lambda W\leq 0, \quad (38)$$

and to define $Y=\frac{1}{2}\rho B$, the third one is

$$-\frac{\partial W}{\partial t}-\frac{\partial W}{\partial x}\cdot \mathrm{f}+\langle \mathrm{A}\ W\rangle+\frac{DD^T}{\mu^2}+\langle BY\rangle+2\lambda W\leq 0. \quad (39)$$

Once the construction of metrics satisfies the modified form, the realtime geodesic will be searched, then the control idea (25) and (26) can achieve the universal input-to-state L^{∞} gain for system (1).

Remark 1 We consider our RCCM for the purpose of solving sum of squares (SOS) programming with additional constraints. For the finite dimensional search of RCCM, one defines the the compact set $x\in\Lambda$ to be a semialgebraic set

$$\Lambda:=\left\{x\in \mathbb{R}^n:\theta_i\left(x\right)\geq 0\right\},$$

and because the consideration on disturbance w is viewed as variables of modified dual RCCM, one defines the the compact set $w\in\Theta$ to be a semialgebraic set

$$\Theta:=\left\{w\in \mathbb{R}^m:\pi_j\left(w\right)\geq 0\right\}.$$

where θ_i and π_j are multivariate polynomials in x and w respectively. Now one can verify a nonnegativity SOS polynomials $p\left(x,w\right)$ by the rule

$$p-\sum_i L_i\theta_i-\sum_j N_i\pi_i \ \text{ is } \ \text{SOS} \qquad (40)$$

in which L_i and N_i should be SOS polynomials. More technology details about how to use SOS programming can be found in [156]. The simulation process takes auxiliary indeterminates corresponding y to the dimension of OPT_{RCCM} , so the every equation is reconstructed. For example, to write inequality (39) as

$$\begin{bmatrix} -\dfrac{\partial W}{\partial t}-\dfrac{\partial W}{\partial x}\cdot \mathrm{f}+\langle \mathrm{A}\ W\rangle+\langle BY\rangle & D \\ D^{T} & \mu^{2} \end{bmatrix} \leq 0, \quad (41)$$

one uses $F(x,w)$ replaces the terms of matrix in (41), then a SOS $p(x,w)$ can be denoted by $-y\ \ Fy$ where the dimension of auxiliary indeterminates y is $n+m$. For the additional constraints such as the semialgebraic sets Λ and Θ, the rule (40) guarantee SOS programming to be true.

5.3.6 RCCM-based Tube

The RCCM-based tube takes from (16). By the Comparison Lemma [157], one can get the upper bound $\dfrac{\mu^2}{2\lambda\underline{\alpha}}\bar{w}^2$, in which $\bar{w}=\sup_2\left\|w-w^{\text{å}}\right\|$, if the Euclidean energy $\left\|x(0)-x^{\text{å}}(0)\right\|^2 \in \left(0,\dfrac{\mu^2}{2\lambda\underline{\alpha}}\bar{w}^2\right)$. Thus, taking the square root of such energy yields a definition:

$$\Omega\left(\rho,x^{*}(t)\right):=\left\{x\in\Lambda:\left\|x(t)-x^{*}(t)\right\|\leq\sqrt{\frac{1}{2\lambda\underline{\alpha}}}\mu\bar{w}:\rho\right\}, \quad (42)$$

where $x(t)$ denotes the actual trajectories deriving from RCCM control law. Due to the fixed size of ñ, it is easier to check collision risk along a planed trajectory as illustrated in Fig. 5.1, and thanks to [158], the designed tube also can be contained in MPC framework in case the tightened constraints satisfying

$$x^{\text{å}}(\cdot)\in\bar{\Lambda}:=\Lambda\oplus(-\Omega),$$

where $\oplus$ denotes the Minkowski sum. We only discuss the tube for our safety control framework in this research, so the next section will introduce some barrier constraints inside the designed tube.

5.4 Control system safety

Though the tube Ω avoiding obstacles that we called outside unsafe factors addressed some safety control problems, there lacks concentrations on inside unsafe factors. Thus, it is necessary to introduce the barrier function into RCCM-based tube as one result of safety critical control. Consider a family of superlevel sets of a continuously differentiable function $h(x):\Lambda\to\mathbb{R}$ and an extended class $\mathcal{K}$ function $\kappa:\Theta\to\mathbb{R}$, which is expressed as

$$\begin{aligned}
\mathcal{C}_{R} &= \left\{x\in\Lambda, w\in\Theta \middle|\ h(x)+\kappa\left(\|w\|^{2}\right)\geq 0\right\} \\
\partial\mathcal{C}_{R} &= \left\{x\in\Lambda, w\in\Theta \middle|\ h(x)+\kappa\left(\|w\|^{2}\right)= 0\right\} \\
\mathrm{int}\mathcal{C}_{R} &= \left\{x\in\Lambda, w\in\Theta \middle|\ h(x)+\kappa\left(\|w\|^{2}\right)> 0\right\}
\end{aligned}$$

satisfying $\Omega\supset\mathcal{C}_{R}\supseteq\mathcal{C}$.

Input-to-state safety developed in related work presented a general safety control framework for systems with disturbances through introducing input-to-state safe set. In comparison to that set, this research focuses on robust safe set, specializing in systems safety running in the created tube. Moreover, geodesic calculation without inequality constraint and faster response of the fixed-size tubes reduce the procedural complexity compared to MPC-based tubes with barrier function constrains [159].

Definition 5 (Robust safety). The system (1) is robust safe with respect to the set $\mathcal{C}_{R}$ if the set $\mathcal{C}_{R}$ is forward invariant.

Definition 5 can be thought of an inside safety of the tube. If every x starts from Λ

stay in set $\mathcal{C}_R$, then control systems can pass the virtual tube and reach the final goal $x(t_{\text{end}})$. This section is divided into three parts as a response to the problem description of Subsection II-C. We will give basic principle of robust safety control including robust control barrier function with relative-degree 1 and 2 . Then, the quadratic-program-based formulations was proposed to unify stability and safety.

5.4.1 Robust control barrier function

To generalize to robust safety, the invariance set $\mathcal{C}_R$ should follow a condition

Definition 6 (Robust Control Barrier Function (RCBF)). Given a continuously differentiable function $h:\Lambda \rightarrow \mathbb{R}$ for the set $\mathcal{C}_R$. Function h is called RCBF for system (1) if there exists an extended class $\mathcal{K}$ function α and a positive constant ι such that:

$$\sup_{u\in \mathbb{R}^m}\left\{L_f h(x)+L_B h(x)u+L_D h(x)w\right\}\geq -\alpha\left(h(x)\right)-\iota w \quad w$$

Then, Theorem 3 gives the result that the set $\mathcal{C}_R \subset \Omega$ is forward invariance when there existing a RCBF.

Theorem 2 Given a system (1) and a continuously differentiable function $h:\Lambda \rightarrow \mathbb{R}$, if h is an $RCBF$ on $\mathcal{C}_R$, then the systems is robust safe with respect to the set $\mathcal{C}_R$.

Proof: Define a new function

$$\eta(x,w):=h(x)+\kappa\left(\| w\|^2\right).$$

If h is a RCBF, one gets

$$
\begin{aligned}
\dot{\eta}(x,w) &= \dot{h}(x) - \frac{d}{dt}\kappa\left(\| w \|^2\right) \\
&\geq -\alpha\left(h(x)\right) - \iota w \;\; w \\
&\geq -\alpha\left(h(x)\right) - \iota \| w \|^2 \\
&= -\alpha\left(\eta(x,w) - \kappa\left(\| w \|^2\right)\right) - \iota \| w \|^2
\end{aligned}
\tag{43}
$$

where η is substituted for h.

For any $x \in \partial\mathcal{C}_R$, by $\eta = 0$, inequality (43) can be reduce to

$$
\dot{\eta}(x,w) \geq -\alpha\left(-\kappa\left(\| w \|^2\right)\right) - \iota \| w \|^2,
$$

therefore to pick κ make

$$
\alpha \circ \kappa\left(\| w \|^2\right) - \iota \| w \|^2 \geq 0, \quad (44)
$$

then $\dot{\eta}(x,w) \geq 0$. According to Nagumos theorem [107], the systems (1) is robust safe with respect to the set $\mathcal{C}_R$.

Corollary 2 Given a system (1) and a continuously differentiable function $h:\mathbb{R}^n \to \mathbb{R}$, if h satisfies

$$
\sup_{u \in \mathbb{R}^m}\left\{ L_f h(x) + L_B h(x) u - \frac{L_D h(x) L_D h(x)}{4\iota} \right\} \geq -\alpha\left(h(x)\right) \quad (45)
$$

then h is a RCBF in $\mathcal{C}_R$.

Proof: Consider the worst-case w such that

$$
\begin{aligned}
\inf_{w \in \mathbb{R}^m}\Big\{ L_f h(x) + L_B h(x) u \quad &+ L_D h(x) w \\
&+ \alpha\left(h(x)\right) + \iota w^{\mathrm{T}} w \Big\} \geq 0
\end{aligned}
\tag{46}
$$

it yields $w = -\dfrac{L_D h(x)}{2\iota}$. Substituting it into (46), then one gets the RCBF based worst-case disturbances.

In Theorem 3, the sufficient condition renders safety has been verified. Then, in Corollary 2, such condition was further reduced to an inequality independent on w

under the worst-case disturbances assumption. As discussed in the safety about the designed tube, one can obtain a safe control set by consider

$$\mathrm{U}_{\text{safe}} := \left\{ u \in \Re^{m} : L_f h(x) + L_B h(x) u + \alpha(h(x)) - \frac{L_D h(x) L_D h(x)}{4\iota} \geq 0 \right\} \tag{47}$$

Notice that κ cannot be apparently confirmed yet, but it is able to deduce by applying the inequality (44). If ι and α are given, one can ensure that at least $\kappa(\cdot) = \iota\alpha^{-1}(\cdot)$, so the safe set C_{R} is in terms of $h(x) + \kappa(\| w \|^2)$.

The control law in (47) is one way achieving robust safety. An alteration is to use the universal robust safe control law by Sontag formula. Define $a = L_f h(x) - \frac{L_D h(x) L_D h(x)}{4\iota} + \alpha(h(x)), b = L_B h(x)$, then the universal robust safe control law is

$$u = \begin{cases} 0, & \text{when} b = 0, \\ -\dfrac{a + \sqrt{a^2 + \| b \|^4}}{\| b \|^2}, & \text{otherwise.} \end{cases} \tag{48}$$

5.4.2 Robust safety control with relative-degree 2

The above subsection showed that robust control barrier functions can address unsafe factors for control systems, with the set U_{safe} or the universal controller in the worst-case RCBF. In fact, such constrains are based on RCBF whose first time-derivative should depend on the control input, satisfying relative-degree one. In contrary, the next contexts develop a way to construct safety control for robotic systems of which safety constraints have to be the relative-degree 2 .

Definition 7 (Exponential Robust Control Barrier Function (ERCBF)). Given a 2-times continuously differentiable function $h:\Lambda \to \mathbb{R}$ for the set $\mathcal{C}_R$. Function h is called ERCBF for system (1) if there exists a vector K function α and a positive constant ι such that:

$$\begin{aligned}\sup_{u\in\mathbb{R}^m}\left\{L_f^2 h(x)+L_B^2 h(x)u \quad +L_D^2 h(x)w\right\}& \\ \geq -K\left[h(x)\,\dot{h}(x)\right]-\iota w \;\; w&\end{aligned} \tag{49}$$

where the elements of $K=\left[K_1 \quad K_2\right]$ are positive constants.

In no disturbance situation, the higher relative-degree barrier function in systems safety can reference [160]. For address disturbance problems, the following analysis was presented

Theorem 3 Given a system (1) and a 2-times continuously differentiable function $h:\Lambda\to\mathbb{R}$, if h is an ERCBF on $\mathcal{C}_R$, then the systems is robust safe with respect to the set $\mathcal{C}_R$.

Proof: First, to define $\eta(x,w):=h(x)+\kappa\left(\| w\|^2\right),\dot{\eta}(x,w):=\dot{h}(x)=L_f h(x)$ and $\ddot{\eta}(x,w)=\ddot{h}(x)=L_f^2 h(x)+L_B^2 h(x)u+L_D^2 h(x)w$ then, to construct the dynamics of η

$$\begin{bmatrix}\dot{\eta}\\ \ddot{\eta}\end{bmatrix}=\begin{bmatrix}0 & 1\\ 0 & 0\end{bmatrix}\begin{bmatrix}\eta\\ \dot{\eta}\end{bmatrix}+\begin{bmatrix}0\\ 1\end{bmatrix}\ddot{\eta}(x,w) \tag{50}$$

Now, let $\mathbf{z}=\left[\eta \quad \dot{\eta}\right]$,$\mathbf{F}=\begin{bmatrix}0 & 1\\ 0 & 0\end{bmatrix},\mathbf{G}=\begin{bmatrix}0\\ 1\end{bmatrix}$ and $\mathbf{u}=\ddot{\eta}(x,w)$ then one obtains differential equation

$$\dot{\mathbf{z}}=\mathbf{F}\mathbf{z}+\mathbf{G}\mathbf{u}. \tag{51}$$

Then, chosen a feedback style

$$\begin{aligned}\mathbf{u} \quad &= -K_1\left(\eta(x,w)-\kappa\left(\|w\|^2\right)\right)-K_2\dot{\eta}(x,w)-\iota\|w\|^2 \\ &\le -K\left[h(x)\dot{h}(x)\right]-\iota w \;\; w\end{aligned} \qquad (52)$$

one can obtain the feedback equation

$$\dot{\mathbf{z}} = (\mathbf{F}-\mathbf{G}K)\mathbf{z}+\mathbf{G}\left(K_1\kappa\left(\|w\|^2\right)-\iota\|w\|^2\right). \quad (53)$$

Since $\mathbf{F}-\mathbf{G}K$ is Hurwitz matrix, one can directly solve (51) to obtain

$$\begin{aligned}\mathbf{z}(t) = \quad & e^{(\mathbf{F}-\mathbf{G}K)t}\mathbf{z}(0) \\ & +\int_0^t e^{(\mathbf{F}-\mathbf{G}K)(t-\tau)}\mathbf{G}\left(K_1\kappa\left(\|w\|^2\right)-\iota\|w\|^2\right)d\tau.\end{aligned} \qquad (54)$$

The above integral term regarding w hold positive if chose the appropriate K_1 and $\kappa, \mathbf{z}(t)$ therefore keep positive. It is easy to obtain $\eta(t)=\mathbf{C}\mathbf{z}(t)$ in which $\mathbf{C}=[1 \quad 0]$. Thus, by the comparison lemma, if chosen

$$\mathbf{u} \ge -K_1\left(\eta(x,w)-\kappa\left(\|w\|^2\right)\right)-K_2\dot{\eta}(x,w)-\iota\|w\|^2, \quad (55)$$

one can obtain a conclusion that

$$\begin{aligned}\eta(t) \ge \quad & \mathbf{C}e^{(\mathbf{F}-\mathbf{G}K)t}\mathbf{z}(0) \\ & +\mathbf{C}\int_0^t e^{(\mathbf{F}-\mathbf{G}K)(t-\tau)}\mathbf{G}\left(K_1\kappa\left(\|w\|^2\right)-\iota\|w\|^2\right)d\tau\end{aligned}$$

Since condition (48) guarantee the minimum feedback $\mathbf{u}$ satisfy (54), one can verify $\eta(t)$ is always in set $\mathcal{C}_R$, then the systems is robust safe with respect to the set $\mathcal{C}_R$.

We are interested on the safety about the designed tube, for h with a relative degree 2 , it can follow the worst-case disturbance to get a safe control set. As described in Corollary 2, one obtains such set

$$\begin{aligned}\mathcal{U}_{\underline{safe}} := \Big\{u \in \mathbb{R}^m : & L_f^2 h(x)+L_B^2 h(x)u+K\left[h(x)\dot{h}(x)\right] \\ & -\frac{L_D^2 h(x)\, L_D^2 h(x)}{4\iota} \ge 0\Big\}.\end{aligned} \qquad (56)$$

Now, let's confirm the safe set $\mathcal{C}_R$. It has been known $\mathbf{z}(t)$ should be positive, which keeps $K_1\kappa\left(\|w\|^2\right)-\iota\|w\|^2$ to be positive. Hence, make a $\kappa\left(\|w\|^2\right)\geq\frac{\iota\|w\|^2}{K_1}$, one can get a robust safe set

$$\mathcal{C}_R=\left\{x\in\Lambda,w\in\Theta\,\middle|\,h(x)+\frac{\iota\|w\|^2}{K_1}\geq 0\right\}$$

As example in Fig 5.3, this robust safe set is bigger than $\mathcal{C}$, with a less conservation.

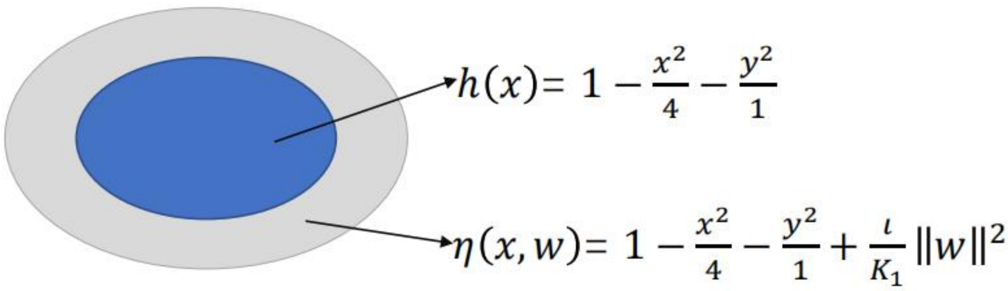

Fig. 5.3. Figure compares the difference between $\mathcal{C}$ and $\mathcal{C}_R$, where grey+blue regions are $\mathcal{C}_R$.

5.4.3 Combining RCCM with RCBF

In this section, the RCCM and the barrier constrains can be unified into one optimization framework for creating tube and the system safety. Consider the following quadratic-program-based controller

$$\begin{aligned} u=&\underset{u\in\mathbb{R}^m}{\operatorname{argmin}}\left(u-u^*\right)^{\mathrm{T}}\left(u-u^*\right)\\ \text{s.t}\quad &\chi_1\left(c_s,c,x,x^*,x,u^*,\mu,\lambda\right)+\chi_2\left(c_s,c,x\right)u\leq 0 \qquad (57)\\ &\xi_1\left(x,\iota\right)+\xi_2\left(x\right)u\geq 0\end{aligned}$$

where χ and ξ are taken from stable set $\mathrm{U}_{\text{stable}}$ in (26) and safe set U_{safe} in (47) respectively, and use χ_1 and ξ_1 to denote the term independent on u, while χ_2 and ξ_2 denote the term dependent on u. Noted that parameters updating for c_s and c is via geodesic calculation (21), while metric M, parameters μ and λ are obtained by the off-line computation of optimization problems described in Section III-D.

For robust safety control with relative-degree 2, one can unifying the safe set U_{safe} in (56) with stable set U_{stable}. It yields

$$\begin{aligned} u &= \underset{u\in \mathbb{R}^m}{\operatorname{argmin}} \left(u-u^*\right)^{\mathrm{T}}\left(u-u^*\right) \\ \text{s.t}\quad & \chi_1\left(c_s, c, x, x^*, x, u^*, \mu, \lambda\right)+\chi_2\left(c_s, c, x\right)u \leq 0 \\ & \underline{\xi}_1\left(x, t\right)+\underline{\xi}_2\left(x\right)u \geq 0 \end{aligned} \qquad (58)$$

where $\underline{\xi}_1$ denotes the term independent on u, while $\underline{\xi}_2$ denotes the term dependent on u. In problems (57) and (58), the first constrain among them creates the RCCM-based tube, which provides a limitation for system's motion, though the second constrains lead such motion to avoid the barrier.

5.5 Simulation

In this section, an example of a planar quadrotor was simulated to illustrate the proposed safety-critical control. The simulated process is done in Matlab R2019a1.

The physical diagram of a planar quadrotor is shown in Fig. 5.4, and the parameters of quadrotor is shown in Tab. I, where u_2, u_1, l, g represent the right thrust forces, left thrust forces, the symmetric thrust moment arm, and gravitational acceleration, respectively. The state equation of planar quadrotor can be presented in affine form as

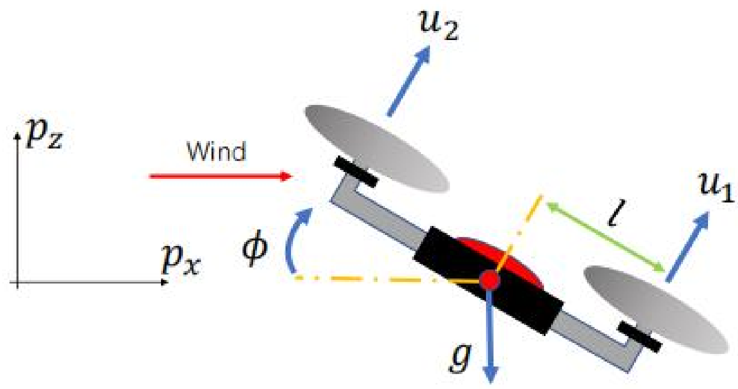

Fig. 5.4. The physical diagram of a planar quadrotor

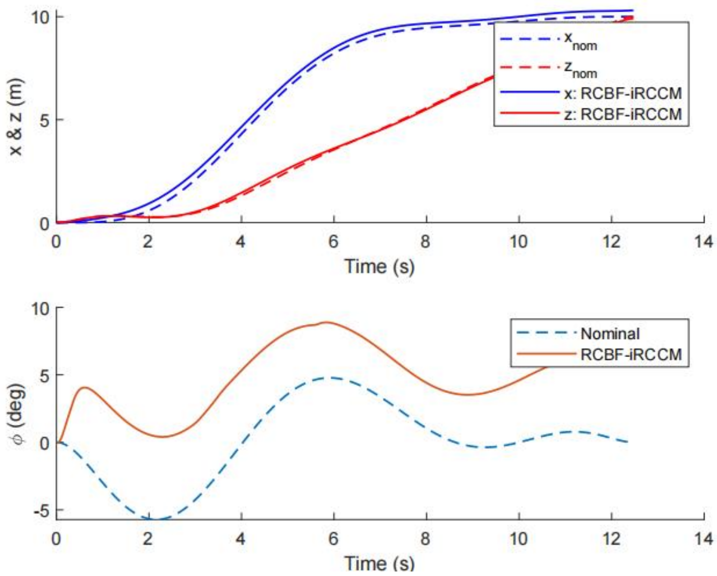

Fig. 5.5. The tracking of nominal trajectory using iRCCM

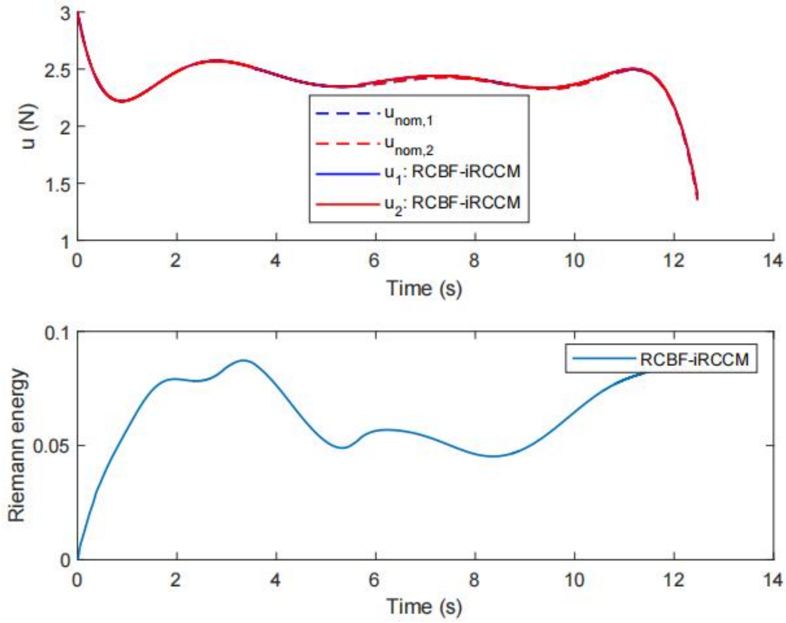

Fig. 5.6. The inputs and Riemann energy using iRCCM

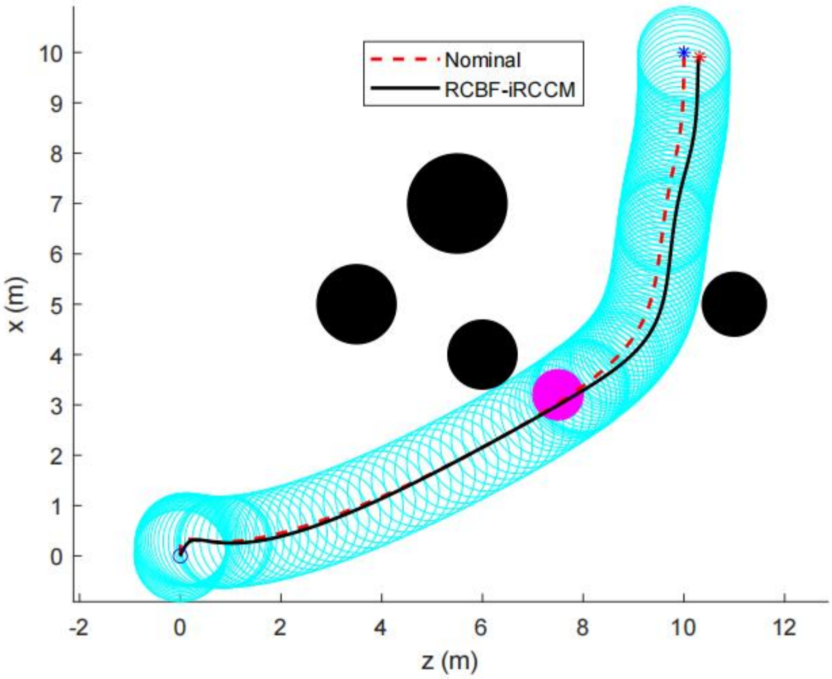

Fig. 5.7. The actual trajectory and the tube in the scenario with multi obstacles and wind disturbances, tracking via iRCCM

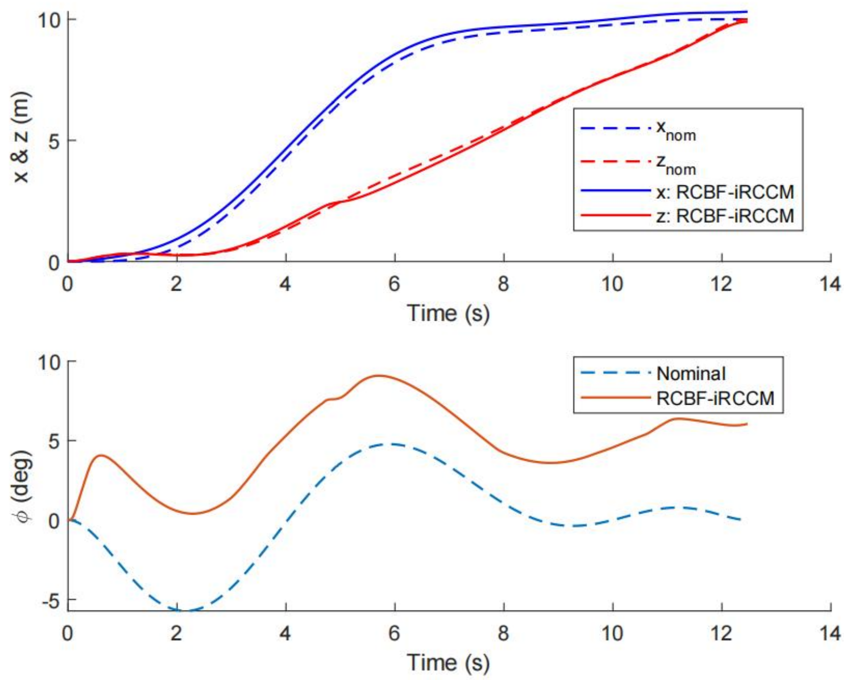

Fig. 5.8. The tracking of nominal trajectory using RCBF-iRCCM

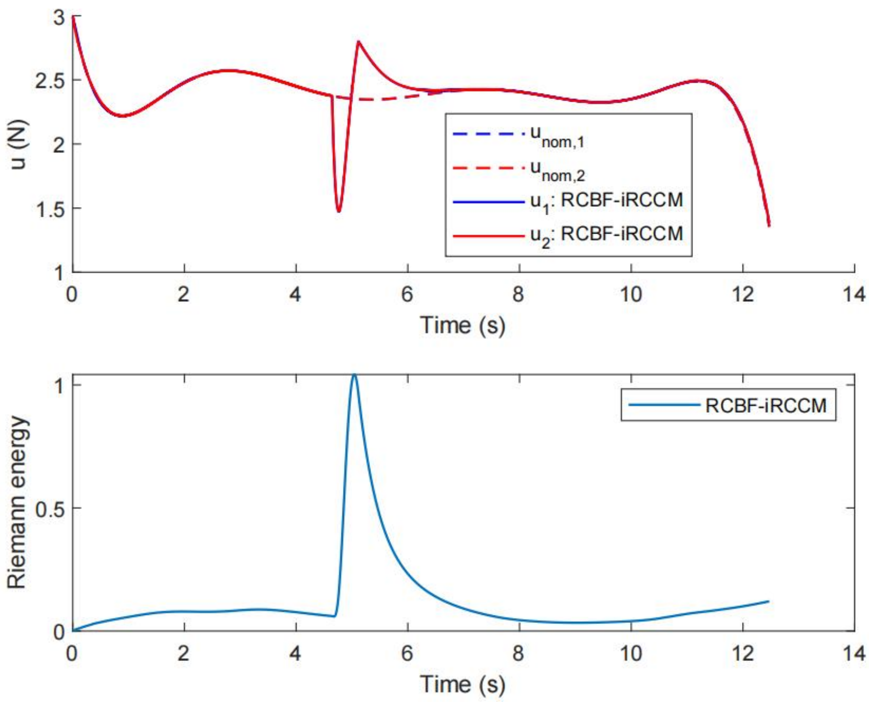

Fig. 5.9. The inputs and Riemann energy using RCBF-iRCCM

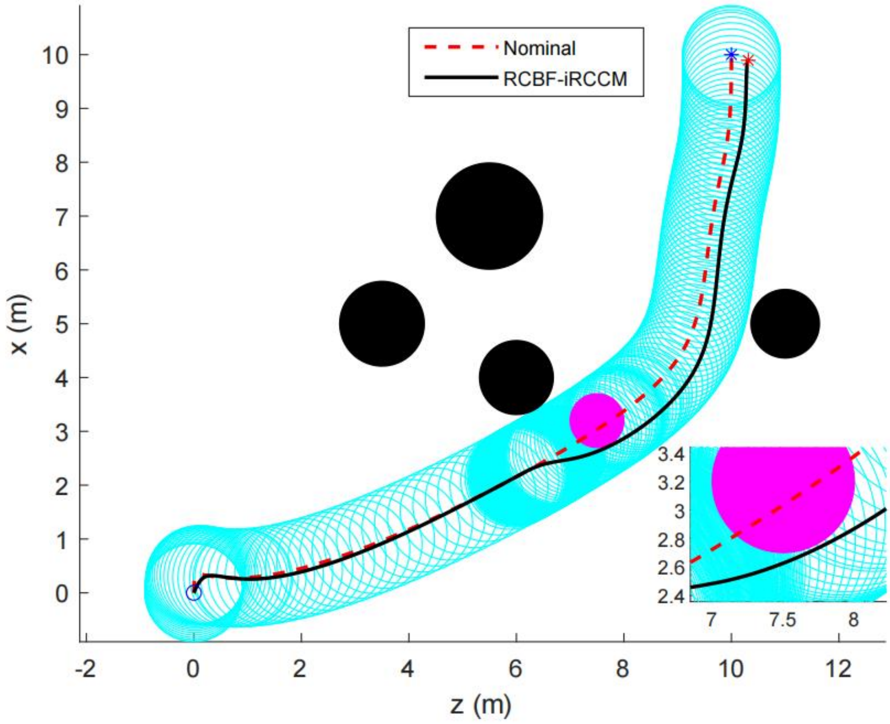

Fig. 5.10. The actual trajectory and the tube in the scenario with multi obstacles and wind disturbances, tracking via RCBF-iRCCM

follows:

$$\dot{x}=\begin{bmatrix} v_x\cos(\phi)-v_z\sin(\phi) \\ v_x\sin(\phi)+v_z\cos(\phi) \\ \dot{\phi} \\ v_z\dot{\phi}-g\sin(\phi) \\ -v_x\dot{\phi}-g\cos(\phi) \\ 0 \end{bmatrix}+\begin{bmatrix} 0 & 0 \\ 0 & 0 \\ 0 & 0 \\ 0 & 0 \\ \frac{1}{m} & \frac{1}{m} \\ \frac{l}{J} & \frac{-l}{J} \end{bmatrix}\begin{bmatrix} u_1 \\ u_2 \end{bmatrix}+\begin{bmatrix} 0 \\ 0 \\ 0 \\ \cos(\phi) \\ -\sin(\phi) \\ 0 \end{bmatrix}w.$$

The planar quadrotor contains six state variables, defined by $x=\left[p_x,p_z,\phi,v_x,v_z,\dot{\phi}\right]^T$, where p_x,p_y denote the horizontal velocity and longitudinal velocity reference ground coordinate, v_x,v_z denote the slip velocity and the velocity along the thrust axis, $\phi,\dot{\phi}$ denote the angle and angular velocity. Since the hardware constraints of the quadrotor, setting the fixed state constraints to be $v_x\in[-2\mathrm{m/s},2\mathrm{m/s}],v_z\in[-1\mathrm{m/s},1\mathrm{m/s}],\phi\in\left[-45^\circ,45^\circ\right]$ and $\dot{\phi}\in[-60,60]^\circ/s$, and assuming that the there is uncertain disturbance caused by the wind, where we artificially set it as $w(t) = 0.8 + 0.2\sin(2\pi t/10)$.

In this simulation, the abbreviation iRCCM was used to denote the robust contraction control metric that results in universal inputto-state L^{∞} gain of the planar quadrotor. For better comparison with safety-critical control, the abbreviation RCBF-iRCCM was used to denote such metric-based method coupled provided robust control barrier functions. We firstly calculated the iRCCM with the SOS optimization of YALMIP tools [151], with the consideration $10I \geq \ W \geq 0.01I$. It can be observed that the disturbance w has a predictable boundary $\bar{w} = 1$, so this simulation applied Corollary 1 to search iRCCM, and since the Killing condition (36) requires that W is independent on v_z and $\dot{\phi}$, we considered each elements of $M(v_x, \phi)$ is the monomials about v_x and ϕ with the maximum degree 4 . For dealing with the hardware constraints $-2 \leq v_x \leq 2$, $-1 \leq v_z \leq 1, -45 \leq \phi \leq 45$ and $-60 \leq \dot{\phi} \leq 60$, considered the semialgebraic set which described in Remark 1 to construct the OPT_{RCCM} problems. The numerical solution of $\underline{\alpha}^{-1}$ is about 0.9999 and μ^2 is about 0.2007 in the determination $\lambda = 1.2$, so the fixed size of RCCM-tube can be solved as $\tilde{n} = 0.9145$ according to the defined $\tilde{n} : \sqrt{\frac{1}{2\lambda\underline{\alpha}}}\mu\bar{w}$ in set (42).

For illustrating that how iRCCM assists with path planning, considered several obstacles in the task scenario. It is showed in Fig. 5.7 and Fig. 5.10, where the black regions are obstacles with different size. If the planned path is close to those obstacles, the actual trajectory of the planar quadrotor may lead a collision with obstacles because of the wind. Hence, the designed tube can be viewed as a redundancy to assist find a desired path. In Fig. 5.7, the desired path can not be allowed to through the obstacles in the left area because of the restriction by the tube's size, but it can pass the spare area in the right area, in which the tube constructed from blue circles showed the planned path is collision-free when the wind interferes with the flying environment.

However, one can see the actual trajectory still collide with the obstacles denoting by purple region that the previous path plan dose not consider. This obstacle is an emergency situation so we should consider safety-critical control. The provided RCBF-iRCCM can solve above problems and the results is showed in Fig. 5.10, where the CBF was designed to the safe distance from the purple obstacle, with an expression $[p_x - p_{ox}, p_z - p_{oz}][p_x - p_{ox}, p_z - p_{oz}] - r^2$ in which p_{ox}, p_{oz} and r denote the center coordinates and the radius of the purple obstacle, respectively. Since the second timederivative depend on the control input, we chose the safety-critical control scheme by robust safety control with relative-degree 2 , where the parameters was determined as $\iota = 10, K_1 = 35$ and $K_2 = 15$ In Fig. 5.10, It can be seen the proposed safety-critical control guarantees that the actual trajectory remain in the tubes, and safely avoid the emergency obstacle inside the tube, though the simulated environment is interfered with the wind. Fig. 5.5, Fig. 5.6, Fig. 5.8 and Fig. 5.9 compared the detailed state in the location px and pz, the input u and the Riemann energy (21), which further illustrated the the effectiveness and applicability of the proposed method.

Noted that the planned nominal input u* and nominal statev x* was solved by

OpimTraj [161]. YALMIP [153] and Mosek solver [162] was required to solve sum-of-squares programs in iRCCM problem. The Chebyshev Pseudospectral method [163] was used to solve geodesic c(s) via nonlinear optimization tools OPTI [164]. Matlab quadprog solver was required for solving quadratic programs for controllers.

TABLE III Parameters of quad-rotor

Term	Value	Unit
m	0.18	Quadrotor mass */kg*
g	9.8	Gravitational acceleration
l	0.086	Quadrotor span */m*
j	$2.5 * 10^{-4}$	Quadrotor moment of Inertia $/kg \cdot m^2$

5.6 Chapter summary

This chapter presents a safety-critical control for nonlinear control-affine systems with disturbance, which creates a contraction-based tube with a predictable fixed size for guaranteeing the robustness of the actual trajectories. It not only can assist the generation of a planned trajectory for avoiding obstacles, but also can ensure the safety inside the tube by coupling with barrier constraints. The effectiveness was verified by the simulation results of a planar quad-rotor.

In summary, this chapter introduces the development of a new UAV flight control algorithm to enhance its safety in the built environment is presented. After validating the effectiveness of the algorithm through simulations, the chapter presents experimental results and discusses the potential and limitations of the algorithm in real-world applications. This chapter not only advances UAV technology in safety-critical applications, but also provides a theoretical basis for optimizing the application of fully automated UAVs in indoor built environments.

Chapter 6. Optimization of fully automatic UAV application in indoor construction environment

This chapter develops a framework for UAV flight control in indoor environments to facilitate path planning for autonomous UAVs. The framework proposed in this chapter integrates 3D construction site maps from BIM models combined with Airsim software in Unreal Engine 4 and Simulink in Matlab. Then, this study developed an algorithm to optimize the drone's flight control. The framework can then calculate a collision-free guidance path and iterate in real time to account for changes in the actual flight process. The framework was validated in a simulated indoor construction site using MATLAB and Unreal Engine 4 (UE4). The planned trajectory demonstrates smoothness, energy efficiency, and adequate coverage.

6.1 Introduction

UAV technology is undoubtedly gaining popularity in the Architecture, Engineering, Construction and Facilities Management (AEC/FM) industry for site management [165], inspection [166] and 3D modeling [167]. Drones are the optimal choice for the smart construction chain due to their unparalleled flexibility. In industrial scenarios with high headroom and poor ground maneuverability (e.g., crowded indoor construction environments), UAVs can cover multiple construction sites in a single flight and outperform ground robots [168]. Recent research has enabled UAVs to fly autonomously in unknown environments using simultaneous localization and mapping (SLAM) techniques [169-172].

However, the current research primarily focuses on point-to-point navigation of UAVs [171,172], with limited attention paid to flight motion planning of drones in actual construction scenarios. It is imperative to consider the motion dynamics of trajectory tracking in path planning for unmanned aerial vehicles (UAVs) [173,174]. Neglecting this crucial aspect can lead to unsafty flight control and increased energy consumption, which pose significant challenges for UAV applications due to the large scale and complexity of construction scenarios, as well as the limited durability of UAVs [175].

Most of the currently widely used UAV flight algorithms rely on preset flight paths and static environment models. In indoor construction environments, these algorithms face many challenges: First, it is difficult to respond in real time to dynamic changes within the construction site, such as temporarily stacked building materials; second, they are often not optimal in terms of energy efficiency, which may result in the need for drones frequent charging affects work efficiency.

This study presents a comprehensive framework for implementing path planning and utilizing new UAV dynamics algorithms to enable complete autonomous UAV applications that can safely operate in indoor construction environments. The framework comprises model construction, path finding and planning, trajectory generation, and flight control. The proposed flights were rigorously validated using simulation environments in MATLAB [176] and Airsim. The trajectories were executed on the platform using a software flight controller. The proposed application scenario is a whole house model that houses mechanical, electrical, and plumbing components, along with other building materials.

The rest of this chapter is as follows: Section 6.2 explains the research methodology, including the conversion and import of BIM 3D models in Airsim software, Implementation of collision-free path finding algorithm, dynamic trajectory generation and flight control algorithm Calculation. Section 6.3 evaluates the performance of the system, and then Section 6.4 discusses the chapter summary.

6.2 Research methodology

This section describes the detailed methodology of the proposed framework. The workflow is overview in Fig. 6.1. The planning phase consists of five steps: (1) 6.2.1 model construction and import, (2) 6.2.2 Collision-free path finding, (3) 6.2.3 trajectory generation, and (4) 6.2.4 flight control, the planning phase is implemented using MATLAB, followed by the validation phase in Section 6.3.

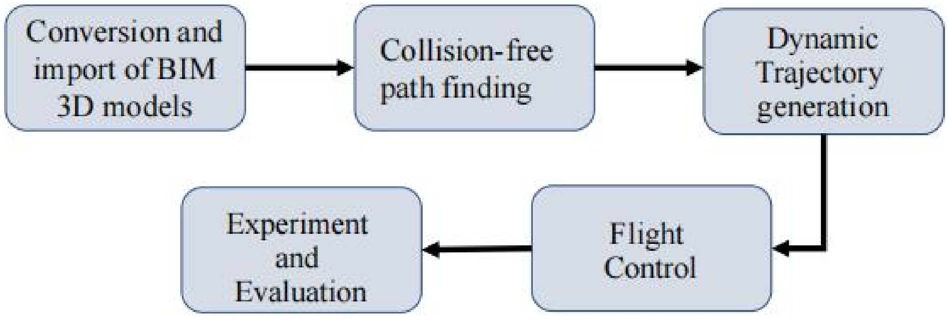

Fig. 6.1. Workflow of the planning phase

6.2.1 Conversion and import of BIM 3D models in Airsim

The platform is the first proposed tool for training operators in the construction environment and with safety considerations. To create the 3D model of a building in the UE platform, a BIM 3D model was exported in .fbx format and introduced to the game engine. The C# scripting language powers the game development in the engine. While the UE platform allows the definition of each subject separately, for this study, the whole building was set as one object. By integrating 4D site-specific temporal and spatial safety information with the UE model, the simulator will allow users to monitor the safety level of each UAV operation or scenario considering the existing plan. The derivation of the flight plan for the semi-autonomous aerial survey is done from the 4D-BIM in the vendor-neutral and open data format IFC or 4D-Software. Based on the 4D-BIM, relevant components are identified as event and demand-oriented by the associated processes analogous to are derived for the UAV-based data acquisition. This is done by deriving the component surfaces of the relevant operations and the corresponding IFC entities (IfcTask, IfcBuldingElement, IfcCartesianPoint). The premise for calculating the POIs is, among others, the configurations of the laser scanner (vertical and horizontal field of view). In this way, it can be ensured that the flight path to be flown provides optimum LiDAR coverage and quality during the data acquisition. The flight plan will then be computed using search algorithms.

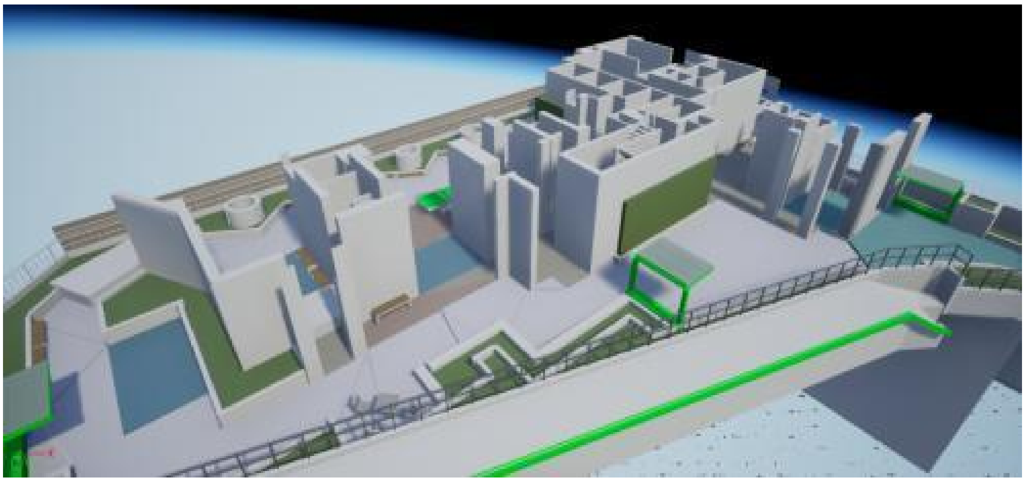

Fig. 6.2. Simulation of UAV-based data acquisition

6.2.2 Collision-free path finding

In this platform, the existing path algorithm can be imported into the system using the ROS system and the connection plug-in of ROS_Airsim. Based on the powerful simulation capability of Airsim, this system can completely simulate the environment when the UAV is flying and verify the performance of the path algorithm at the software level. Therefore, in this research, the focus is mainly on completing the communication links between the software.

After algorithm research, we learned that the RRT method (rapidly expanded random tree) and the PRM method (probabilistic roadmap method) can realize path planning under global obstacle information. In Airsim, the UAV can obtain the simulated signal of obstacles by simulating its attached detector. The PRM method samples points in the map and obtains feasible paths through the sampling points. The RRT method expands nodes from the starting point each time there is a certain probability of expanding to the target point or a random point and finally generates a tree that contains feasible paths. Path tree. Algorithms such as A* can be used to find the optimal path in the current sampling point.

Therefore, in this study, the RRT path planning method and A* algorithm are selected as the path algorithm of the UAV. Through the simulation of Airsim, we found that the algorithm can make the UAV safely carry out path planning flight in the simulated construction site. In addition, Airsim can also simulate radar and computer vision detection methods for path discovery and restore the entire flight process of the drone. This makes the simulated flight results of the simulation system have greater credibility.

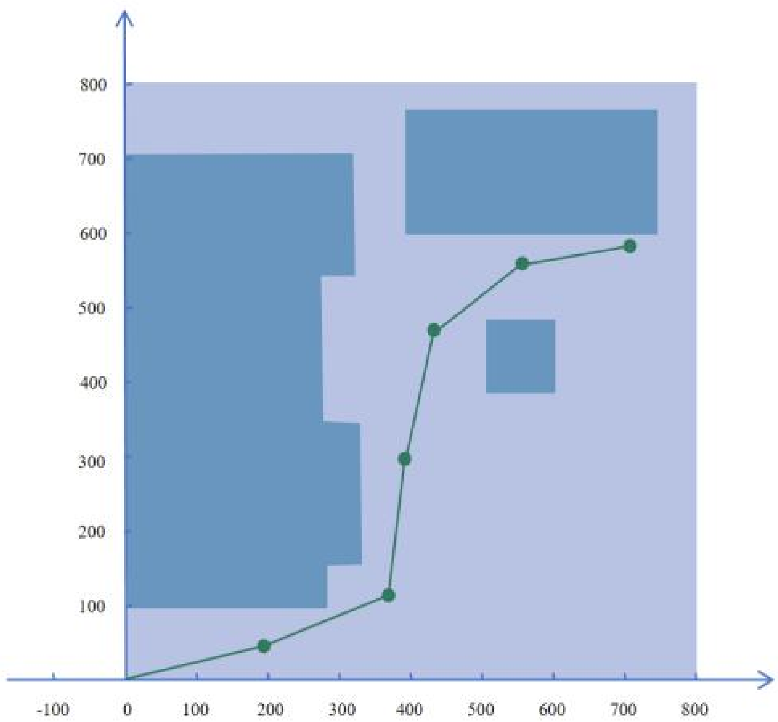

Fig. 6.3 Path finding Algorithm Labeling Diagram

6.2.3 Dynamic trajectory generation

6.2.3.1. Problem statement

In order to generate an approximate trajectory in indoor construction environment, the first thing we need do is to write down the dynamics of our UAV, which describe how the UAV system moves. We use $\mathbf{v}^b$ for velocities of UAVs (body), $\mathbf{J}$; $\boldsymbol{G}$; $\mathbf{R}^{b2g}\mathbf{e}_3$ for inertia matrix, gyro torque and rotation matrix, m; g for mass and gravitational acceleration,and F; τ for control:

$$\begin{aligned} \dot{\mathbf{v}}^b &= g\mathbf{e}_3 - \frac{F}{m}\mathbf{R}^{b2g}\mathbf{e}_3 \\ \mathbf{J}\cdot\dot{\omega}^b &= -\,\omega^b \times \left(\mathbf{J}\cdot\omega^b\right) + \mathbf{G} + \tau \end{aligned} \tag{1}$$

We want the UAV to move one unit of distance in one unit of time, and it should be stationary at both start and finish. These requirements are illustrated in Fig. 6.6. Now the trajectory optimization problem of UAV can be described as

$$\min_{t_0,t_F,x(t),u(t)} J_B\big(t_0,t_F,x(t_0),x(t_F)\big) + \int_t^{t_F} J_P\left(\tau,x(\tau),u(\tau)\right)d\tau$$

subsject to

$$\begin{aligned} &\dot{x}(t) = f\big(t,x(t),u(t)\big) \\ &C_p\big(t,x(t),u(t)\big) \le 0 \\ &C_B\left(t_0,t_f,x(t_0),x\big(t_f\big)\right) \le 0 \\ &x_{\text{low}} \le x(t) \le x_{\text{up}} \\ &u_{\text{low}} \le u(t) \le u_{\text{up}} \\ &x_{0,\text{low}} \le x(t_0) \le x_{0,\text{up}} \\ &x_{F,\text{low}} \le x\big(t_f\big) \le x_{F,\text{up}} \\ &t_{\text{low}} \le t_0 \le t_F \le t_{\text{up}} \end{aligned}$$

Discrete The time t and function x(t) and u(t) to the discrete sets of real numbers

$$
\begin{aligned}
t &\rightarrow [t_0, t_1, \dots, t_N] \\
x(t) &\rightarrow [x_0, x_1, \dots, x_N] \\
u(t) &\rightarrow [u_0, u_1, \dots, u_N]
\end{aligned}
$$

where N denotes the number of grid points. For finding the optimal trajectories $x(t)^*$ and $u(t)^*$, it is reliable to use the scheme of collocation using trapezoid method. To use trapezoid method, therefore, rewrites the discrete form of above problem as an approximate NLP

$$
\min_{\substack{u_0,\dots,u_N \\ x_0,\dots,x_N \\ t_0 \\ t_F}} \mathrm{J}_B\,(t_0, t_F, x_0, x_N) \sum_{k=0}^{N-1} \frac{h_k}{2} \mathrm{J}_P\,(t_k, x_k, u_k)
$$

Subsject to

$$
\begin{gathered}
\frac{h_k}{2}(f_{k+1} + f_k) = x_{k+1} - x_k \\
\mathrm{C}_p\,(t_k, x_k, u_k)\ 0 \\
\mathrm{C}_B\,(t_0, t_N, x_0, x_N)\ 0 \\
x_{low} \le x_k \le x_{up} \\
u_{low} \le u_k \le u_{up} \\
x_{0,\,low} \le x_0 \le x_{0,\,up} \\
x_{F,\,low} \le x_N \le x_{F,\,up} \\
t_{low} \le t_0 \le t_F \le t_{up}
\end{gathered}
$$

where $h_k = t_{k+1} - t_k$ denotes the time interval and $k \in [0, N-1]$.

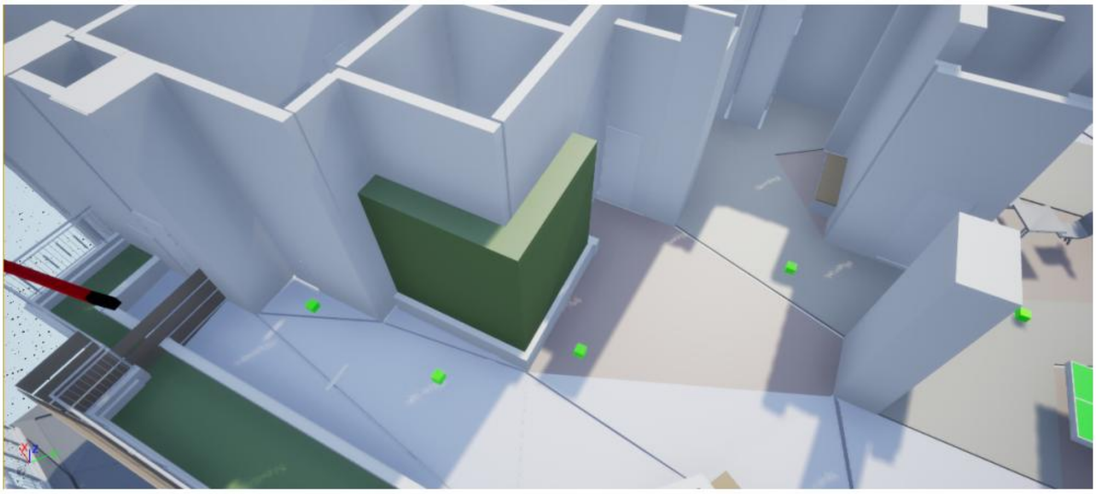

Fig. 6.4.Flight trajectory labeling diagram in 3D BIM models

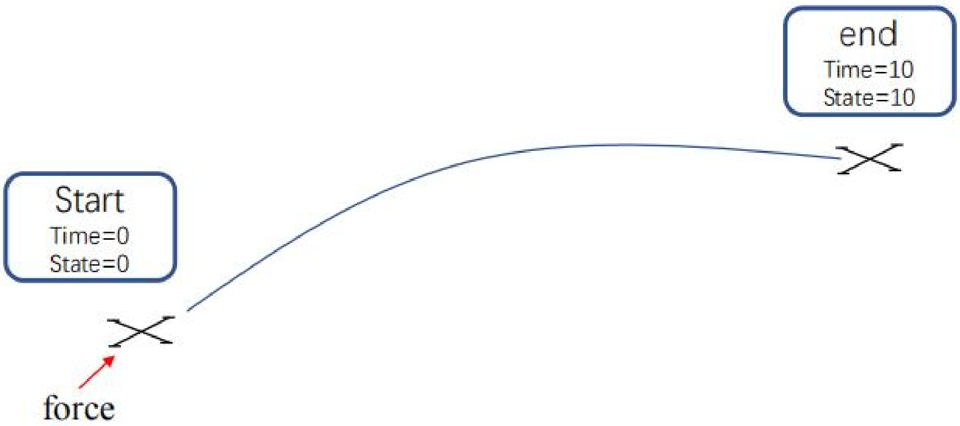

Fig. 6.5. Illustration of the boundary conditions for the UAV, where state denote the position px, py, pz specifically

Remark 1. *It should be noticed that the dynamics system for constrain is converted to collocation constrain which enforces the decision variables are at the collocation points. The details of such transformation come from the integration expression of dynamics system. Assume dynamics and control are linear between grid points, then let it*

$$
\begin{aligned}
\dot{x}(t) &= f\big(t, x(t), u(t)\big) \\
\Rightarrow x(t_{k+1}) &= x(t_k) + \int_{t}^{t_{k+1}} f\left(\tau, x(\tau), u(\tau)\right) d\tau
\end{aligned}
$$

Applying trapezoid method for the integral part of above equation, then we have $\int_{t_k}^{t_{k+1}} f\left(\tau, x(\tau), u(\tau)\right) d\tau = \frac{h_k}{2}(f_{k+1} + f_k)$.

6.2.3.2 UAV Example: Trapezoidal Collocation

Dynamics system (1) is a bit complicated, so let us use a simple model to reduce the complexity of our optimization problem. The parameters see Table IV. To linearize the nonlinear dynamics to get

$$\dot{x}(t) = Ax(t) + Bu(t) + D \qquad (2)$$

where $x = \left[p_x v_x p_y v_y p_z v_z \phi \dot{\phi} \theta \dot{\theta} \psi \psi\right]^{\top}, u = [F \tau_1 \tau_2 \tau_3]^{\top}, D = [0_{5\times1} g 0_{6\times1}]^{\top}$ and

The estimate linear dynamic (2) now can be approximated using trapezoidal quadrature, it yields

$$
\begin{aligned}
&\int_{t}^{t_{k+1}} \dot{x}\,(t) dt = \int_{t}^{t_{k+1}} (Ax(\tau) + Bu(\tau) + D)\, d\tau \\
&\Longrightarrow x_{k+1} - x_k \approx \frac{h_k}{2}(Ax_{k+1} + Bu_{k+1} + Ax_k + Bu_k + 2D)
\end{aligned}
$$

$$
A = \begin{bmatrix}
0 & 0 & 0 & 1 & 0 & 0 & 0 & 0 & 0 & 0 & 0 & 0 \\
0 & 0 & 0 & 0 & 1 & 0 & 0 & 0 & 0 & 0 & 0 & 0 \\
0 & 0 & 0 & 0 & 0 & 1 & 0 & 0 & 0 & 0 & 0 & 0 \\
0 & 0 & 0 & 0 & 0 & 0 & -g\sin(\psi) & -g\cos(\psi) & 0 & 0 & 0 & 0 \\
0 & 0 & 0 & 0 & 0 & 0 & g\cos(\psi) & -g\sin(\psi) & 0 & 0 & 0 & 0 \\
0 & 0 & 0 & 0 & 0 & 0 & 0 & 0 & 0 & 0 & 0 & 0 \\
0 & 0 & 0 & 0 & 0 & 0 & 0 & 0 & 0 & 1 & \tan(\theta)\sin(\phi) & \tan(\theta)\cos(\phi) \\
0 & 0 & 0 & 0 & 0 & 0 & 0 & 0 & 0 & 0 & \cos(\phi) & -\sin(\phi) \\
0 & 0 & 0 & 0 & 0 & 0 & 0 & 0 & 0 & 0 & \frac{\sin(\phi)}{\cos(\theta)} & \frac{\cos(\phi)}{\cos(\theta)} \\
0 & 0 & 0 & 0 & 0 & 0 & 0 & 0 & 0 & 0 & 0 & 0 \\
0 & 0 & 0 & 0 & 0 & 0 & 0 & 0 & 0 & 0 & 0 & 0
\end{bmatrix}
\qquad
B = \begin{bmatrix}
0 & 0 & 0 & 0 \\
0 & 0 & 0 & 0 \\
0 & 0 & 0 & 0 \\
0 & 0 & 0 & 0 \\
0 & 0 & 0 & 0 \\
\frac{1}{m} & 0 & 0 & 0 \\
0 & 0 & 0 & 0 \\
0 & 0 & 0 & 0 \\
0 & 0 & 0 & 0 \\
0 & \frac{l}{I_x} & 0 & 0 \\
0 & 0 & \frac{l}{I_y} & 0 \\
0 & 0 & 0 & \frac{1}{I_z}
\end{bmatrix}
$$

Here, we use a common cost function. It is an integral of control efort squared:

$$\min_{u(t),x(t),t_0,t_F} \int_{t}^{t_f} u\,(\tau)^2 d\tau$$

This integral also can be approximated using trapezoidal quadrature as

$$\min_{\substack{u_0,\dots,u_N \\ x_0,\dots,x_N \\ t_0 \\ t_F}} \sum_{k=0}^{N-1} \frac{h_k}{2}\left(u_{k+1}^2 + u_k^2\right)$$

Let us consider the additional constrains including state and control, boundary constrains. It should be note that there is an assumption, that is, the UAV can fly freely so the path constraints does not exist in our optimization problem. For the purpose of simulation, configuring state and control limitation, which is

$$\begin{bmatrix} -\infty \\ -\infty \\ -\infty \\ 0/\mathrm{s} \\ 0/\mathrm{s} \\ 0/\mathrm{s} \\ -40^\circ \\ -40^\circ \\ -40^\circ \\ -40^\circ/\mathrm{s} \\ -40^\circ/\mathrm{s} \\ -40^\circ/\mathrm{s} \end{bmatrix} \le x_k \le \begin{bmatrix} \infty \\ \infty \\ \infty \\ 2\mathrm{m/s} \\ 2\mathrm{m/s} \\ 2\mathrm{m/s} \\ 40^\circ \\ 40^\circ \\ 40^\circ \\ 40^\circ/\mathrm{s} \\ 40^\circ/\mathrm{s} \\ 40^\circ/\mathrm{s} \end{bmatrix} \quad \text{for } \forall k$$

Configuring boundary limitations, which are

$$x_0 = [000000000000]^{\mathsf{T}},$$
$$x_N = [101010000000000]^{\mathsf{T}}.$$

Finally, we need to solve above NLP.

TABLE IV Parameters

Mass (m)(kg)	1.4	Moment of inertia(I_x, I_Y, I_2)(kg/m^2)	[0.05 0.05 50.24]
Wheelbase (l)(m)	0.56	Attitude angle (ϕ, θ, ψ)	$-40 \sim 40$
Velocity of attitude angle $(\dot{\phi}, \dot{\theta}, \dot{\psi})(\circ/\mathbf{s})$	$-40 \sim 40$	Torque(τ_1, τ_2)(N. m)	-6.25 ~ 6.25
Pull force (F)($\mathbb{N}$)	$0 \sim 43.5$	Torque(τ_3)(N. m)	$-2.25 \sim 2.25$
Velocity of body (v_x, v_Y, v_Y)(m/s)	0~2		

6.2.3.3 Constructing a standard form of NLP

In section 6.2.3.2, we make an example explaining the trajectory optimization of UAV. In this section, our aim is to construct a standard form of above NLP. The reason is to make program conveniently.

$$\min_{\mathbf{Z}} J(\mathbf{Z}) \quad \text{subsject to}$$
$$\mathbf{f}(\mathbf{Z}) \leq 0$$
$$\mathbf{g}(\mathbf{Z}) = 0$$
$$\mathbf{Z}_{low} \leq \mathbf{Z} \leq \mathbf{Z}_{up}$$

We now known the decision variable is $\mathbf{Z} = [t_0, t_F, x_k^\top, u_k^\top]^\top$, where $\mathbf{Z} \in \mathbb{R}^{2+N(n+m)}$.

It should be noted that each $k \in N$ and hence $[x_1^\top, \dots, x_N^\top]^\top \in \mathbb{R}^{Nn}$ and $[u_1^\top, \dots, u_N^\top]^\top \in \mathbb{R}^{Nm}$.

6.2.4 Flight control system

The PID control, widely used in the automatic system field, usually requires a demanding skills on choosing parameter. Therefore, a valid tool called contraction theory was utilized for executing the generated trajectory in this thesis, it has several advantages to analysis the stability of UAV system so that adjusting parameters has been changed easier. The more detailed description on contraction theory can be found in [177,178] and in this section the main design process and some basic conception are provided to illustrate how to track planned trajectories. The definition about contraction matrix is a symmetric and uniformly positive matrix $G(x; t)$ satisfying

$$\frac{d}{dt}\langle\delta_x, \delta_x\rangle_G \leq -\beta\langle\delta_x, \delta_x\rangle_G$$

where β denote contraction rete, and the notation $\langle\delta_x, \delta_x\rangle_G = \delta_x^{\mathsf{T}} G(x, t)\delta_x$. The δx is a variation around any given trajectory in a control system, which means the planned trajectory denoted by x^* can be connected to the actual trajectory x by a curve produced in the manifold of that system. For a simple linear case, the curve should be a straight line, so δx can be approximated as $x - x^*$: In this chapter, we use the linearized model of UAV and design contraction theory-based controller to achieve the track purpose. A double-loop control framework was taken and it is shown in Fig. 6.6, where inputs $\mathbf{p}^*$; $\mathbf{v}^*$ generated from the previous trajectory planning.

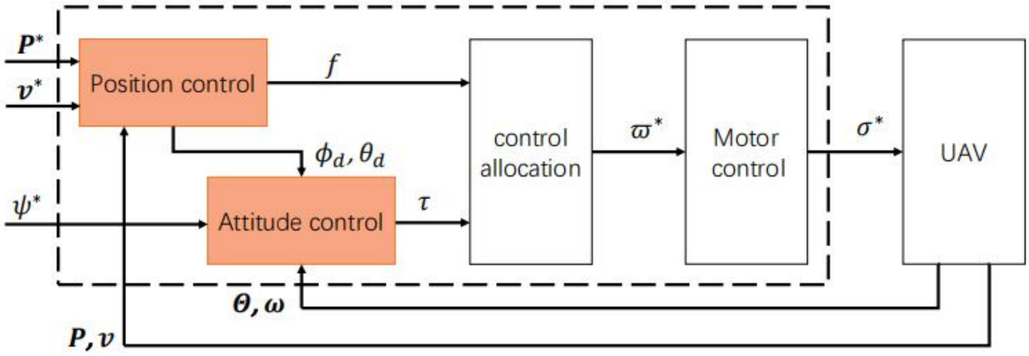

Fig. 6.6 Workflow of flight control

6.2.4.1 Position Control

To execute the desired path, position control is used to create the desired attitude. Meanwhile, it forms an outer loop feedback, by which the thrust f reach the module of control allocation to further produce rotor command to release voltage for control the rotation of four rotors. Finally, the motion along the perpendicular direction of the UAV was executed.

Consider the altitude model around equilibrium point

$$\dot{p}_z = v_z, \quad \dot{v}_z = g - \frac{f}{m} \tag{3}$$

The z-axis direction control on Earth coordinate is

$$f = f^* + mg + m(\lambda_{pz}(p_z - p_z^*) + \lambda_{vz}(v_z - v_z^*))$$

where, the parameters $\lambda(\cdot)$ was choose as an appropriate value to lead the stability. We given a simple derivation about the controller, for avoiding repeating of derivation, only to take the altitude control as an example. Taking the diferential dynamic of system (3), it yields

$$\dot{\delta}_{p_z} = \delta_{vz}, \quad \dot{\delta}_{v_z} = g - \frac{\delta_f}{m}$$

which can be denoted by matrix form

$$\begin{bmatrix} \dot{\delta}_{p_z} \\ \dot{\delta}_{v_z} \end{bmatrix} = \begin{bmatrix} 0 & 1 \\ 0 & 0 \end{bmatrix} \begin{bmatrix} \delta_{p_z} \\ \delta_{v_z} \end{bmatrix} + \begin{bmatrix} 0 \\ g \end{bmatrix} + \begin{bmatrix} 0 \\ -\frac{1}{m} \end{bmatrix} \delta_f \qquad (4)$$

So, to choose δf to make equation (4) negative, one selection is $\delta f = m(g + \lambda_{pz}\, \delta_{pz} + \lambda_{vz}\, \delta_{vz})$. The actual controller can be written as

$$f = f^* + \int_0^1 \delta_f \, ds = f^* + m(g + \lambda_{pz}\delta_{pz} + \lambda_{vz}\delta_{vz}))$$

Consider the horizon model around equilibrium point

$$\dot{\mathbf{p}}_h = v_h, \quad \dot{\mathbf{v}}_h =- gA_\psi \Theta_{h_d}$$

Similarly, the x-axis and y-axis direction control on Earth coordinate are

$$\Theta_{h^d} = \Theta_h^* + g^{-1}A_\psi^{-1}(\lambda_{p^z}(p_z - p_z^*) + \lambda_{v^z}(v_z - v_z^*))$$

The desired attitude Θ_{hd} reaches the module of attitude control, leading to the desired torque, which further provide data to forms the feedback control in the inter loop.

6.2.4.2 Attitude Control

The goal of attitude control ensures that desired attitude $\Theta_d = [\Theta_{h_d}^{\top} \psi_d]^{\top}$ can be tracked, thereby converging to the desired path of UAV. In this chapter, Θ_{hd} is given by the module of position control and ψ_d is a constant given by control panel desired path of UAV. In this thesis, Θ_{hd} is given by the module of position control and

ψd is a constant given by control panel.

Consider the attitude model around equilibrium point

$$\dot{\Theta} = \omega, \quad \dot{\omega} = \tau$$

Similarly, the required torque that adjusting attitudes is

$$\tau = \tau^* - \lambda_\Theta(\Theta - \Theta_d) - \lambda_\omega\big(\omega - (\Theta - \Theta_d)\big)$$

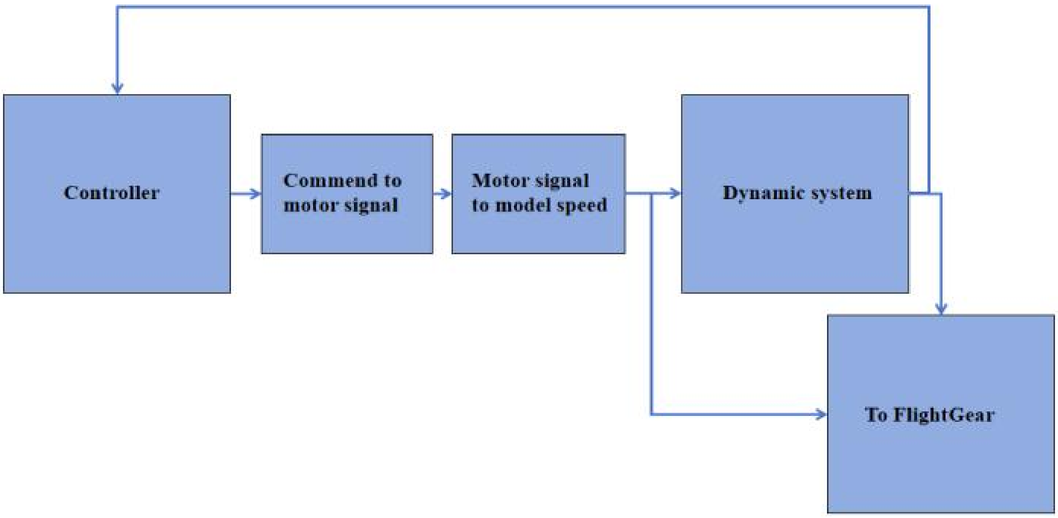

Fig. 6.7 Workflow of flight control

6.3 Experiment and Evaluation

6.3.1MATLAB simulation

The MATLAB/Simulink simulation was designed to ensure the physical feasibility of the trajectory and provide convenient visualization. The Simulink simulator was created based on the desired states, true states, flight controller.and dynamic model referring to Fig. 6.8. The desired states were published from the trajectory generator

(Section 6.2.3) at a frequency of 200 Hz, and the true states were obtained from numerical integration using the Ode3 solver. The flight controller was programmed following the contraction-based controller described in Section 6.2.4, where the gain parameters of the flight controller were tuned manually to obtain the best performance.

In comparison to PID controller, the contraction-based controller exhibits advantages in controlling the fight of unmanned aerial vehicles (UAVs), as it effectively mitigates position errors in x, y, and z coordinates. This is based on the results of the UAV trajectory in the simulation shown in Fig. 6.8(b), 6.8(c), 6.8(d). According to the specific data given in Fig. 6.8, it can be concluded that during this simulation process, desired_position is 17.32 units in length, PID_position is 19.05 units in length, and contraction_position is 18.18 units in length. And at position XYZ, contraction_position has smaller perturbation performance than PID_position, especially at position Z. The specific data is shown as Table V.

Therefore, based on experimental data, the new algorithm improves energy efficiency optimization and real-time path update efficiency by 5% from the perspective of simulation experiments.

TABLE V Contraction_position and PID_position data contrast

Term	Contraction_position	PID_position	Unit
Average response speed	0.188	0.2	s
Stability error	0.24	0.5	/
Actual flight distance	18.18	19.05	/

6.3.2 Display of multi-data results of flight simulation experiments

In order to evaluate the performance of the collaborative software system and determine the success of UAV simulation output data and calculations, the system was tested using the actual construction BIM model as the simulated site. Fig. 6.8 and Fig. 6.9 is a recorded image of the collaboration software system. As expected, in the collaborative software, when the UAV performs a simulated flight in Airsim, its flight control algorithm, and path planning algorithm can produce the same effect as set, and the flight data required for the experiment can be transmitted synchronously in real-time into Matlab for use with Simulink.

Therefore, the collaborative system has met the basic requirements of the initial development, which can simulate the flight state of the UAV in the indoor environment to the greatest extent and can import the improved algorithm and verify it.

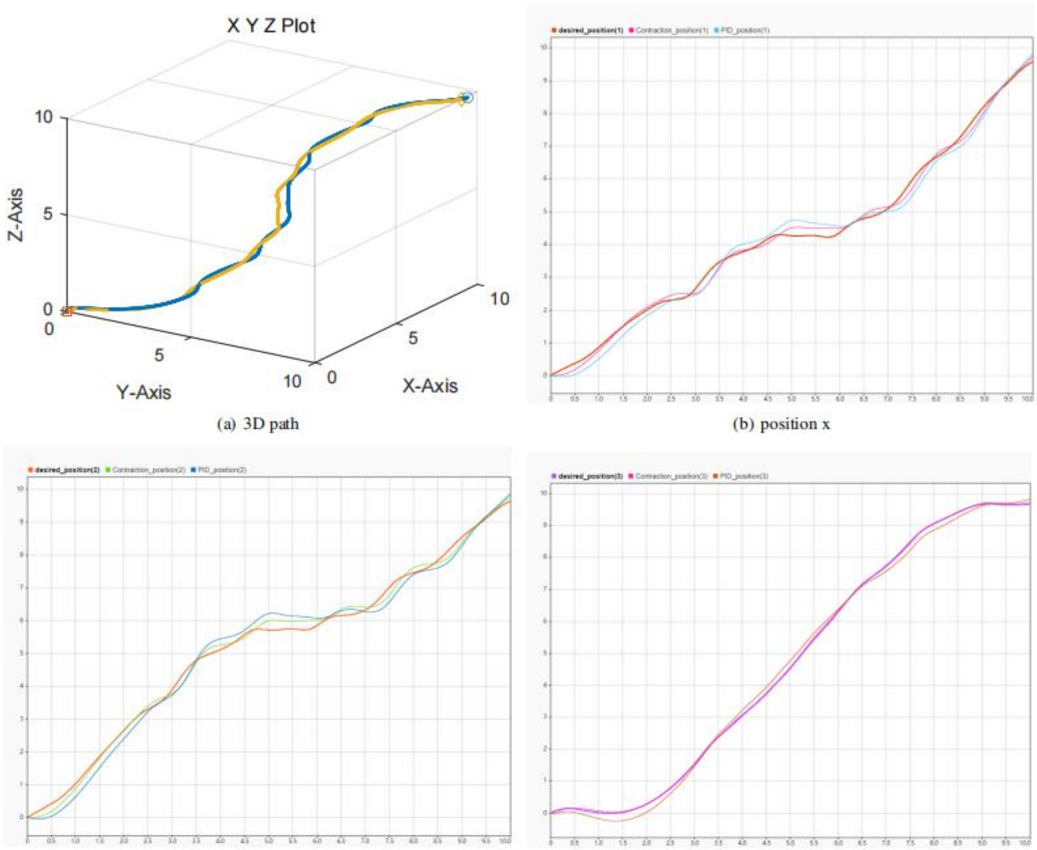

(a) 3D path (b) position x

(c) position y (d) position z

Fig. 6.8. Simulation Result

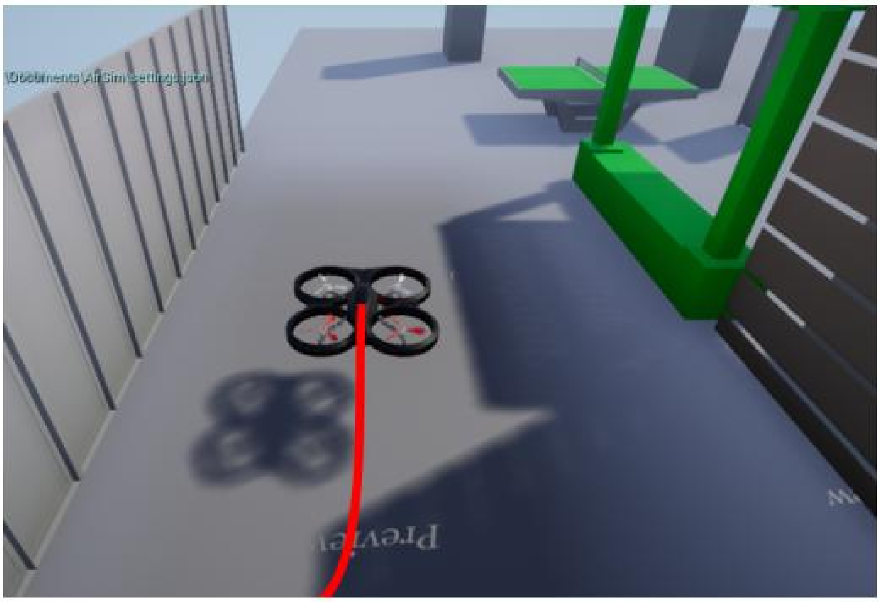

Fig. 6.9. 3D scene simulation of UAV flight with trajectory supported by Airsim software

6.4 Chapter summary

This chapter describes developing and testing a flight simulation system for a collaborative indoor environment. The system mainly consists of Airsim software based on UE4 and Simulink based on Matlab. The Airsim software is responsible for simulating the indoor environment based on the BIM model and the simulated flight of the drone. Simulink is responsible for adjusting the flight control algorithm and obtaining the experimental data of the simulated flight. The ROS software system is responsible for linking these two software platforms. Airsim can use its powerful simulation capabilities to improve the simulation of the flight simulation experiment environment and UAV flight by importing the BIM model and providing a guarantee for the simulation experiment results for reference in subsequent actual aircraft experiments. At the same time, we use ROS as a tool to import the UAV path planning algorithm and transfer the flight data from Airsim to Matlab. In Simulink, we developed a new UAV flight control algorithm and conducted flight simulation experiments through Airsim for performance verification, and finally got the data and

results. This algorithm improves the flight control of UAVs in indoor building environments, improves the accuracy of flight routes, and reduces the extra energy required by UAVs in complex environments to ensure their flight attitude and other factors consumption. The system is an improvement and integration of existing UAV simulation software and UAV development software. Compared with other methods using a single simulation software, the method proposed in this study is more accurate and reliable. The feasibility of the developed system can be illustrated by experimental verification using the newly developed algorithm. Improving drones flying in indoor construction environments through simulation software is a new development in smart building construction. Based on this system, drones can participate in various construction tasks faster. In addition, the UAV simulation system developed by this research institute can also be embedded into the building digital twin system in the future, making the function of the building digital twin system more perfect and powerful.

Of course, this needs further research and exploration. In future work, the first is to combine the simulation experiment with the real machine experiment to provide more reliable and sufficient experimental data. A more powerful experimental platform is needed to carry out simultaneous experiments of simulation and real machines. Therefore, future research must develop a software platform that can simultaneously conduct real UAV flight experiments while conducting simulated flight experiments at the construction site that provides the BIM model.

Chapter 7. Cost-effective collaborative framework between UAV and robot for recycling construction waste

Construction and demolition waste (CDW) significantly impedes the progress, productivity, and safety of construction activities. Traditional CDW treatment methods, which rely heavily on manual labor, are inefficient and resource-intensive. This chapter introduces a cost-effective, autonomous recycling system for construction waste, leveraging the combined capabilities of automated robots and unmanned aerial vehicles (UAVs). By integrating neural network-based computer vision technology, UAVs and robots can identify construction waste in real-time within complex construction environments. Additionally, coordinate positioning technology enables precise localization and collection of waste by robots, the improved flight algorithm enables the drone to fly safely and smoothly in indoor environments. Unlike conventional ground-based robots, drones offer a comprehensive aerial perspective, enhancing the detection and localization of waste that might otherwise be missed. Field tests demonstrate that this UAV-robot system mitigates the limitations of purely vision-based robots and provides a more effective waste management solution. This innovative system not only promises significant improvements in automated waste recycling but also lays the groundwork for broader applications in construction automation, potentially revolutionizing the industry.

7.1 Introduction

Construction waste is defined as garbage generated from construction activities and abandoned whether or not processing has been adopted [179]. One of the traditional ways to handle construction waste is through landfill. This method generally consumes tremendous land resources and may be harmful to the entire ecosystem in toxic industrial products. Dealing with construction waste efficiently and environmentally has become an essential issue in many countries and regions such as the United States, China, and South Korea [180]. Such an environmental issue is especially urgent for Hong Kong. According to the report from the Environmental Protection Agency of Hong Kong [181], about 25% of all kinds of waste are construction wastes, and lands available for landfill may be exhausted in the next few decades. Thus, it is necessary to explore more efficient ways to deal with construction waste. Generally, there are five strategies in Hong Kong to handle issues of construction waste [182], including “avoid”, “minimize”, “recycle”, “treat” and “dispose”. Among these five strategies, “avoid” and “minimize” are two top-ranking strategies according to their desirability. These two strategies may solve or alleviate construction waste from the source and save the further cost of treatment. However, due to the current level of onsite construction management, avoiding construction waste is ideal while efficient minimization is also comparatively difficult. For other strategies like “treat” and “dispose”, additional cost is usually needed, and direct disposal may lead to severe environmental issues in extreme cases. Thus, the “recycle” strategy is an optimal option compared to the other four strategies, which may balance efficiency and cost.

From the perspective of project management, construction waste generated during the construction process would have a great impact on construction site environment [183]. For current construction site management, construction wastes are regularly cleared and transported. However, construction wastes are still available during the construction process, which makes them inevitable. Various construction wastes, such as broken bricks, nails, concrete, etc., may cause harm to workers on construction site [184]. At the same time, these wastes would also affect the construction status of workers, requiring them to spend extra energy to pay attention and avoid them during the construction process [185,186]. These factors could affect the safety management and schedule management of construction. Given the above, timely recycling of construction wastes on the construction site is critically necessary and should be investigated.

With the recent concepts of information-based automated construction, robots have a greater advantage in recycling on-site construction wastes as compared with traditional methods (e.g., manpower) [187]. However, most construction sites are still recycling waste through manual working processes (e.g., workers). Relying on on-site workers or allocating extra manpower to dispose of construction waste would cause inefficient manpower resources and unsatisfactory recycling processes [188].

The construction site environment is very complex and changeable [189]. As such, it is difficult for automated robots to complete the recycling work independently when a fixed path cannot be set. Although many researchers have improved construction waste recycling robots. For example, Wang et al. [190] improved the computer vision function and path planning function of construction waste recycling robot. Xiao et al. [191] developed of an automatic sorting robot for construction and demolition waste and use of height maps and near-infrared (NIR) hyperspectral images to locate the ROI of objects and to do online statistic pixel-based classification in contours. Chen et al. [192] developed a novel simultaneous localization and mapping (SLAM) method for high efficiency and high accuracy robot localization.

However, these studies also demonstrate that researchers usually focus on how robots detect CDWs to improve automated recycling robots. For this reason, this study chose to improve the automatic construction waste recycling robot through other external support.

Therefore, this chapter proposes a combined system based on drones and automated construction waste collection robots. This is actually a way to improve the detection methods and capabilities of robots. Compared with ground robots, drones that work in the air have a better field of vision, and can be used as the "eyes" of automated robots to quickly identify and locate garbage, and plan the work path in real-time. In the proposed system, drones and robots need to use computer vision technology to identify construction waste, and can transmit positioning coordinates through image positioning technology. Therefore, Yolov3 training is used to create a dedicated training data set to recycle the system. It can convert real-time environmental information into neural activities to ensure efficient recognition.

The rest of this chapter is as follows: Section 7.2 explains the design of the system, including the hardware equipment information of the robot and UAV and the target detection and positioning method. Section 7.3 evaluates the performance of the system, and then Section 7.4 discusses the conclusions of this research and future works.

7.2 Collaboration between robot and UAV

The construction waste recycling system faces two main challenges. First, although drones can help robots obtain target information more quickly and comprehensively, it is necessary to convert the target location information from the drone's perspective into coordinate positioning information that the robot can understand. Secondly, in this system, the robot completes the final recycling operation, which requires the robot to be able to recognize all kinds of construction waste in real-time. To meet these challenges, it is necessary to refine the robot's hardware and software in more detail and choose a coordinated conversion method that can meet the conditions of use.

7.2.1 Robot system

A four-wheel-drive robotics platform is used in the project. this robotics platform is specially tailored for outdoor applications such as the construction site where terrain maneuverability is required. It is configured with large torque stepper motors, 8-inch pneumatic wheels, and high chassis. This design ensures a maximum carrying capacity of 50kg while running at full speed.

On the other hand, the robot utilizes ROS (Robot Operating System) to organize all the SLAM (Simultaneous localization and mapping) and navigation functions. With all the data from the mounted sensors, the running ROS can locate the robot and continuously conduct a path planner to find an optimal route and generate surrounding environment models.

An Integrated PC is specialized in AI computing and vision-based solutions. Plenty of sensors are adopted and mounted on the proposed platform, including four proximity sensors, three RGB cameras, one 2D Lidar, one depth camera, and one global positioning system (GPS) module. All these sensors and the Integrated PC constitute the navigation, guidance and control system and endow the robotics platform with intelligence. The ROS robot key node relationship and vision detection system are shown in Fig. 7.1 and the robot vision detection system is shown in Fig. 7.2.

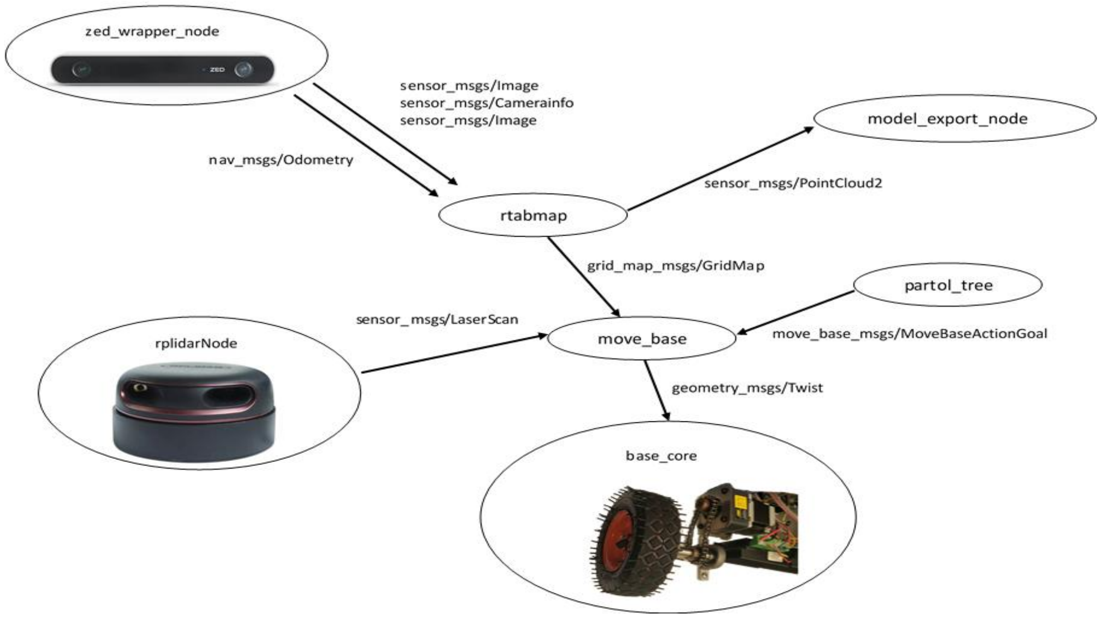

Fig. 7.1 Key node relationship of ROS robot

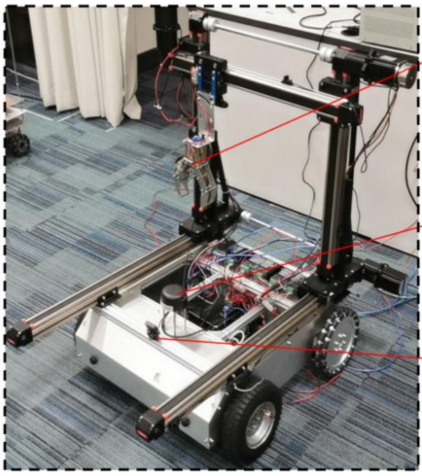

Fig. 7.2 Robot Vision Detection System

7.2.2 UAV system

The construction site is a complex environment. As a result, the drones working in this environment must be small and portable. In order to cope with increasingly stringent drone aviation control regulations in Hong Kong, this thesis chooses the DJI (Da-Jiang Innovations) Mavic drone as UAV hardware equipment of the combined system. To further use the UAV to identify and locate the construction waste, it is necessary to use computer vision technology to identify the video pictures taken by the UAV and calibrate the related camera parameters of the UAV. After obtaining the correlation matrix information data, the following section will discuss the conversion formula of pixel coordinates and world coordinates for subsequent positioning.

As a light civilian drone shown in Fig. 7.3, the DJI Mavic's single maximum flight time can basically meet the requirements of automatic waypoint flight in this project. Otherwise, the drone is equipped with the newly developed flight control algorithm in the previous chapter. This algorithm improves the drone's stability and navigation within confined and complex spaces.

Fig. 7.3. Drone flying on construction site

7.2.3 Collaborative framework between robot and UAV

In this research, the UAV and the robot are combined into a complete cooperative system by using the computer as the ground base station. The cooperative framework is shown in Fig. 7.4 and schematic diagram is shown in Fig. 7.5. In this combined system, the computer will act as the central station of the cooperative system to connect the drones in the air with the robots on the ground.

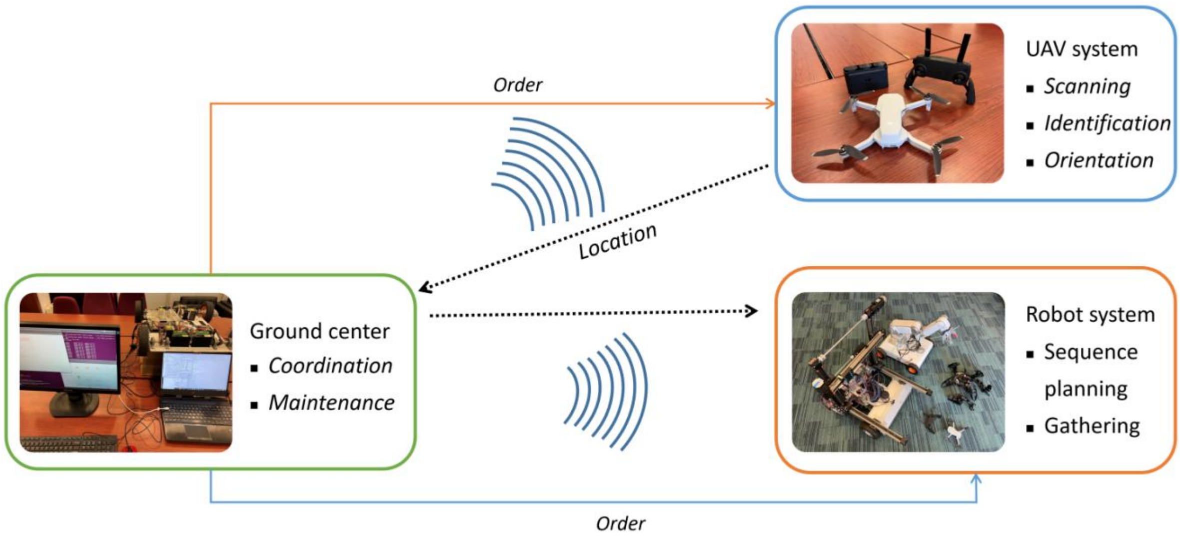

Fig. 7.4. Collaborative framework between UAV and robotics

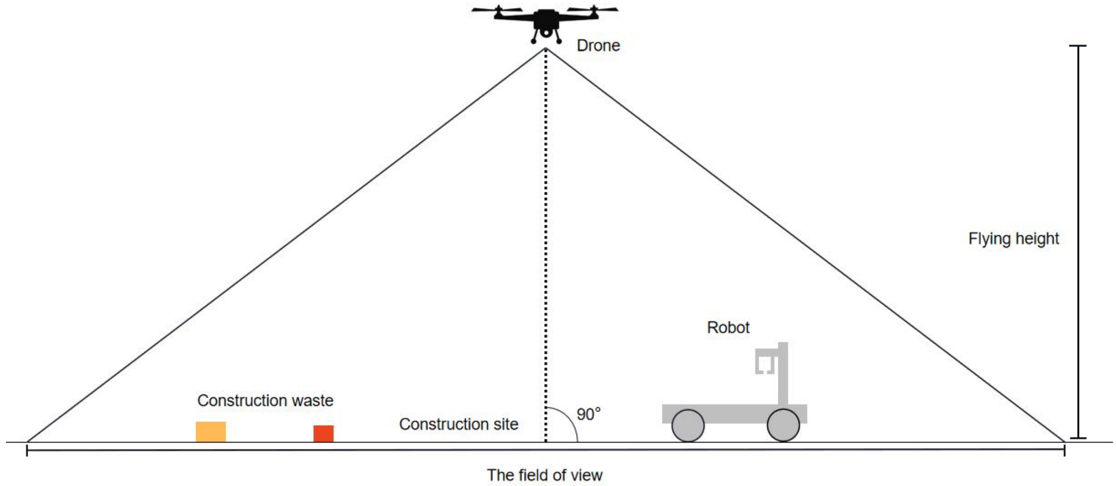

Fig. 7.5. Schematic diagram of the drone-robot collaboration system

According to the preceding section, the GPS is widely used for device positioning in the UAV and robot collaboration framework relying on its powerful functions and economical equipment cost. However, the civil GPS has an absolute error of 2.5-5 meters inaccuracy [193], which reduces the precision of cooperation work. To make up for such limitation of the civil GPS, it is necessary to use a new positioning method.

The new method contains three main steps. In the first step, automatic waypoint flight of the UAV is arranged, which will obtain the GPS coordinates of each waypoint shooting point shown in Fig. 7.6. Take the current DJI UAV as an example, this function can be realized by extracting GPS information from the photo taken by the automatic positioning waypoint. The accuracy of the GPS information of coordinates does not need to be particularly precise. This is because the GPS information is only used as a reference coefficient.

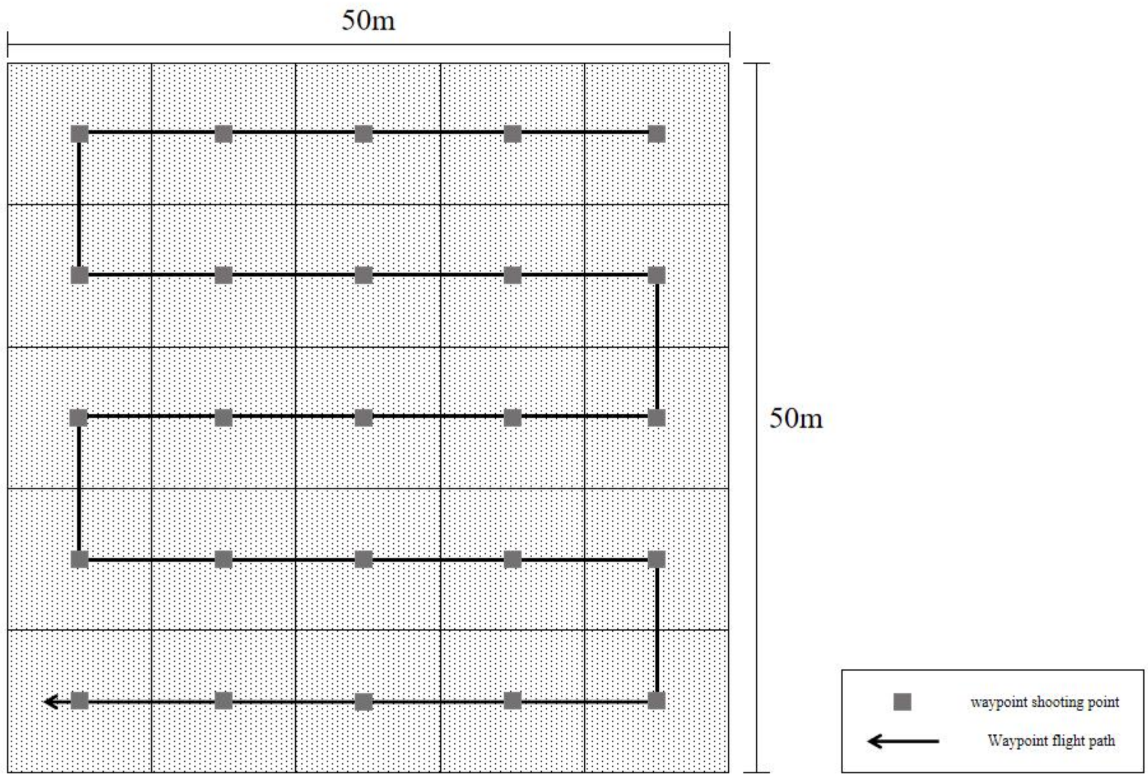

Fig. 7.6. UAV automatic waypoint flight

Furthermore, the indoor environment is insufficiently spacious for the drone to fly in a straight line in accordance with the automatic cruise path. Consequently, obstacles on the flight path are likely to affect the drone's data collection. To mitigate the impact of this issue, the enhanced flight control algorithm, as previously outlined, can be employed in conjunction with the obstacle avoidance sensor on the DJI drone to address the interference. Furthermore, the drone equipped with the new flight control algorithm can also be utilized to assess the efficacy and viability of the flight control algorithm in subsequent field trials of the collaborative framework.

Along with obtaining GPS information data, the number of detected construction waste based on computer vision techniques can also be determined, which can be used to draw a heat point map. Such heat-point map will provide main distribution information of construction waste, as shown in Fig. 7.7. As a result, the cleaning robot can plan a cleaning route in advance, which may effectively boost the entire cleaning efficiency.

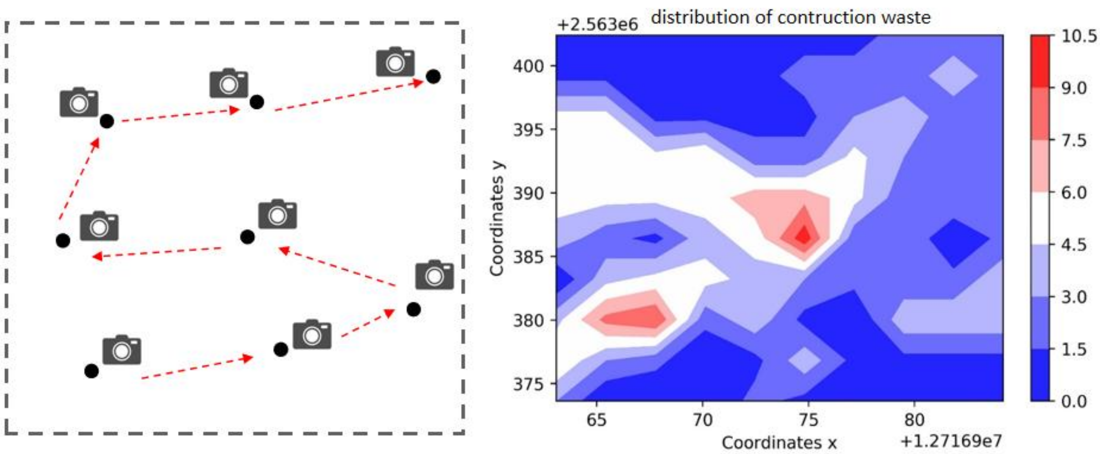

Fig. 7.7. Waypoint hotspot map for construction waste

For the second step, the drone will choose the most densely distributed area to hover over it according to the obtained the GPS coordinates. For the third step, the cleaning robot on the ground will enter the surveillance area where the drone is hovering. The hovering drone will take pictures at a certain interval. Both construction waste and cleaning robot will be detected in the picture. As a result, the cleaning robot will get the direction information of waste from the hovering UAV. In addition, according to the calibration of the drone camera lens, the Pixel position coordinates of the location of the robot and construction waste can be converted to real world position, which will also provide the approximate distance between the robot and construction waste. Such information will help the cleaning robot determine whether the battery is sufficient to accomplish the cleaning task. Since both robot and construction waste are simultaneously detected in the taken picture, the relative direction from the robot to construction waste can be determined without knowing the exact GPS coordinates. Thus, the limited precision of civil GPS information will not affect the normal working of the entire system. More details will be described in details in the following sections.

7.3 Experiments and Evaluation

7.3.1 Vision program

Considering the overall balance between accuracy and efficiency of detection, a deep learning convolutional neural network called YOLO is used [194]. The third version of YOLO is applied, which will be abbreviated as YOLOv3 throughout the whole thesis. In this section, the related training, testing, and application process of the model will be introduced. A large number of diversified training and test data are established to ensure the reliability and stability of the model. After the model is validated, it is used for real-time videosto ensure the feasibility of the model in the real-time detection process.

There are many types of construction waste. To achieve an efficient test on the proposed system, bricks and nails are used as prototype targets for target detection. The underlying theories of detection for other types of construction waste are similar to the chosen two types of waste, which will not affect the overall reliability of the model.

7.3.1.1 Data Collection and Description

The data set for this study comes from aerial videos of drones in different construction site scenarios. The videos that make up the data set vary greatly in quality, height, and scenes. They contain images of common construction waste from various construction site environments in the real world and provide us with various objects in different occlusions and different background environments. In addition, the quality of light during the shooting also varies with scene factors. This allows us to create a training data set that fits real-world conditions very well.

Our training data comes from videos marked as containing construction waste. From this part of the data, we further selected all video clips that seemed to contain scraps such as different kinds of nails and bricks. Part of the reason for this is to reduce the scope of waste types to a manageable scale. At this point, each video is sampled at a rate of 30 frames per second to generate images that can be annotated in preparation for use in the learning model. This sampling produced more than 6000 frames, which were searched for the best examples of construction waste and then labeled. The final training data set consists of 2000 images.

Fig. 7.8. Prepossessing the training datasets

7.3.1.2 YOLOv3 Model Training and Testing

After collecting the data, we manually annotated the data using the graphical image annotation tool. The prepossessing of the prepared data set is shown in Fig. 7.8. Then we saved the file in the specified directory and trained the model using YOLOv3. To ensure the reliability of the model, we set the stage for YOLOv3 to 20,000 iterations. The result shows that the model's mean average precision for brick and nail is 95%. We tested the model repeatedly with video and images. Typical results are shown in Fig. 7.9. Using the YOLOv3 model, the UAV camera can accurately identify the target object and provide an accurate relative position. Hence, we can convert the relative position coordinate taken by the UAV into the absolute position of the object and control the robot to pick it up. The specific coordinate conversion method will be explained below.

Fig. 7.9. Video frame and object detection results

7.3.2 Coordinate transformation and positioning between robot and UAV

With the accomplished real-time target detection on images, the next step is to obtain the accurate position information of the target. As mentioned above, the first step is to convert the pixel coordinates of the located garbage and the robot itself into world coordinates through coordinate system conversion formula [195]. After obtaining the world coordinates of both parties, the specific distance and angle vector of the locked construction waste is calculated by the vector calculation formula and transmitted to the robot.

7.3.2.1 Coordinate transformation process

The image sensor of the DJI Mavic drone camera uses 1/2.3 inch CMOS, and its effective pixels are 12 million, which can fully meet the requirements for aerial target recognition of UAVs. A well-trained YOLOv3 model can detect object classes and coordinates of pixel boxes in drone footage [196] However, the bounding box of the detected object cannot be easily used for localization.

The first reason is the drone footage needs calibrate. There are four coordinate systems in the camera [197], namely: world coordinate system (Xw, Yw, Zw), camera coordinate system (Xc, Yc, Zc), image coordinate system (x, y), and pixel coordinate system (u, v). After calibrating the camera to obtain the internal and external parameter matrix, these coordinates can be transformed. Therefore, it is necessary to calibrate the drone camera.

By using Matlab camera calibration experiment method, we can find the internal and external parameters of the camera [198], as well as the distortion parameters. Using the calibration method as Fig 7.10 shown, we obtained the internal and external parameters of the UAV camera, as shown in the following formulas(1).

$$K=\begin{bmatrix}1/dx & 0 & u_0\\ 0 & 1/dy & v_0\\ 0 & 0 & 1\end{bmatrix}\begin{bmatrix}f & 0 & 0\\ 0 & f & 0\\ 0 & 0 & 1\end{bmatrix}=\begin{bmatrix}699.06 & 0 & 327.60\\ 0 & 698.05 & 245.64\\ 0 & 0 & 1\end{bmatrix} \tag{1}$$

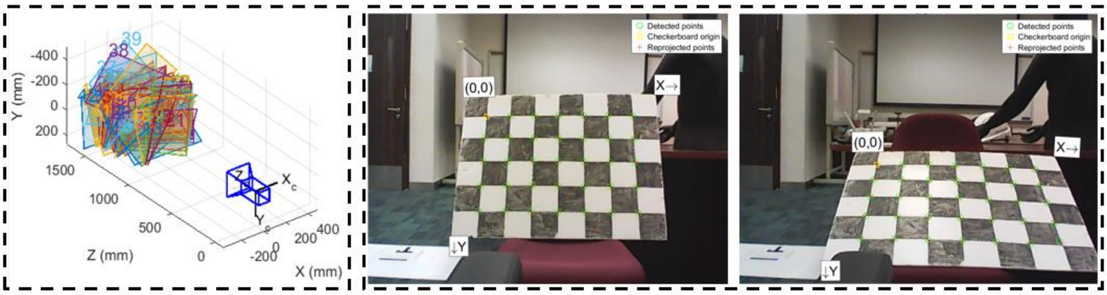

Fig. 7.10. Conveniently calibrated with chess-board process

After that, the transformation formula Eq. (2) is used to convert the pixel coordinates and the world coordinates [199]. In Eq. (2), the first matrix on the right is the camera internal parameter matrix, and the second matrix is the camera external parameter matrix.

$$z\begin{bmatrix}u\\ v\\ 1\end{bmatrix}=\begin{bmatrix}1/dx & 0 & c_x\\ 0 & 1/dy & c_y\\ 0 & 0 & 1\end{bmatrix}\begin{bmatrix}f & 0 & 0\\ 0 & f & 0\\ 0 & 0 & 1\end{bmatrix}\begin{bmatrix}r11 & r12 & r13 & t1\\ r21 & r22 & r23 & t2\\ r31 & r32 & r33 & t3\end{bmatrix}\begin{bmatrix}X_W\\ Y_W\\ Z_W\\ 1\end{bmatrix} \tag{2}$$

The second reason is the output of the YOLOv3 detection needs to be projected from the drone view into the orthogonal grid system, this mathematical transformation can be determined by the pixel position of the centroid point of the bounding box (in the view of the drone) of waste and robot. For pixel coordinates, with the uppermost left pixel of the image serving as the origin, rows parallel to the X-axis, and columns parallel to the Y-axis, the pixel coordinates of the centroid of the detected bounding box are determined. Using the following multiple formulas, the pixel coordinates of the detection target and the robot can be converted into a grid system, which is determined based on the fixed shooting angle and shooting height of the drone.

Using the formula Eq. (3) described below, the pixel coordinates of the target construction waste and the robot captured by the drone can be converted into camera coordinates.

$$\mathrm{z}\begin{bmatrix} u \\ v \\ 1 \end{bmatrix} = \begin{bmatrix} f_x & 0 & c_x \\ 0 & f_y & c_y \\ 0 & 0 & 1 \end{bmatrix} \begin{bmatrix} x \\ y \\ 1 \end{bmatrix} = K \begin{bmatrix} x \\ y \\ 1 \end{bmatrix} \tag{3}$$

Multiplying both sides by the inverse of K derives get Eq(4):

$$\begin{bmatrix} x \\ y \\ 1 \end{bmatrix} = K^{-1} \begin{bmatrix} u \\ v \\ 1 \end{bmatrix} \tag{4}$$

The next step is to transform from the camera coordinate system to the world coordinate system using formula (5):

$$\begin{bmatrix} X_c \\ Y_c \\ Z_c \end{bmatrix} = R \begin{bmatrix} X \\ Y \\ Z \end{bmatrix} + t \tag{5}$$

7.3.2.2 The vector positioning process

This method is designed based on the fixed flying height of the drone during aerial photography and a constant shooting angle of 90 degrees perpendicular to the ground. Based on the vertical perspective, there is no error in the traveling angle of the robot under the observation of the drone. Let the ground space be a 2-dimension space denoted by the notation $\mathbb{R}^2$, in which both drone and robot are viewed as rigid bodies that have different coordinate systems. We mainly utilize a Cartesian coordinate system to denote the location of each body. For conveniently distinguishing the drone from robot, the fixed frame $\mathcal{A}$ was introduced to represent the coordinate of the drone such that $(p_x, p_y)_{\mathcal{A}}$ is a location in frame $\mathcal{A}$, where p_x and p_y are straight-line distances on the rotation x and y in frame $\mathcal{A}$, respectively. The fixed frame $\mathcal{B}$ was introduced to represent the coordinate of the robot such that $(q_x, q_y)_{\mathcal{B}}$ is a location in frame $\mathcal{B}$. Particularly, we use $\mathcal{B}_{t(i)}$, to denote the frame at time $t(i)$, $i = 1,2, \cdots, n$ for distinguishing the location of the target garbage in the frame $\mathcal{B}$ at different times.

The standard coordinate transformation was introduced in our image-based method to calculate the location where construction waste is relatively referenced to the drone. The angle was observed by the drone, the traveling angle of the robot directly in front of the robot's head, which is denoted by a notation ϕ and represents the degree from rotation y. So at time $t(i)$, if the location of robot reference to frame $\mathcal{A}$ is obtained as $(p_x, p_y)_{\mathcal{A}}$, and the location of garbage reference to the frame $\mathcal{B}_{t(i)}$ is obtained as $(q_x, q_y)_{\mathcal{B}_{t(i)}}$, we can get a formula, which is shown as follows.

$$\begin{bmatrix} r_x \\ r_x \end{bmatrix} = \begin{bmatrix} p_x \\ p_y \end{bmatrix} + \begin{bmatrix} \cos\phi & -\sin\phi \\ \sin\phi & \cos\phi \end{bmatrix} \begin{bmatrix} q_x \\ q_y \end{bmatrix},$$

Where $[r_x \quad r_x]^T$ denotes the location of garbage reference to frame $\mathcal{A}$ at time $t(i)$. After the theoretical calculation formula is obtained, the specific orientation method is: Let the drone hover over the target waypoint and take pictures every n second. The robot is also recognized by the deep learning network. Then calculate the position of the robot at different times in each picture, and determine the specific position information by calculating the vector angle and the distance to the target.

Fig. 7.11. Examples of coordinate system of the construction site experiment.

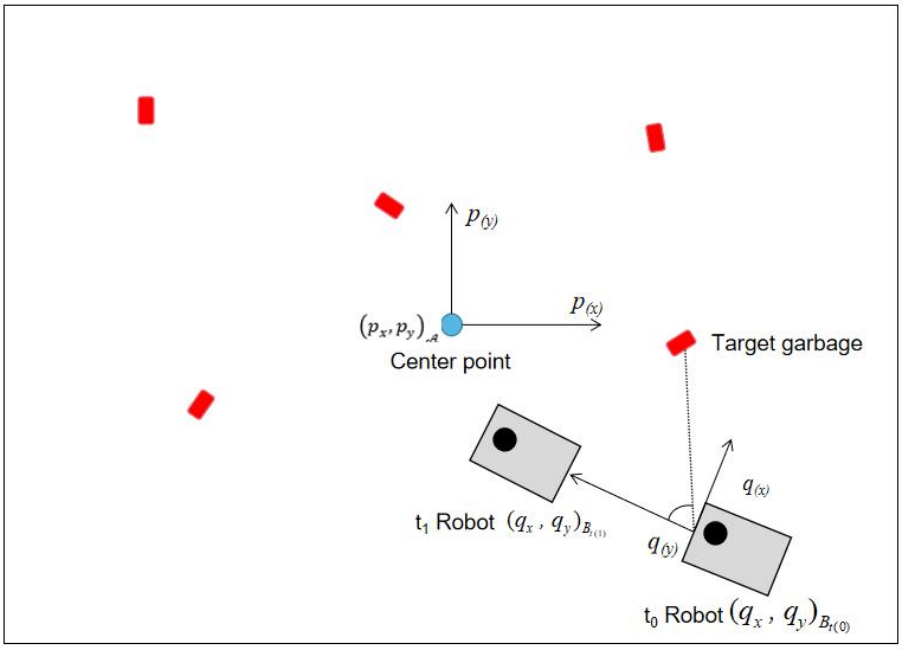

Fig. 7.12. Calculate position of robot at times t0 and t1

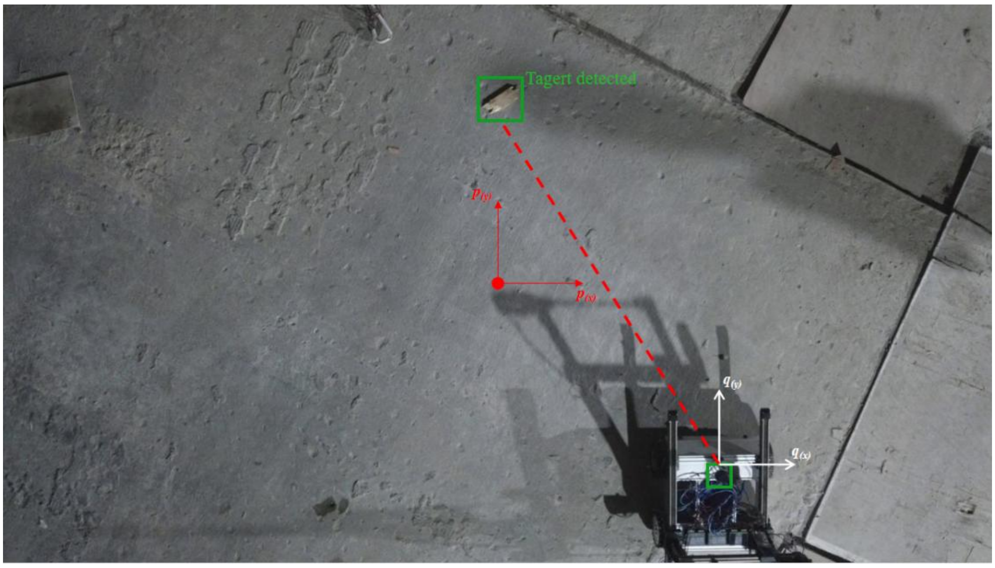

Fig. 7.13. Calculate process at a real construction site

7.3.3 Collaborative system pick-up test

To evaluate the performance of the collaborative system and determine how successful the robot is in picking up the construction waste, and verify the feasibility of the flight algorithm. The system conducted a real-world pick-up experiment on an actual construction site. To give the collaborative system a realistic construction site working environment, the construction trashes were spread on the construction site beforehand, Fig. 7.14(a) is the recorded image of the experiment. Guided by the trained YOLO model, the drones and robots detected the target garbage distributed on the construction in the air and the ground. Moreover, in this complex environment, the drone successfully performed obstacle avoidance flight and automatically planned the flight route, which proves the real feasibility of using computer vision technology to identify trash on the construction site and the feasibility of the developed flight algorithm at the practical level. With the help of the self-developed positioning technology, the robot reached the location of the garbage without any failure and carried out a successful pick-up operation, as shown in Fig. 7.14(b).

Fig. 7.14(a). Construction site experiment process

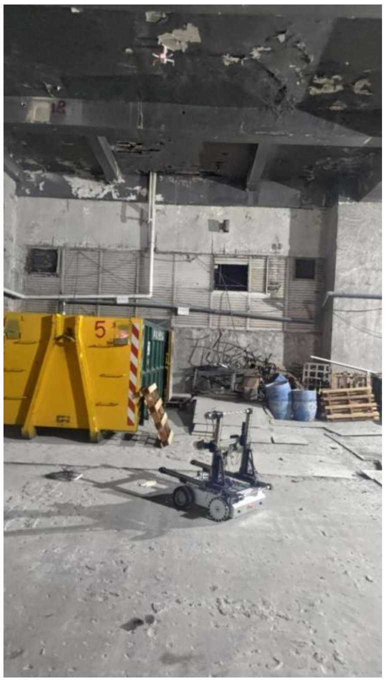

Fig. 7.14(b). The robotic garbage pick-up

7.4 Chapter summary

This chapter describes the development and testing of a collaboration construction waste recycling system. The system consists of two parts: a drone and a robot. The drone is responsible for identifying and locating construction waste. The robot is responsible for going to the target location for recycling construction waste. The drone can use its wide field of view to improve the detection and location capability of construction waste. We utilize YOLOv3 as a computer vision algorithm to implement these functions and developed a new vector positioning formula. This positioning formula realizes the positioning and guidance of the drone between the construction waste and the robot. The robot is equipped with cameras and a robotic arm, which can collect and classify target objects at close range.

This system only requires software improvements to existing drones and robots, compared with other methods that need to be improved on hardware, the method proposed in this research is more stable and convenient. The feasibility and efficiency of the developed system are verified and illustrated by going to a real construction site to conduct experiments.

The research presented in this chapter has the potential to significantly reduce the most critical cost issue associated with intelligent construction, extend the service life of automation equipment, enhance the flexibility and adaptability of the equipment, and improve the performance and efficiency of the equipment by optimizing algorithms and improving codes. Should new requirements emerge in conjunction with this system, additional hardware can be incorporated to enhance its functionality. This method encourages technological innovation, facilitates rapid distribution and deployment, and benefits a greater number of practitioners. Concurrently, it conserves resources for the fabrication and conveyance of hardware, while curbing the consumption of physical resources. Moreover, through the implementation of software updates, potential vulnerabilities can be promptly addressed, thereby enhancing the overall security and stability of the system. In light of the aforementioned advantages, it is evident that the method presented in this chapter offers a compelling alternative in terms of cost-effectiveness, resource utilization, environmental protection, innovation, and popularity.

In regard to computer vision algorithms, our findings indicated that enhancements were necessary for real-time detection algorithms to be effectively implemented in the context of drones in indoor construction environments. The construction site environment is characterized by a high degree of complexity and variability, with a multitude of both moving and stationary objects. The algorithm must be capable of efficiently detecting and identifying multiple categories of objects. Furthermore, as the operation of the system on the construction site necessitates a high degree of real-time performance, the algorithm's reasoning speed must be capable of meeting the demands of real-time detection and response. Furthermore, the construction site environment is distinctive and necessitates rigorous safety standards and uninterrupted operation. Consequently, the algorithm must demonstrate robust detection capabilities in low-light and low-resolution conditions.

Chapter 8. Discussion and Conclusion

A comprehensive simulation software framework and a collaborative framework for combining drones with ground robots were developed to improve the adaptability and applicability of unmanned aerial vehicles (UAVs) in indoor construction environments. This study addressed major challenges such as obstacle avoidance, flight stability, energy efficiency, and navigation without GPS signals. Laboratory experiments and field tests in real construction environments validated the effectiveness of the proposed solutions. The results showed that the UAV flight control algorithm and the integration of drones with ground robots for construction waste recovery were significantly improved.

8.1 Contributions

This study makes several theoretical and practical contributions to the field of indoor construction management and UAV technology. Firstly, it introduces an advanced flight control algorithm tailored to the specific needs of indoor construction environments. Unlike previous methods, the proposed algorithm enhances real-time obstacle avoidance and flight stability, crucial for navigating complex and dynamic indoor spaces. This improvement significantly reduces the risk of collisions and flight disruptions, ensuring safer and more efficient operations in confined construction sites.

Secondly, the integration of Building Information Modeling (BIM) with flight simulation software, such as Airsim and MATLAB/Simulink, represents a significant advancement. This integration allows for the creation of a realistic simulation environment where UAV algorithms can be tested and optimized before deployment, ensuring higher accuracy and feasibility. The use of these sophisticated simulation tools enables comprehensive pre-deployment testing, which minimizes potential errors and enhances the reliability of UAV operations in actual construction environments.

Thirdly, this research develops a novel collaborative framework for UAVs and ground robots to efficiently manage construction waste. The framework leverages the UAV's aerial perspective for comprehensive site surveillance and the robot's ground capabilities for precise waste collection. This collaboration enhances the efficiency and effectiveness of construction waste management, promoting sustainable construction practices. By combining the strengths of both aerial and ground robotics, the system ensures thorough coverage and efficient waste removal, contributing to cleaner and safer construction sites.

Compared to previous research on UAV applications in construction, this study offers several distinct advantages. The use of advanced algorithms and simulation models ensures that the results are objective and quantifiable, enabling precise assessments and improvements. This methodological rigor provides a solid foundation for future research and development in UAV technology. Unlike earlier methods that were limited to specific tasks or environments, the proposed approach can adapt to various construction scenarios, making it more versatile and applicable to different project needs. This adaptability is crucial for addressing the diverse and dynamic challenges encountered in modern construction projects.

Furthermore, the integration of multiple factors such as UAV flight stability, obstacle avoidance, and energy efficiency provides a comprehensive solution that addresses several critical aspects of UAV deployment in construction. This holistic approach ensures that the UAVs perform optimally across a range of operational conditions, enhancing their utility and effectiveness. The continuous and non-invasive data collection enabled by the developed framework allows for ongoing monitoring of construction sites without disrupting ongoing activities. This capability is essential for maintaining real-time oversight and ensuring timely interventions when necessary.

In addition, the collaborative framework between UAVs and ground robots facilitates a seamless integration of aerial and terrestrial operations, leading to more coordinated and effective construction site management. This synergy enhances the overall efficiency of construction processes and contributes to better resource utilization. The proposed system's ability to generate objective and quantifiable results through advanced simulation and data analysis tools ensures that improvements are based on robust empirical evidence. This scientific rigor enhances the credibility and reliability of the findings, paving the way for wider acceptance and adoption of UAV technologies in the construction industry.

8.2 Limitations

Despite the significant contributions, this study has a few limitations. First, the simulation framework, while robust, may not fully capture the variability and unpredictability of real-world construction environments. Although it can simulate various construction scenarios, there may still be unforeseen challenges when deploying UAVs in different real-world conditions. The dynamic and ever-changing nature of construction sites, with frequent layout changes and unexpected obstacles, can pose significant challenges that are difficult to replicate accurately in a simulated environment. To mitigate this, future research should focus on enhancing the simulation framework to incorporate more sophisticated modeling techniques and real-time data integration from actual construction sites.

Second, the reliance on computer vision for target detection may face challenges in low-light conditions or environments with significant visual obstructions. While the integration with ground robots mitigates some of these issues, the overall system performance could be affected by factors such as poor lighting, dust, and debris, which are common in construction sites. Improving the robustness of the computer vision system through the incorporation of additional sensors, such as thermal cameras and LIDAR, could help address these challenges and enhance the system's reliability in various environmental conditions.

Thirdly, the training dataset for the UAV's computer vision system is limited to a specific set of construction waste types (e.g., bricks and nails). This limitation may affect the system's generalization ability to detect and manage other types of construction waste not included in the training data. Expanding the training dataset to include a wider variety of waste types and environmental conditions would improve the system's adaptability and effectiveness in diverse construction scenarios. Additionally, the development of more advanced machine learning algorithms capable of generalizing from limited data could further enhance the system's performance.

Privacy concerns may also arise from the use of cameras and sensors to monitor construction sites. Workers may feel uncomfortable being constantly observed, and regulations in some regions may restrict the use of such technologies, impacting the deployment of the proposed system. Addressing these concerns through the development of privacy-preserving data collection methods and ensuring compliance with relevant regulations will be crucial for the broader acceptance and implementation of the system.

Lastly, the experimental validation was conducted in controlled environments and selected construction sites. While the results are promising, further large-scale field tests are necessary to fully understand the system's robustness and scalability in diverse indoor construction scenarios. Conducting extensive field trials across different types of construction sites, including large-scale infrastructure projects and smaller residential developments, would provide valuable insights into the system's performance and identify areas for further improvement.

8.3 Discussion and suggestions on future research directions

The findings of this research highlight the transformative potential of UAV technology when applied to indoor construction environments. By addressing unique challenges such as real-time obstacle avoidance, flight stability, and collaboration with ground robots, this study provides a significant step toward the practical integration of UAVs in construction management. However, several aspects merit further exploration to ensure broader adoption and sustained impact.

The practical integration of UAV systems into real-world construction projects presents challenges related to scalability. Construction sites are highly dynamic, with frequent layout changes, temporary obstructions, and varying environmental conditions that are difficult to fully replicate in simulations. For instance, the unpredictability of worker movement or the placement of materials may require further refinement of path planning and positioning systems. To overcome these limitations, future efforts should focus on testing the system across larger, more diverse construction sites to better understand its constraints and adaptability.

Another area for improvement lies in enhancing UAV perception systems. The reliance on computer vision as the primary sensing modality, although effective under controlled conditions, reveals limitations in environments with poor lighting, heavy dust, or significant occlusions. While integrating LiDAR or thermal imaging sensors could improve robustness, such additions may increase system complexity and cost. A hybrid perception system that combines multiple sensing technologies could be a promising direction for future research. Such an approach would compensate for the shortcomings of individual methods, significantly improving detection accuracy and operational reliability in challenging environments.

The collaboration between UAVs and ground robots, which proved successful in construction waste management, also has room for optimization. The UAV’s aerial perspective enhances waste detection, while the robot’s precision enables effective collection. However, the coordination between the two systems currently relies on periodic data exchange, which may introduce delays in dynamic environments. Developing real-time communication protocols and joint decision-making algorithms would enable seamless interaction between UAVs and robots, resulting in faster and more efficient task execution.

In addition to technical challenges, ethical and regulatory considerations must also be addressed to ensure the successful adoption of UAVs in construction. Privacy concerns related to continuous site surveillance, data security issues, and compliance with aviation regulations could hinder deployment. Proactively engaging with regulatory bodies and industry stakeholders to establish clear guidelines and standards for UAV use is essential. Furthermore, ensuring transparency in UAV operations and addressing worker concerns about privacy and safety will foster greater acceptance of the technology.

This study opens several avenues for future research. For example, integrating UAVs with digital twin technologies could allow real-time UAV data to continuously update virtual construction models, enabling construction managers to dynamically monitor progress and make informed decisions. Additionally, applying advanced machine learning algorithms for autonomous decision-making would enable UAVs to adapt to unforeseen challenges in real time without human intervention. Expanding the collaborative framework to include multiple UAVs and robots could also address tasks requiring extensive coverage or simultaneous operations, such as large-scale site monitoring or waste segregation. Research into multi-agent systems and swarm robotics could provide valuable insights into achieving such coordination.

Lastly, long-term studies evaluating the environmental and economic impacts of UAV integration in construction would offer a more comprehensive understanding of their benefits. Quantifying cost savings, reductions in material waste, and improvements in worker safety could help build a stronger case for widespread adoption.

In summary, this discussion emphasizes the practical significance of the proposed UAV systems while acknowledging the challenges that remain. By addressing scalability, perception limitations, ethical concerns, and exploring innovative research directions, UAVs have the potential to become an integral part of the construction industry, driving it toward greater efficiency, sustainability, and safety.

Reference

[1] Mohamed, N., Al-Jaroodi, J., Jawhar, I., Idries, A., & Mohammed, F. (2020). Unmanned aerial vehicles applications in future smart cities. *Technological forecasting and social change*, *153*, 119293.

[2] Alizadehsalehi, S., Yitmen, I., Celik, T., & Arditi, D. (2020). The effectiveness of an integrated BIM/UAV model in managing safety on construction sites. *International journal of occupational safety and ergonomics*, *26*(4), 829-844.

[3] Azhar, S. (2011). Building information modeling (BIM): Trends, benefits, risks, and challenges for the AEC industry. *Leadership and management in engineering*, *11*(3), 241-252.

[4] Bock, T., & Linner, T. (2015). *Robot oriented design*. Cambridge university press.

[5] Halder, S., & Afsari, K. (2023). Robots in inspection and monitoring of buildings and infrastructure: A systematic review. *Applied Sciences*, *13*(4), 2304.

[5] Martinez, J. G., Gheisari, M., & Alarcón, L. F. (2020). UAV integration in current construction safety planning and monitoring processes: Case study of a high-rise building construction project in Chile. *Journal of Management in Engineering*, *36*(3), 05020005.

[6] Hassanalian, M., & Abdelkefi, A. (2017). Classifications, applications, and design challenges of drones: A review. *Progress in Aerospace sciences*, *91*, 99-131.

[7] Irizarry, J., & Costa, D. B. (2016). Exploratory study of potential applications of unmanned aerial systems for construction management tasks. *Journal of Management in Engineering*, *32*(3), 05016001.

[8] Kopsida, M., Brilakis, I., & Vela, P. A. (2015, October). A review of automated construction progress monitoring and inspection methods. In *Proc. of the 32nd CIB W78 Conference 2015* (pp. 421-431).

[9] Gheisari, M., & Esmaeili, B. (2019). Applications and requirements of unmanned aerial systems (UASs) for construction safety. *Safety science*, *118*, 230-240.

[10] Zhou, Z., Goh, Y. M., & Li, Q. (2015). Overview and analysis of safety management studies in the construction industry. *Safety science*, *72*, 337-350.

[11] Choi, H. W., Kim, H. J., Kim, S. K., & Na, W. S. (2023). An overview of drone applications in the construction industry. *Drones*, *7*(8), 515.

[12] Olomolaiye, A., & Egbu, C. (2004, September). The significance of human resource issues in knowledge management within the construction industry–people, problems and possibilities. In *Proceedings of the Twentieth Annual Conference, Association of Researchers in Construction Management, Heriot Watt University* (pp. 533-540).

[13] Ofori, G. (2015). Nature of the construction industry, its needs and its development: A review of four decades of research. *Journal of construction in developing countries*, *20*(2), 115.

[14] Siebert, S., & Teizer, J. (2014). Mobile 3D mapping for surveying earthwork projects using an Unmanned Aerial Vehicle (UAV) system. *Automation in construction*, *41*, 1-14.

[15] Zhong, R. Y., Peng, Y., Xue, F., Fang, J., Zou, W., Luo, H., ... & Huang, G. Q. (2017). Prefabricated construction enabled by the Internet-of-Things. *Automation in Construction*, *76*, 59-70.

[16] Golizadeh, H., Hosseini, M. R., Martek, I., Edwards, D., Gheisari, M., Banihashemi, S., & Zhang, J. (2020). Scientometric analysis of research on "remotely piloted aircraft" A research agenda for the construction industry. *Engineering, Construction and Architectural Management*, *27*(3), 634-657.

[17] Ghamari, M., Rangel, P., Mehrubeoglu, M., Tewolde, G. S., & Sherratt, R. S. (2022). Unmanned aerial vehicle communications for civil applications: A review. *IEEE Access*, *10*, 102492-102531.

[18] Umar, T. (2021). Applications of drones for safety inspection in the Gulf Cooperation Council construction. *Engineering, Construction and Architectural Management*, *28*(9), 2337-2360.

[19] Rashdi, R., Martínez-Sánchez, J., Arias, P., & Qiu, Z. (2022). Scanning technologies to building information modelling: A review. *Infrastructures*, *7*(4), 49.

[20] Li, C. Z., Xue, F., Li, X., Hong, J., & Shen, G. Q. (2018). An Internet of Things-enabled BIM platform for on-site assembly services in prefabricated construction. *Automation in construction*, *89*, 146-161.

[21] Shakhatreh, H., Sawalmeh, A. H., Al-Fuqaha, A., Dou, Z., Almaita, E., Khalil, I., ... & Guizani, M. (2019). Unmanned aerial vehicles (UAVs): A survey on civil applications and key research challenges. *Ieee Access*, *7*, 48572-48634.

[22] Rachmawati, T. S. N., & Kim, S. (2022). Unmanned Aerial Vehicles (UAV) integration with digital technologies toward construction 4.0: A systematic literature review. *Sustainability*, *14*(9), 5708.

[23] Li, Y., & Liu, C. (2019). Applications of multirotor drone technologies in construction management. *International Journal of Construction Management*, *19*(5), 401-412.

[24] Setyawan, A. A., Taftazani, M. I., Bahri, S., Noviana, E. D., & Faridatunnisa, M. (2022). Drone LiDAR application for 3D city model. Journal of Applied Geospatial Information, 6(1), 572-576.

[25] Agueera-Vega, F., Carvajal-Ramirez, F., Martínez-Carricondo, P., López, J. S. H., Mesas-Carrascosa, F. J., García-Ferrer, A., & Pérez-Porras, F. J. (2018).

Reconstruction of extreme topography from UAV structure from motion photogrammetry. Measurement, 121, 127-138.

[26] Jacob-Loyola, N., Muñoz-La Rivera, F., Herrera, R. F., & Atencio, E. (2021). Unmanned aerial vehicles (UAVs) for physical progress monitoring of construction. Sensors, 21(12), 4227.

[27] Sulaiman, M. A. M. (2022). UAV-Driven Building Inspection and Integrated Facility Maintenance Management. Western Michigan University.

[28] Kas, K. A., & Johnson, G. K. (2020). Using unmanned aerial vehicles and robotics in hazardous locations safely. Process safety progress, 39(1), e12066.

[29] York, D. D., Al-Bayati, A. J., & Al-Shabbani, Z. Y. (2020, March). Potential applications of uav within the construction industry and the challenges limiting implementation. In Construction Research Congress 2020 (pp. 31-39). Reston, VA: American Society of Civil Engineers.

[30] Onososen, A. O., Musonda, I., Onatayo, D., Tjebane, M. M., Saka, A. B., & Fagbenro, R. K. (2023). Impediments to construction site digitalisation using Unmanned Aerial Vehicles (UAVs). Drones, 7(1), 45.

[31] Liang, H., Lee, S. C., Bae, W., Kim, J., & Seo, S. (2023). Towards UAVs in construction: advancements, challenges, and future directions for monitoring and inspection. Drones, 7(3), 202.

[32] Alizadehsalehi, S., Hadavi, A., & Huang, J. C. (2019, June). BIM/MR-Lean construction project delivery management system. In *2019 IEEE Technology & Engineering Management Conference (TEMSCON)* (pp. 1-6). IEEE.

[33] Alizadehsalehi, S., Hadavi, A., & Huang, J. C. (2020). From BIM to extended reality in AEC industry. *Automation in construction*, *116*, 103254.

[34] Ibrahim, A., & Golparvar-Fard, M. (2019, June). 4D BIM based optimal flight planning for construction monitoring applications using camera-equipped UAVs. In *ASCE International Conference on Computing in Civil Engineering 2019* (pp. 217-224). Reston, VA: American Society of Civil Engineers.

[35] Lee, S., & Choi, Y. (2016). Reviews of unmanned aerial vehicle (drone) technology trends and its applications in the mining industry. *Geosystem Engineering*, *19*(4), 197-204.

[36] Kim, D. H., Lee, B. K., & Sohn, S. Y. (2016). Quantifying technology–industry spillover effects based on patent citation network analysis of unmanned aerial vehicle (UAV). *Technological Forecasting and Social Change*, *105*, 140-157.

[37] Dorafshan, S., & Maguire, M. (2018). Bridge inspection: Human performance, unmanned aerial systems and automation. *Journal of Civil Structural Health Monitoring*, *8*, 443-476.

[38] Moud, H. I., Razkenari, M. A., Flood, I., & Kibert, C. (2019). A flight simulator

for unmanned aerial vehicle flights over construction job sites. *Advances in Informatics and Computing in Civil and Construction Engineering*, 609-616.

[39] Feifei, X., et al. "Study on construction of 3D building based on UAy images." The International Archives ofthePhotogrammetry, Remote Sensing and Spatial Information Sciences 39 (2012): B1.

[40] Wang, J., Zhang, S., & Teizer, J. (2015). Geotechnical and safety protective equipment planning using range point cloud data and rule checking in building information modeling. *Automation in Construction*, *49*, 250-261.

[41] Asnafi, M. (2016). *3D/4D BIM-Based Hazard Identification, Safety Regulations and Safety Monitoring of Construction Projects in Pre-construction and Construction Phases* (Master's thesis, Eastern Mediterranean University (EMU)-Doğu Akdeniz Üniversitesi (DAÜ)).

[42] Alizadehsalehi, S., Asnafi, M., Yitmen, I., & Celik, T. (2017, June). UAS-BIM based real-time hazard identification and safety monitoring of construction projects. In *9th Nordic Conference on Construction Economics and Organization 13-14 June, 2017 at Chalmers University of Technology, Göteborg, SWEDEN* (Vol. 13, p. 22).

[43] Freimuth, H., & König, M. (2015, October). Generation of waypoints for UAV-assisted progress monitoring and acceptance of construction work. In *15th International Conference on Construction Applications of Virtual Reality* (Vol. 13, No. 4, pp. 77-86).

[44] Chen Y, Zhang J, Min B C. Applications of BIM and UAV to construction safety[C]//CSCE Annual Conference. 2019: 1-7.

[45] Kaamin M, Razali S N M, Ahmad N F A, et al. The application of micro UAV in construction project[C]//AIP Conference Proceedings. AIP Publishing LLC, 2017, 1891(1): 020070.

[46] Asadi K, Suresh A K, Ender A, et al. An integrated UGV-UAV system for construction site data collection[J]. Automation in Construction, 2020, 112: 103068.

[47] Ku Y D, Yang J H, Fang H Y, et al. Optimization of grasping efficiency of a robot used for sorting construction and demolition waste[J]. International Journal of Automation and Computing, 2020, 17(5): 691-700.

[48] Zhang Z, Wang H, Song H, et al. Industrial robot sorting system for municipal solid waste[C]//International Conference on Intelligent Robotics and Applications. Springer, Cham, 2019: 342-353.

[49] Gao X, Zhu L, Cui H, et al. Complete and Accurate Indoor Scene Capturing and Reconstruction Using a Drone and a Robot[J]. IEEE Sensors Journal, 2020, 21(10): 11858-11869.

[50] Oleynikova, H., Taylor, Z., Siegwart, R., & Nieto, J. (2018). Safe local exploration for replanning in cluttered unknown environments for microaerial vehicles. *IEEE Robotics and Automation Letters*, *3*(3), 1474-1481.

[51] Shi, C., Lai, G., Yu, Y., Bellone, M., & Lippiello, V. (2023). Real-Time

Multi-Modal Active Vision for Object Detection on UAVs Equipped With Limited Field of View LiDAR and Camera. *IEEE Robotics and Automation Letters*.

[52] Chen, L., Yuan, X., Xiao, Y., Zhang, Y., & Zhu, J. (2020). Robust autonomous landing of UAV in non-cooperative environments based on dynamic time camera-LiDAR fusion. *arXiv preprint arXiv:2011.13761*.

[53] Yan, C., Xiang, X., & Wang, C. (2020). Towards real-time path planning through deep reinforcement learning for a UAV in dynamic environments. *Journal of Intelligent & Robotic Systems*, *98*, 297-309.

[54] Walker, O., Vanegas, F., Gonzalez, F., & Koenig, S. (2019, March). A deep reinforcement learning framework for UAV navigation in indoor environments. In *2019 IEEE Aerospace Conference* (pp. 1-14). IEEE.

[55] Bolognini, M. (2022). Path planning for multicopter networks and applications to the condition monitoring of the built environment.

[56] Elmokadem, T., & Savkin, A. V. (2021). A hybrid approach for autonomous collision-free uav navigation in 3d partially unknown dynamic environments. *Drones*, *5*(3), 57.

[57] Mangalam, K., An, Y., Girase, H., & Malik, J. (2021). From goals, waypoints & paths to long term human trajectory forecasting. In *Proceedings of the IEEE/CVF International Conference on Computer Vision* (pp. 15233-15242).

[58] Wen, N., Zhao, L., Su, X., & Ma, P. (2015). UAV online path planning algorithm in a low altitude dangerous environment. *IEEE/CAA Journal of Automatica Sinica*, *2*(2), 173-185.

[59] Lyu, H. (2018, October). Detect and avoid system based on multi sensor fusion for UAV. In *2018 International Conference on Information and Communication Technology Convergence (ICTC)* (pp. 1107-1109). IEEE.

[60] Jordan, S., Moore, J., Hovet, S., Box, J., Perry, J., Kirsche, K., ... & Tse, Z. T. H. (2018). State-of-the-art technologies for UAV inspections. *IET Radar, Sonar & Navigation*, *12*(2), 151-164.

[61] Pokhrel, N. (2018). Drone obstacle avoidance and navigation using artificial intelligence.

[62] Giagkos, A., Tuci, E., Wilson, M. S., & Charlesworth, P. B. (2021). UAV flight coordination for communication networks: genetic algorithms versus game theory. *Soft computing*, *25*(14), 9483-9503.

[63] Kazim, M., Azar, A. T., Koubaa, A., & Zaidi, A. (2021). Disturbance-rejection-based optimized robust adaptive controllers for UAVs. IEEE Systems Journal, 15(2), 3097-3108.

[64] Wu, J., Wang, H., Liu, Y., Zhang, M., & Wu, T. (2022). Learning-based fixed-wing UAV reactive maneuver control for obstacle avoidance. Aerospace Science and Technology, 126, 107623.

[65] Lin, H. Y., & Zhan, J. R. (2023). GNSS-denied UAV indoor navigation with UWB incorporated visual inertial odometry. Measurement, 206, 112256.

[66] Bouhamed, O., Ghazzai, H., Besbes, H., & Massoud, Y. (2020, October). Autonomous UAV navigation: A DDPG-based deep reinforcement learning approach. In 2020 IEEE International Symposium on circuits and systems (ISCAS) (pp. 1-5). IEEE.

[67] Du, Y., Zhang, X., & Nie, Z. (2019). A real-time collision avoidance strategy in dynamic airspace based on dynamic artificial potential field algorithm. IEEE Access, 7, 169469-169479.

[68] Gudmundsson, S., Golubev, V., Drakunov, S., & Reinholtz, C. (2019). Bio-Inspired Methodologies for Energy Conservation and Harvesting Flight-Path Modeling for Unmanned Aerial System. Journal of Aerospace Information Systems, 16(7), 289-295.

[69] Ebeid, E., Skriver, M., Terkildsen, K. H., Jensen, K., & Schultz, U. P. (2018). A survey of open-source UAV flight controllers and flight simulators. Microprocessors and Microsystems, 61, 11-20.

[70] Rezwan, S., & Choi, W. (2022). Artificial intelligence approaches for UAV navigation: Recent advances and future challenges. IEEE access, 10, 26320-26339.

[71] Stevens, B. L., & Lewis, F. L. (2003). Aircraft Control and Simulation. Wiley. *New york*.

[72] Beard, R. W., & McLain, T. W. (2012). *Small unmanned aircraft: Theory and practice*. Princeton university press.

[73] Franklin, G. F., Powell, J. D., Emami-Naeini, A., & Powell, J. D. (2002). *Feedback control of dynamic systems* (Vol. 4). Upper Saddle River: Prentice hall.

[74] Anderson, B. D., & Moore, J. B. (2007). *Optimal control: linear quadratic methods*. Courier Corporation.

[75] Hartley, E. N., & Maciejowski, J. M. (2014). Reconfigurable predictive control for redundantly actuated systems with parameterised input constraints. *Systems & Control Letters*, *66*, 8-15.

[76] Mnih, V., Kavukcuoglu, K., Silver, D., Rusu, A. A., Veness, J., Bellemare, M. G., ... & Hassabis, D. (2015). Human-level control through deep reinforcement learning. *nature*, *518*(7540), 529-533.

[77] Ames, A. D., Xu, X., Grizzle, J. W., & Tabuada, P. (2016). Control barrier function based quadratic programs for safety critical systems. *IEEE Transactions on Automatic Control*, *62*(8), 3861-3876.

[78] Ames, A. D., Coogan, S., Egerstedt, M., Notomista, G., Sreenath, K., & Tabuada, P. (2019, June). Control barrier functions: Theory and applications. In *2019 18th European control conference (ECC)* (pp. 3420-3431). IEEE.

[79] Kolathaya, S., & Ames, A. D. (2018). Input-to-state safety with control barrier functions. *IEEE control systems letters*, *3*(1), 108-113.

[80] Zhao, P., Mao, Y., Tao, C., Hovakimyan, N., & Wang, X. (2020, December). Adaptive robust quadratic programs using control Lyapunov and barrier functions. In *2020 59th IEEE Conference on Decision and Control (CDC)* (pp. 3353-3358). IEEE.

[81] Taylor, A. J., & Ames, A. D. (2020, July). Adaptive safety with control barrier functions. In *2020 American Control Conference (ACC)* (pp. 1399-1405). IEEE.

[82] Wills, A. G., & Heath, W. P. (2004). Barrier function based model predictive control. *Automatica*, *40*(8), 1415-1422.

[83] Zeng, J., Zhang, B., & Sreenath, K. (2021, May). Safety-critical model predictive control with discrete-time control barrier function. In *2021 American Control Conference (ACC)* (pp. 3882-3889). IEEE.

[84] Grandia, R., Taylor, A. J., Ames, A. D., & Hutter, M. (2021, May). Multi-layered safety for legged robots via control barrier functions and model predictive control. In *2021 IEEE International Conference on Robotics and Automation (ICRA)* (pp. 8352-8358). IEEE.

[85] Lohmiller, W., & Slotine, J. J. E. (1998). On contraction analysis for non-linear systems. *Automatica*, *34*(6), 683-696.

[86] Manchester, I. R., & Slotine, J. J. E. (2017). Control contraction metrics: Convex and intrinsic criteria for nonlinear feedback design. *IEEE Transactions on Automatic Control*, *62*(6), 3046-3053.

[87] Zhao, P., Lakshmanan, A., Ackerman, K., Gahlawat, A., Pavone, M., & Hovakimyan, N. (2022). Tube-certified trajectory tracking for nonlinear systems with robust control contraction metrics. *IEEE Robotics and Automation Letters*, *7*(2), 5528-5535.

[88] Lakshmanan, A., Gahlawat, A., & Hovakimyan, N. (2020, December). Safe feedback motion planning: A contraction theory and $\mathscr{L}$ 1-adaptive control based approach. In *2020 59th IEEE Conference on Decision and Control (CDC)* (pp. 1578-1583). IEEE.

[89] Singh, S., Landry, B., Majumdar, A., Slotine, J. J., & Pavone, M. (2023). Robust feedback motion planning via contraction theory. *The International Journal of Robotics Research*, *42*(9), 655-688.

[90] Raković, S. V., Levine, W. S., & Açikmese, B. (2016, July). Elastic tube model predictive control. In *2016 American Control Conference (ACC)* (pp. 3594-3599). IEEE.

[91] Choset, H., Lynch, K. M., Hutchinson, S., Kantor, G. A., & Burgard, W. (2005). *Principles of robot motion: theory, algorithms, and implementations*. MIT press.

[92] Chen, Y. B., Luo, G. C., Mei, Y. S., Yu, J. Q., & Su, X. L. (2016). UAV path

planning using artificial potential field method updated by optimal control theory. *International Journal of Systems Science*, *47*(6), 1407-1420.

[93] Shukla, A., Singla, E., Wahi, P., & Dasgupta, B. (2013). A direct variational method for planning monotonically optimal paths for redundant manipulators in constrained workspaces. *Robotics and Autonomous Systems*, *61*(2), 209-220.

[94] Liu, H., Li, X., Fan, M., Wu, G., Pedrycz, W., & Suganthan, P. N. (2020). An autonomous path planning method for unmanned aerial vehicle based on a tangent intersection and target guidance strategy. *IEEE Transactions on Intelligent Transportation Systems*, *23*(4), 3061-3073.

[95] Li, B., & Chen, B. (2021). An adaptive rapidly-exploring random tree. *IEEE/CAA Journal of Automatica Sinica*, *9*(2), 283-294.

[96] Economou, J. T., Kladis, G., Tsourdos, A., & White, B. A. (2007, July). UAV optimum energy assignment using Dijkstra's Algorithm. In *2007 European Control Conference (ECC)* (pp. 287-292). IEEE.

[97] Yan, F., Zhuang, Y., & Xiao, J. (2012, December). 3D PRM based real-time path planning for UAV in complex environment. In *2012 IEEE international conference on robotics and biomimetics (ROBIO)* (pp. 1135-1140). IEEE.

[98] Bai, X., Jiang, H., Cui, J., Lu, K., Chen, P., & Zhang, M. (2021). UAV path planning based on improved A* and DWA algorithms. *International journal of aerospace engineering*, *2021*(1), 4511252.

[99] Reif, J., & Sharir, M. (1994). Motion planning in the presence of moving obstacles. *Journal of the ACM (JACM)*, *41*(4), 764-790.

[100] Kelly, M. (2017). An introduction to trajectory optimization: How to do your own direct collocation. *SIAM Review*, *59*(4), 849-904.

[101] Geiger, B., Horn, J., DeLullo, A., Niessner, A., & Long, L. (2006, August). Optimal path planning of UAVs using direct collocation with nonlinear programming. In *AIAA Guidance, Navigation, and Control Conference and Exhibit* (p. 6199).

[102] Kim, S. H., Padilla, G. E. G., Kim, K. J., & Yu, K. H. (2019). Flight path planning for a solar powered UAV in wind fields using direct collocation. *IEEE Transactions on Aerospace and Electronic Systems*, *56*(2), 1094-1105.

[103] Mirinejad, H., & Inanc, T. (2017). An RBF collocation method for solving optimal control problems. *Robotics and Autonomous Systems*, *87*, 219-225.

[104] Hashemi, D., & Heidari, H. (2020). Trajectory planning of quadrotor UAV with maximum payload and minimum oscillation of suspended load using optimal control. *Journal of Intelligent & Robotic Systems*, *100*(3), 1369-1381.

[105] Morbidi, F., & Pisarski, D. (2021, May). Practical and accurate generation of energy-optimal trajectories for a planar quadrotor. In *2021 IEEE International Conference on Robotics and Automation (ICRA)* (pp. 355-361). IEEE.

[106] Couturier, A., & Akhloufi, M. A. (2021). A review on absolute visual localization for UAV. *Robotics and Autonomous Systems*, *135*, 103666.

[107] Cadena, C., Carlone, L., Carrillo, H., Latif, Y., Scaramuzza, D., Neira, J., ... & Leonard, J. J. (2016). Past, present, and future of simultaneous localization and mapping: Toward the robust-perception age. *IEEE Transactions on robotics*, *32*(6), 1309-1332.

[108] Li, C. T., Cheng, J. C., & Chen, K. (2020). Top 10 technologies for indoor positioning on construction sites. *Automation in construction*, *118*, 103309.

[109] Caldas, C. H., Torrent, D. G., & Haas, C. T. (2006). Using global positioning system to improve materials-locating processes on industrial projects. *Journal of Construction Engineering and Management*, *132*(7), 741-749.

[110] Razavi, S. N., & Moselhi, O. (2012). GPS-less indoor construction location sensing. *Automation in Construction*, *28*, 128-136.

[111] Ibrahim M, Moselhi O. Inertial measurement unit based indoor localization for construction applications[J]. Automation in Construction, 2016, 71: 13-20.

[112] Goodrum, P. M., McLaren, M. A., & Durfee, A. (2006). The application of active radio frequency identification technology for tool tracking on construction job sites. *Automation in construction*, *15*(3), 292-302.

[113] Jang, Won-Suk, and Miroslaw J. Skibniewski. "A wireless network system for automated tracking of construction materials on project sites." *Journal of civil engineering and management* 14.1 (2008): 11-19.

[114] Dissanayake, M. G., Newman, P., Clark, S., Durrant-Whyte, H. F., & Csorba, M. (2001). A solution to the simultaneous localization and map building (SLAM) problem. *IEEE Transactions on robotics and automation*, *17*(3), 229-241.

[115] Ren S, He K, Girshick R, et al. Faster r-cnn: Towards real-time object detection with region proposal networks[J]. Advances in neural information processing systems, 2015, 28.

[116] Redmon J, Farhadi A. YOLO9000: better, faster, stronger[C]//Proceedings of the IEEE conference on computer vision and pattern recognition. 2017: 7263-7271.

[117] Lin T Y, Dollár P, Girshick R, et al. Feature pyramid networks for object detection[C]//Proceedings of the IEEE conference on computer vision and pattern recognition. 2017: 2117-2125.

[118] Redmon J, Divvala S, Girshick R, et al. You only look once: Unified, real-time object detection[C]//Proceedings of the IEEE conference on computer vision and pattern recognition. 2016: 779-788.

[119] Davis P, Aziz F, Newaz M T, et al. The classification of construction waste material using a deep convolutional neural network[J]. Automation in construction, 2021, 122: 103481.

[120] Redmon J, Farhadi A. Yolov3: An incremental improvement[J]. arXiv preprint arXiv:1804.02767, 2018.

[121] Aziz F, Arof H, Mokhtar N, et al. Waste level detection and HMM based collection scheduling of multiple bins[J]. Plos one, 2018, 13(8): e0202092.

[122] Davis P, Sher W, Tang P, et al. Factors affecting waste management on New South Wales construction sites[J]. COBRA 2018, 2018.

[123] Begum R A, Siwar C, Pereira J J, et al. Attitude and behavioral factors in waste management in the construction industry of Malaysia[J]. Resources, Conservation and Recycling, 2009, 53(6): 321-328.

[124] Bao Z, Lee W M W, Lu W. Implementing on-site construction waste recycling in Hong Kong: Barriers and facilitators[J]. Science of the Total Environment, 2020, 747: 141091.

[125] Ali T H, Akhund M A, Memon N A, et al. Application of artifical intelligence in construction waste management[C]//2019 8th International Conference on Industrial Technology and Management (ICITM). IEEE, 2019: 50-55.

[126] Jex, H., & Culick, F. (1985). Flight control dynamics of the 1903 Wright Flyer. In *12th Atmospheric Flight Mechanics Conference* (p. 1804).

[127] Wang, W., Jiang, B., Yang, J., & Li, C. (2021, February). Research on UAV application in mountain anti-terrorism combat. In *Journal of physics: conference series* (Vol. 1792, No. 1, p. 012079). IOP Publishing.

[128] Mullen, J., Bailey, S. C., & Hoagg, J. B. (2016). Filtered dynamic inversion for altitude control of fixed-wing unmanned air vehicles. *Aerospace Science and Technology*, *54*, 241-252.

[129] Yan, Y., Yang, J., Liu, C., Coombes, M., Li, S., & Chen, W. H. (2020). On the actuator dynamics of dynamic control allocation for a small fixed-wing UAV with direct lift control. *IEEE Transactions on Control Systems Technology*, *28*(3), 984-991.

[130] Zheng, Z. Jin, L. Sun, and M. Zhu, “Adaptive sliding mode relative motion control for autonomous carrier landing of fixed-wing unmanned aerial vehicles,” *IEEE Access*, vol. 5, pp. 5556–5565, 2017.

[131] Guclu, A., Kurtulus, D. F., & Arikan, K. B. (2016). Attitude and altitude stabilization of fixed wing VTOL unmanned air vehicle. In *AIAA Modeling and Simulation Technologies Conference* (p. 3378).

[132] Zhang, C., Zhang, G., & Dong, Q. (2021). Multi-variable finite-time observer-based adaptive-gain sliding mode control for fixed-wing UAV. *IET control theory & applications*, *15*(2), 223-247.

[133] Shuo, K. U., Da-li, D., Wei-li, Y., & Wen-qiang, Z. (2020). Attitude control of fixed-wing UCAV based on adaptive fuzzy PID. In *IOP Conference Series: Materials Science and Engineering* (Vol. 715, No. 1, p. 012099). IOP Publishing.

[134] Lungu, M. (2020). Backstepping and dynamic inversion combined controller for auto-landing of fixed wing UAVs. *Aerospace Science and Technology*, *96*, 105526.

[135] Ulus, Ş., & Eski, I. (2021). Neural network and fuzzy logic-based hybrid attitude controller designs of a fixed-wing UAV. *Neural Computing and Applications*, *33*(14), 8821-8843.

[136] Hamissi, A., Bouzid, Y., Dabouze, N., Zaouche, M., Busawon, K., & Hamerain, M. (2019). Combining homogeneous high order sliding mode and nonlinear dynamic inversion for fixed wing aircraft attitude and speed control. *IFAC-PapersOnLine*, *52*(12), 304-309.

[137] Zhai, R., Zhou, Z., Zhang, W., Sang, S., & Li, P. (2014). Control and navigation system for a fixed-wing unmanned aerial vehicle. *Aip Advances*, *4*(3).

[138] Kanellis, E., & Vasov, G. (2016). *Real time NMPC for fixed wing UAV applications* (Doctoral dissertation, Master's thesis, Aalborg university, Electronics and IT).

[139] Ingabire, A., & Sklyarov, A. A. (2019). Control of longitudinal flight dynamics of a fixedwing UAV using LQR, LQG and nonlinear control. In *E3S Web of Conferences* (Vol. 104, p. 02001). EDP Sciences.

[140] Anjali, B. S., Vivek, A., & Nandagopal, J. L. (2016). Simulation and analysis of integral LQR controller for inner control loop design of a fixed wing micro aerial vehicle (MAV). *Procedia Technology*, *25*, 76-83.

[141] Manchester, I. R., & Slotine, J. J. E. (2017). Control contraction metrics: Convex and intrinsic criteria for nonlinear feedback design. *IEEE Transactions on Automatic Control*, *62*(6), 3046-3053.

[142] Forni, F., & Sepulchre, R. (2013). A differential Lyapunov framework for contraction analysis. *IEEE transactions on automatic control*, *59*(3), 614-628.

[143] Papachristodoulou, A., Anderson, J., Valmorbida, G., Prajna, S., Seiler, P., Parrilo, P., ... & Jagt, D. (2013). SOSTOOLS version 4.00 sum of squares optimization toolbox for MATLAB. *arXiv preprint arXiv:1310.4716*.

[144] Leung, K., & Manchester, I. R. (2017, May). Nonlinear stabilization via control contraction metrics: A pseudospectral approach for computing geodesics. In *2017 American Control Conference (ACC)* (pp. 1284-1289). IEEE.

[145] Ducard, G. J. (2009). *Fault-tolerant flight control and guidance systems: Practical methods for small unmanned aerial vehicles*. Springer Science & Business Media.

[146] Lijia, C., Yu, T., & Guo, Z. (2019). Adaptive observer-based fault detection and active tolerant control for unmanned aerial vehicles attitude system. *IFAC-PapersOnLine*, *52*(24), 47-52.

[147] Manchester, I. R., & Slotine, J. J. E. (2018). Robust Control Contraction Metrics: A Convex Approach to Nonlinear State-Feedback ${H}^\infty$ Control. *IEEE Control Systems Letters*, *2*(3), 333-338.

[148] Singh, S., Majumdar, A., Slotine, J. J., & Pavone, M. (2017, May). Robust online motion planning via contraction theory and convex optimization. In *2017 IEEE International Conference on Robotics and Automation (ICRA)* (pp. 5883-5890). IEEE.

[149] Blanchini, F. (1999). Set invariance in control. *Automatica*, *35*(11), 1747-1767.

[150] Carmo, D., Perdigao, M., & Flaherty, F. J. (1992). Riemannian Geometry, vol. 6. *Cham, Switzerland: Springer*.

[151] Aylward, E. M., Parrilo, P. A., & Slotine, J. J. E. (2008). Stability and robustness analysis of nonlinear systems via contraction metrics and SOS programming. *Automatica*, *44*(8), 2163-2170.

[152] Prajna, S., Papachristodoulou, A., & Parrilo, P. A. (2002, December). Introducing SOSTOOLS: A general purpose sum of squares programming solver. In *Proceedings of the 41st IEEE Conference on Decision and Control, 2002.* (Vol. 1, pp. 741-746). IEEE.

[153] Lofberg, J. (2004, September). YALMIP: A toolbox for modeling and optimization in MATLAB. In *2004 IEEE international conference on robotics and automation (IEEE Cat. No. 04CH37508)* (pp. 284-289). IEEE.

[154] ApS, M. (2019). Mosek optimization toolbox for matlab. *User's Guide and Reference Manual, Version*, *4*(1).

[155] Manchester, I. R., & Slotine, J. J. E. (2014, November). Output-feedback control of nonlinear systems using control contraction metrics and convex optimization. In *2014 4th Australian control conference (AUCC)* (pp. 215-220). IEEE.

[156] Parrilo, P. A. (2000). *Structured semidefinite programs and semialgebraic geometry methods in robustness and optimization*. California Institute of Technology.

[157] Hassan K. Khalil, *Nonlinear systems; 3rd ed.* Upper Saddle River, NJ: Prentice-Hall, 2002. The book can be consulted by contacting: PH-AID: Wallet, Lionel.

[158] Singh, S., Landry, B., Majumdar, A., Slotine, J. J., & Pavone, M. (2023). Robust feedback motion planning via contraction theory. *The International Journal of Robotics Research*, *42*(9), 655-688.

[159] Yu, Y., Shan, D., Benderius, O., Berger, C., & Kang, Y. (2022). Formally robust and safe trajectory planning and tracking for autonomous vehicles. *IEEE Transactions on Intelligent Transportation Systems*, *23*(12), 22971-22987.

[160] Nguyen, Q., & Sreenath, K. (2016, July). Exponential control barrier functions for enforcing high relative-degree safety-critical constraints. In *2016 American Control Conference (ACC)* (pp. 322-328). IEEE.

[161] Kelly, M. (2017). An introduction to trajectory optimization: How to do your own direct collocation. *SIAM Review*, *59*(4), 849-904.

[162] Andersen, E. D., & Andersen, K. D. (2000). The MOSEK interior point optimizer for linear programming: an implementation of the homogeneous algorithm. In *High performance optimization* (pp. 197-232). Boston, MA: Springer US.

[163] Leung, K., & Manchester, I. R. (2017, May). Nonlinear stabilization via control contraction metrics: A pseudospectral approach for computing geodesics. In *2017 American Control Conference (ACC)* (pp. 1284-1289). IEEE.

[164] Currie, J., Wilson, D. I., Sahinidis, N., & Pinto, J. (2012). OPTI: Lowering the barrier between open source optimizers and the industrial MATLAB user. *Foundations of computer-aided process operations*, *24*, 32.

[165] Bosché, F., Ahmed, M., Turkan, Y., Haas, C. T., & Haas, R. (2015). The value of integrating Scan-to-BIM and Scan-vs-BIM techniques for construction monitoring using laser scanning and BIM: The case of cylindrical MEP components. *Automation in Construction*, *49*, 201-213.

[166] Wang, Q., Kim, M. K., Cheng, J. C., & Sohn, H. (2016). Automated quality assessment of precast concrete elements with geometry irregularities using terrestrial laser scanning. *Automation in construction*, *68*, 170-182.

[167] Chen, K., Lu, W., Xue, F., Tang, P., & Li, L. H. (2018). Automatic building information model reconstruction in high-density urban areas: Augmenting multi-source data with architectural knowledge. *Automation in Construction*, *93*, 22-34.

[168] Li, J., Deng, G., Luo, C., Lin, Q., Yan, Q., & Ming, Z. (2016). A hybrid path planning method in unmanned air/ground vehicle (UAV/UGV) cooperative systems. *IEEE Transactions on Vehicular Technology*, *65*(12), 9585-9596.

[169] Lin, Y., Gao, F., Qin, T., Gao, W., Liu, T., Wu, W., ... & Shen, S. (2018). Autonomous aerial navigation using monocular visual-inertial fusion. *Journal of Field Robotics*, *35*(1), 23-51.

[170] Huang, A. S., Bachrach, A., Henry, P., Krainin, M., Maturana, D., Fox, D., & Roy, N. (2017). Visual odometry and mapping for autonomous flight using an RGB-D camera. In *Robotics Research: The 15th International Symposium ISRR* (pp. 235-252). Springer International Publishing.

[171] Gao, F., Wu, W., Gao, W., & Shen, S. (2019). Flying on point clouds: Online

trajectory generation and autonomous navigation for quadrotors in cluttered environments. *Journal of Field Robotics*, *36*(4), 710-733.

[172] Zhou, B., Gao, F., Wang, L., Liu, C., & Shen, S. (2019). Robust and efficient quadrotor trajectory generation for fast autonomous flight. *IEEE Robotics and Automation Letters*, *4*(4), 3529-3536.

[173] Li, F., Zlatanova, S., Koopman, M., Bai, X., & Diakité, A. (2018). Universal path planning for an indoor drone. *Automation in Construction*, *95*, 275-283.

[174] Bolourian, N., & Hammad, A. (2020). LiDAR-equipped UAV path planning considering potential locations of defects for bridge inspection. *Automation in Construction*, *117*, 103250.

[175] Liu, P., Chen, A. Y., Huang, Y. N., Han, J. Y., Lai, J. S., Kang, S. C., ... & Tsai, M. H. (2014). A review of rotorcraft unmanned aerial vehicle (UAV) developments and applications in civil engineering. *Smart Struct. Syst*, *13*(6), 1065-1094.

[176] MathWorks, MATLA B. htps:./www.mathworks.com/products/matlab.html s_ tid=hp products matlab, 1984 (accessed June5.2022).

[177] Lohmiller, W., & Slotine, J. J. E. (1998). On contraction analysis for non-linear systems. *Automatica*, *34*(6), 683-696.

[178] Yu, Y., Zhang, G., He, P., Li, H., Cao, J., & Deng, F. (2022). Tracking attitude with sum-of-squares programming for a fixed-wing air vehicle. *IEEE Transactions on Circuits and Systems II: Express Briefs*, *69*(8), 3450-3454.

[179] Ferronato N, Torretta V. Waste mismanagement in developing countries: A review of global issues[J]. *International journal of environmental research and public health*, 2019, 16(6): 1060.

[180] Li C Z, Zhao Y, Xiao B, et al. Research trend of the application of information technologies in construction and demolition waste management[J]. *Journal of Cleaner Production*, 2020, 263: 121458.

[181] Statistics Unit, Environmental Protection Department, "Monitoring of Solid Waste in Hong Kong- Waste Statistics for 2019" December 2020

[182] Lu W, Yuan H. Off-site sorting of construction waste: what can we learn from Hong Kong?[J]. *Resources, conservation and recycling*, 2012, 69: 100-108.

[183] Shen L Y, Tam V W Y. Implementation of environmental management in the

Hong Kong construction industry[J]. *International Journal of Project Management*, 2002, 20(7): 535-543.

[184] Tam V W Y, Tam C M. A review on the viable technology for construction waste recycling[J]. *Resources, conservation and recycling*, 2006, 47(3): 209-221.

[185] Mahfuth K, Loulizi A, Al Hallaq K, et al. Implementation phase safety system for minimising construction project waste[J]. *Buildings*, 2019, 9(1): 25.

[186] Niskanen, Toivo, and Olli Saarsalmi. "Accident analysis in the construction of buildings." *Journal of occupational accidents* 5.2 (1983): 89-98.

[187] Melenbrink N, Werfel J, Menges A. On-site autonomous construction robots: Towards unsupervised building[J]. *Automation in construction*, 2020, 119: 103312.

[188] Aziz R F, Hafez S M. Applying lean thinking in construction and performance improvement[J]. *Alexandria Engineering Journal*, 2013, 52(4): 679-695.

[189] Li C T, Cheng J C P, Chen K. Top 10 technologies for indoor positioning on construction sites[J]. *Automation in Construction*, 2020, 118: 103309.

[190] Wang Z, Li H, Zhang X. Construction waste recycling robot for nails and screws: Computer vision technology and neural network approach[J]. *Automation in Construction*, 2019, 97: 220-228.

[191] Xiao, W., Yang, J., Fang, H. et al. Development of an automatic sorting robot for construction and demolition waste. *Clean Techn Environ Policy 22*, 1829–1841 (2020). https://doi.org/10.1007/s10098-020-01922-y

[192] Chen X, Huang H, Liu Y, et al. Robot for automatic waste sorting on construction sites[J]. *Automation in Construction*, 2022, 141: 104387.

[193] Feng Z, Guan N, Lv M, et al. Efficient drone hijacking detection using onboard motion sensors[C]//*Design, Automation & Test in Europe Conference & Exhibition (DATE)*, 2017. IEEE, 2017: 1414-1419.

[194] Yeh C C, Chang Y L, Alkhaleefah M, et al. YOLOv3-based matching approach for roof region detection from drone images[J]. *Remote Sensing*, 2021, 13(1): 127.

[195] Siswantoro J, Prabuwono A S, Abdullah A. Real world coordinate from image coordinate using single calibrated camera based on analytic geometry[C]//*International Multi-Conference on Artificial Intelligence Technology*. Springer, Berlin, Heidelberg, 2013: 1-11.

[196] Zhang J, Wu Y, Liu W, et al. Novel approach to position and orientation estimation in vision-based UAV navigation[J]. *IEEE Transactions on Aerospace and*

Electronic Systems, 2010, 46(2): 687-700.

[197] Hong-jie G, Fu-zhou D. Real-time Projection Method for Augmented Reality Assisted Assembly[C]//*MATEC Web of Conferences. EDP Sciences*, 2018, 175: 02026.

[198] Fetić A, Jurić D, Osmanković D. The procedure of a camera calibration using Camera Calibration Toolbox for MATLAB[C]//*2012 Proceedings of the 35th International Convention MIPRO. IEEE*, 2012: 1752-1757.

[199] Tan M, Zheng Y, Chen M, et al. Design and development of locust monitoring system[C]//*Journal of Physics: Conference Series. IOP Publishing*, 2021, 2005(1): 012090.